Decomposition of Hexamethyldisilazane on Hot Metal Filaments and its Gas-phase Chemistry in a Hot-wire Chemical Vapor Deposition Reactor

Ampong, Eric

UNIVERSITY OF CALGARY

Decomposition of Hexamethyldisilazane on Hot Metal Filaments and its Gas-phase Chemistry in a Hot-wire Chemical Vapor Deposition Reactor

by

Eric Ampong

A THESIS
SUBMITTED TO THE FACULTY OF GRADUATE STUDIES
IN PARTIAL FULLFILMENT OF THE REQUIREMENTS FOR THE
DEGREE OF MASTER OF SCIENCE

GRADUATE PROGRAM IN CHEMISTRY
CALGARY, ALBERTA
SEPTEMBER, 2019

Abstract

Hot-wire chemical vapor deposition (HWCVD) has been used to produce silicon-containing thin films, nanomaterials, and functional polymer coatings for applications in microelectronic and photovoltaic devices. Silicon carbonitride (SiC_yN_z) thin films, deposited by HWCVD, have found a wide range of applications due to their nonstoichiometric component that exhibits unique properties from a combination of SiC and Si_3N_4 binary compounds. Most CVD growth of SiC_yN_z proceeds through the use of separate Si-containing (SiH_4), C-bearing (CH_4) and NH_3 precursors. Handling of pyrophoric silane is difficult, and the process optimization with multiple source gases is extremely complex. This has urged interest in exploring alternative single-source precursors for SiC_yN_z deposition.

1,1,1,3,3,3-Hexamethyldisilazane (HMDSZ), a non-pyrophoric and non-corrosive molecule, is one of the single-source precursors for use in HWCVD of SiC_yN_z thin films. In this work, single-photon ionization using vacuum ultraviolet wavelength at 118 nm coupled with time-of-flight mass spectrometry is employed to examine the products from primary decomposition on tungsten and tantalum filaments under collision-free conditions and from secondary gas-phase reactions in a HWCVD reactor. It has been shown that HMDSZ decomposes on the heated metal filaments to produce methyl radicals via Si-CH_3 bond cleavage. The methyl radical formation is controlled by surface reactions at filament temperatures ranging from 1600 to 2400 ^oC. The activation energy for the formation of methyl radicals on the W and Ta filament has been determined to be 71.2 ± 9.1 to 76.7 ± 8.1 kJ/mol, respectively. A comparison with the theoretical energy (363 kJ/mol) required for the homolytic cleavage of Si-CH_3 bond in the gas phase

indicates that the dissociation of HMDSZ on the W and Ta surfaces to produce methyl radicals is a catalytic cracking process.

Aside from the homolytic cleavages, other decomposition routes of HMDSZ, both concerted and stepwise ones, have been systematically explored in this work. The concerted formation of trimethylsilylamine and 1,1-dimethylsilene was found to be the most kinetically favorable route of all, with an activation barrier of 278 kJ/mol. It is also interesting to find that both the elimination of CH_3 radical from a methylated silylamino radical and elimination of H atom from the C atom attached to a Si atom in a silyl radical site proceed without an activation barrier.

In the secondary gas-phase reactions, radical-radical and radical-molecule reactions are dominant. Formation of 1,1-dimethylsilanimine ($(CH_3)_2Si=NH$) was detected from the HWCVD reactor when HMDSZ was introduced. 1,1-dimethylsilanimine undergoes head-to-tail cycloaddition and nucleophilic addition reaction with the abundant HMDSZ molecules to form 1,1,3,3-tetramethylcyclodisilazane and octamethyltrisilazane that were both detected in this work. The secondary gas-phase reactions are also characterized by a free radical short-chain reaction initiated by the primary decomposition of HMDSZ on the metal filaments to produce methyl radicals. Hydrogen abstraction by methyl radical is the main propagation step in the reactor, and biradical recombination reactions terminate the chain reaction to form various stable products with high molecular masses that were also detected in this work.

Acknowledgement

I would like to express my profound gratitude to God for the gift of life and His mercies. I would also like to express my heartfelt appreciation to my supervisor Dr. Yujun Shi for giving me the opportunity to work in her group and for her guidance and supervision throughout these years. Beside my supervisor, I like to thank my supervisory committee members, Dr. Marriott and Dr. Heyne for their time in my annual meetings and their insightful discussion and contributions. Special thanks to Dr. Arvi Rauk for his help in the theoretical calculations used in this work. I also thank Dr. Roland Roesler and his research group members for their help in the synthesis of chemicals used in this work.

It has been a great pleasure working with all the members in Dr. Shi's lab. I would like to thank Taozhe (Evan) Wu for all his help with the instrumentation and for being such a good friend. I specially thank Ebenezer and his family for their help when I first joined the group. I also thank the team at the science workshop, the glass workshop, the electronic workshop, especially Edward Cairns and the instrumentation facility at the department of chemistry, especially Wade White. Finally, I am grateful to my mother, Lucy, my father, Samuel, my brother, Frimpong, my sister, Abigail, and Mr. Kwarteng for their love, support and encouragement.

To my mother (Lucy), my father (Samuel) and
my siblings (Frimpong and Abigail)

Table of Contents

List of Tables

List of Figures and Illustrations

List of Symbols, Abbreviations and Nomenclature

Symbol	Definition
ALD	Atomic layer deposition
Amu	Atomic mass unit
APCVD	Atmospheric-pressure chemical vapor deposition
B3LYP	Becke 3-Parameter, Lee-Yang-Parr
CCSD(T)	Coupled cluster with single, double and perturbative triple
CVD	Chemical vapor deposition
E_a	Activation energy
E_a^{APP}	Apparent activation energy
HMDSZ	1,1,1,3,3,3-Hexamethyldisilazane
HWCVD	Hot-wire chemical vapor deposition
IE	Ionization energy
IRC	Intrinsic reaction coordinate
LiF	Lithium Fluoride
LPCVD	Low-pressure chemical vapor deposition
MFC	Mass flow controller
MWCVD	Microwave chemical vapor deposition
MS	Mass spectrometry
Nd:YAG	Neodymium: yttrium aluminium garnet
PECVD	Plasma-enhanced chemical vapor deposition
PVD	Physical vapor deposition

REMPI	Resonance-enhanced multiphoton ionization
SiC_yN_z	Silicon carbonitride
SPI	Single photon ionization
T_f	Filament temperature
TIMS	Threshold ionization mass spectrometry
TMDSZ	1,1,3,3-Tetramethyldisilazane
TOF-MS	Time-of-flight mass spectrometry
VUV	Vacuum ultraviolet
ZPE	Zero-point energy
ΔG	Change in Gibbs free energy
ΔH	Change in enthalpy
ΔS	Change in entropy

List of Scheme

Epigraph

"Science without religion is lame, religion without science is blind"

Albert Einstein

Chapter One: Introduction and Background

Deposition technology can be regarded as the major key to the creation of devices such as computers and transistors because microelectronic solid-state devices are all based on materials created by thin film deposition. Electronic engineers have continuously sought films of improved quality and sophistication for solid-state devices, requiring a rapid evolution of deposition technology. A high priority for deposition technology is the fabrication of semiconductor materials, an industry that is heavily dependent on the formation of thin solid films of a variety of materials by deposition from gas, liquid, or solid phase. Another reason for the rapid growth of deposition technology is the improved understanding in the chemistry of surfaces, interfaces and microstructures.[1] There are numerous deposition technologies and these technologies can be categorized as via either physical or chemical processes.[2, 3]

Physical vapor deposition (PVD) processes involve materials vaporised from solid or liquid sources in the form of atoms or molecules, and subsequent transportation in the form of a vapor through a vacuum or low-pressure gaseous environment to the substrate where it condenses. PVD processes are used to deposit films with thickness in the range of a few nanometers to thousands of nanometers that can be used to fabricate optical, magnetic and optoelectronic devices.[4] In spite of the high-quality thin films produced by PVD, this technology suffers from its line-of-sight covering, high capital cost, and the need for operation at high vacuum and high temperatures, at which most of these materials are thermally unstable.

Chemical vapor deposition (CVD) has grown very rapidly in the past two decades. Applications of this fabrication process are now key elements for many industrial products, such as optoelectronics, optics, cutting tools, and refractory fibers.[5] CVD involves flowing a precursor gas or gases into a chamber containing a heated substrate to be coated. Chemical reactions occur in the gas phase, and on or near the heated substrate, resulting in the deposition of a thin film on the surface.[5-7] CVD has several advantages which makes it the predominantly preferred process in most cases. For example, this technique offers relatively high deposition rate, a wide variety of precursors that can be chosen from, conformal deposition, and no requirement of ultra-high vacuum reactors as PVD does.[8] Despite the numerous advantages, the technique of CVD has limitations, including the type of substrate to be coated on, relatively high substrate temperatures, and the requirement of volatile precursors. Notwithstanding the numerous deposition techniques available, a deposition technique that has low substrate temperature, high deposition rate, minimal damage to the deposited film, and low equipment cost would be an ideal technique. Hot-wire chemical vapor deposition meets these requirements.

1.1 Hot-Wire Chemical Vapor Deposition

Hot-wire chemical vapor deposition (HWCVD),[9] also known as catalytic chemical vapor deposition (Cat-CVD),[10] is a promising method for preparing silicon-based thin films, such as hydrogenated amorphous silicon (a-Si:H), hydrogenated microcrystalline silicon (μc-Si:H), and polycrystalline silicon (poly-Si).[11] HWCVD has many advantages compared to the conventionally used CVD techniques, such as low-pressure CVD (LPCVD) and plasma enhanced CVD (PECVD).[12] Specifically, the HWCVD method can be used to prepare Si-containing films with a high deposition rate, low equipment cost,

high gas utilization efficiency, large-area uniformity, and lack of plasma-induced damage.[13 14]

The HWCVD technique has been widely investigated particularly in Europe, the United States, and Japan.[15] Applications in various devices, such as solar cells[16] and thin film transistors (TFTs),[17] have been reported. The concept to use catalytic reactions in a CVD process first appeared in a patent by Yamazaki in 1968.[18] Later in 1979, Wiesmann *et al.* reported that amorphous silicon (a-Si) films were deposited by the decomposition of silane (SiH_4) gas on a heated tungsten (W) filament or a carbon rod.[19] However, their work did not receive much attention since the film quality was much worse than those produced by PECVD. In 1985, Matsumura *et al.* succeeded in preparing high-quality a-Si films using the SiF_4 and H_2 mixtures as the source gas on a heated W wire.[20] Amorphous silicon germanium (a-$SiGe_x$),[21] silicon nitride (SiN_x),[22] and poly-Si [23] thin films were successfully prepared by Matsumura *et al*. in the next 6 years. They reported the production of high-quality films deposited using filament temperatures in the range of 1300 - 1900 ^oC with deposition rates between 5 and 20 Å/s.

HWCVD consists of three processes: (a) catalytic decomposition of source gases by resistively heated filament to produce reactive radical species; (b) the secondary radical-radical and radical-molecule reactions in the gas phase under practical deposition pressures from milliTorrs to hundreds of Torrs; and (c) surface reactions with the final mixture of growth precursors on the substrate placed near the heated filament, but kept at relatively low temperature (~300 ^oC), leading to film growth.[24] Hence, film growth in HWCVD is induced by reactive species in the gas phase. These film growth precursors come from direct decomposition on the filament and/or from secondary reactions in the

gas phase. It is therefore important to identify the reactive species in the HWCVD processes and to understand the chemical kinetics in the gas phase.[25] A schematic diagram illustrating the various processes in HWCVD is shown in Figure 1-1.

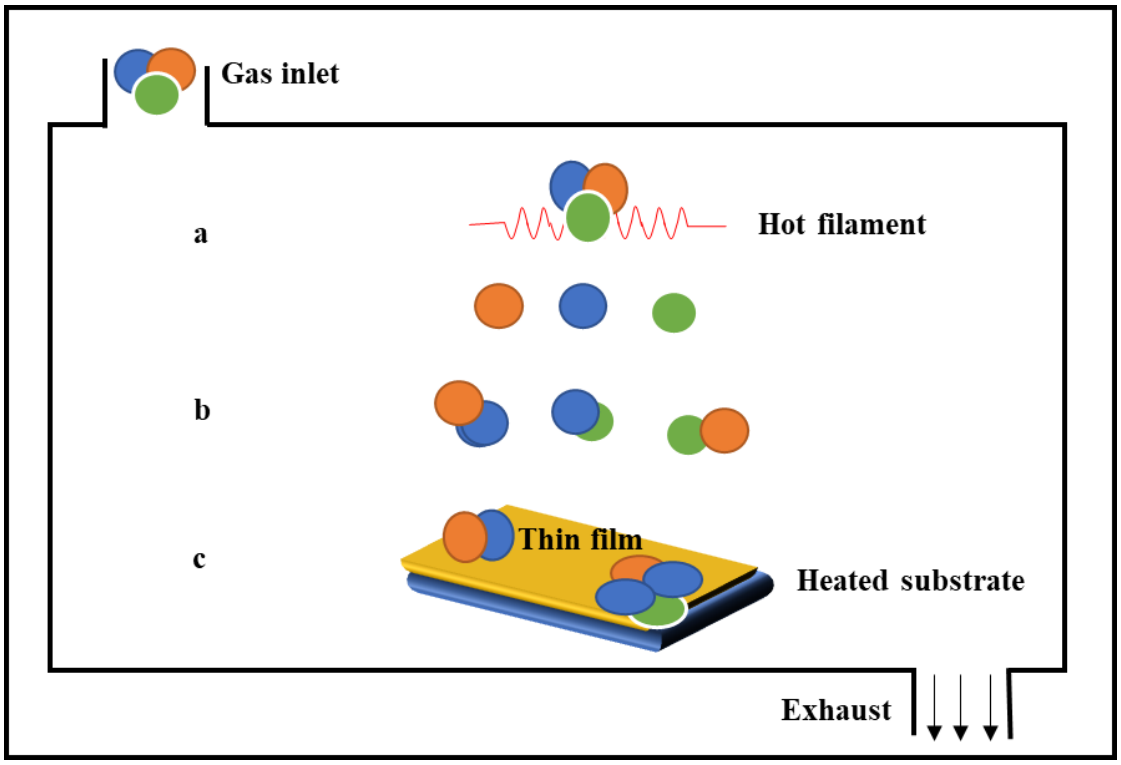

Figure 1-1: A schematic diagram illustrating various processes involved in HWCVD. a) catalytic decomposition of the source gases on heated filament surface in the vacuum chamber, b) secondary gas-phase reactions, and c) surface reactions on the substrate.[26]

1.2 Applications of Hot-Wire Chemical Vapor Deposition (HWCVD) Processes

1.2.1 HWCVD of Hydrogenated Silicon Thin Films

HWCVD of amorphous hydrogenated silicon (a-Si:H) thin films was first introduced by Wiesmann *et al*. in 1979.[19] They deposited a-Si:H by the then-new technique of thermal decomposition of SiH_4 on a hot W filament heated to about 1600 ^oC. The authors

observed that the deposited films have a fairly high photo-response with a photoconductivity of 1.2×10^{-7} $(\Omega\ cm)^{-1}$. They found that introduction of NH_3 along with SiH_4 enhanced the photoconductivity quite significantly from 5.4×10^{-9} $(\Omega\ cm)^{-1}$ to 1.2×10^{-7} $(\Omega\ cm)^{-1}$. The films obtained by Wiesmann *et al*. were of poor quality and no further attempts to improve the quality of the film were made at the time. Only in the late 1980's was the method again studied, first by Doyle *et al*.[27] They studied high-quality a-Si:H produced by decomposition of low-pressure SiH_4 gas on a hot W surface followed by deposition on a substrate. The authors have shown that high-temperature W filament provides the surface for heterogenous thermal decomposition of the low-pressure SiH_4 and subsequent evaporation of atomic silicon and hydrogen. They observed that it was the evaporated species that primarily induced a-Si:H growth on the substrate.

During the same time period, Matsumura's group[28] also produced high-quality silicon films with an improved photoconductivity in the range of 10^{-4} - 10^{-3} $(\Omega\ cm)^{-1}$ on a substrate using SiH_4 and H_2 as source gases at high pressures in HWCVD. They observed that the properties of the films were dependent on the filament temperature, and that the generation of chemical species at the filament depended on the filament aging. Both Doyle *et al*. and Matsumura *et al*. reported the production of high-quality a-Si:H films. In 1995, Brogueira *et al*.[29] reported the deposition of a-Si:H films from SiH_4 and H_2 by HWCVD using a low W filament temperature of 1200 ^oC while varying the substrate temperature between 180 and 290 ^oC. They found that the accumulation time under which a filament is subjected to deposition is an important parameter in determining the optical, electronic and structural properties of the deposited films. The thin films of

silicon and its alloys have large potential for application in low-cost photovoltaic devices (solar cell) and thin film transistors (TFTs).[30]

1.2.2 HWCVD of Diamond Coatings

Diamond, the sp^3-bonded allotrope of carbon, has many unique properties, such as extreme mechanical hardness, high thermal conductivity, and wide band gap. This has encouraged its applications in wear-resistant coatings, optical transparent windows, and cutting tools.[31] The early 80's saw the first demonstration of the growth of polycrystalline diamond thin films by CVD methods.[32] Diamond crystals were grown on various substrates, *e.g.*, diamond, silicon, tungsten, molybdenum.[31, 33]

Matsumoto *et al.*[33] reported the formation of diamond particles on silicon and molybdenum wafers using CH_4/H_2 as precursor gases in HWCVD. From their results, both multiply twinned crystals and cubo-octahedral crystals were obtained. In a similar study, Motahari *et al.*[34] deposited nano- and micro-crystalline diamonds on the surface of substrate using $CH_4/H_2/N_2$ gas mixtures in a tubular quartz vacuum chamber. In their system, the W filaments can heat the substrate and act as thermal activator for gas species at the same time. They found that, apart from the nano- and micro-crystalline diamonds observed in coatings, disordered diamond and some non-diamond phases such as graphitic carbons were present in the coating layers.

1.2.3 HWCVD of Silicon Carbide Thin Films

Silicon carbide (μc-SiC or a-SiC) thin films have received considerable attention after the pioneering work presented by Anderson *et al.*[35] Their unique properties, such as wide band gap and high carrier mobility, make them an excellent candidate for use in various

optoelectronic devices, including blue light-emitting diodes (LEDs) and high-speed, high-power, or high-temperature electronic devices.[35] The conventional approach to the fabrication of SiC thin films proceeds through the use of separate Si-containing (*e.g.*, SiH_4 or $SiH_{4-x}Cl_x$, x = 1-4) and C-bearing (*e.g.*, CH_4) source gases. Tehrani *et al.*[36] reported low-pressure synthesis and characterization of multiphase SiC films by HWCVD method using CH_4/SiH_4 gas mixtures. They used Fourier-transform infrared (FTIR) absorption spectra and X-ray diffraction (XRD) to analyze the deposited SiC films. The deposition rate was found to be significantly influenced by the change in the CH_4 flow rate. Multiphase SiC films consisting of a-Si, a-SiC, and c-SiC phases were observed. When low CH_4 and SiH_4 flow rates were used, crystalline SiC films were obtained with low deposition rates. At higher CH_4 flow rates, higher deposition rate of SiC films were observed with high carbon incorporation, but the presence of a-Si and a-SiC phases were prominent.

In studying SiC:H thin films, Kamble *et al.*[37] demonstrated a high deposition rate in the fabrication of SiC films by the HWCVD method using CH_4 and SiH_4 as source gases. According to their results, the deposition rate of the SiC film was between 9.4 nm/s and 15.54 nm/s. They observed amorphization of the SiC:H films when the deposition pressure was increased. The density of C-H bond decreased, while those of Si-C and Si-H bonds increased, with an increase in the deposition pressure. The C-C bond was absent in the SiC films and nearly stoichiometric SiC:H films were achieved. They concluded that CH_4 can be used as an effective carbon source in HWCVD to fabricate stoichiometric SiC:H films.

In spite of the numerous studies, the use of gas mixtures as source gases have several limitations. Handling pyrophoric silane and highly corrosive chlorosilanes is difficult. Furthermore, the process optimization is extremely complex with multiple source gases. This has urged interest in exploring alternative single-source precursors containing both Si and C, for example, organosilicon compounds.

Bent and coworkers[38] explored the use of mono-, tri-, and tetra-methylsilanes as single-source precursors in HWCVD to deposit a-SiC:H thin films on Si wafers. They employed the in-situ multiple internal reflection FTIR spectroscopy and temperature programmed reactions and desorption techniques to analyze the film structure and thermal reactivity. The formation of films containing mixed silicon hydrides (SiH_x, x = 1-3) and methyl groups was observed when monomethylsilane and trimethylsilane were used as single-source precursors. When tetramethylsilane was used as the single-source precursor, no substantial film growth was observed, which is consistent with the film growth mechanism involving a Si-H bond cleavage. At high temperatures, hydrogen desorption and hydrocarbon evolution from the grown films were observed. Methane was the main hydrocarbon evolved from films grown with monomethylsilane, whereas acetylene was the main hydrocarbon evolved when trimethylsilane was used. They ascribed the formation of acetylene to the higher concentration of methyl group in films grown with trimethylsilane.

1.2.4. HWCVD of Silicon Nitride (SiN_x) and Silicon Carbonitride (SiC_yN_z) Thin Films

The fabrication of silicon nitride (SiN_x) and silicon carbonitride (SiC_yN_z) by HWCVD has attracted much attention. This is because device quality thin films can be

obtained at low substrate temperatures. These device quality films can be fabricated either by the use of mixture of source gases (*e.g.,* SiH_4 and NH_3) or single source gas (*e.g.,* tris(dimethylamino)silane).

1.2.4.1 HWCVD of SiN_x Films Using Silane and Ammonia (SiH_4/NH_3) Mixtures

HWCVD of silicon nitride (SiN_x) thin films have attracted increasing research interest owing to their wide range of applications as passivation layer, diffusion barrier, anti-reflection coating, and gate insulators in semiconductors.[39, 40] Due to the ability to grow high-quality films at low substrate temperatures while avoiding plasma-induced damages to the films, there is an increased interest in the use of HWCVD for SiN_x thin films. Conventionally, the fabrication of SiN_x thin films uses a mixture of separate Si-containing (*e.g.,* SiH_4, $SiH_{4-x}Cl_x$, x=1-4) and NH_3 precursors.

Takano *et al.*[41] studied the conformal step coverage of SiN_x films prepared on a Si substrate using SiH_4/NH_3 gaseous mixtures by HWCVD. The authors found that increasing the catalyzer-substrate distance improved the step coverage from 46 to 67 % on a 1.0 μm line and space pattern. They also found that the deposited SiN_x films exhibited a passivation effect. This suggests that the SiN_x films fabricated by HWCVD are suitable for passivation and interlayer films in microelectronic devices.

Stannowski *et al.*[42] studied the growth process of SiN_x deposition by HWCVD using SiH_4/NH_3 gaseous mixtures. They have shown that SiH_4 is cracked efficiently at the filaments, whereas NH_3 species are scarcely dissociated at the filament, but rather in the gas phase by the atomic hydrogen originating from the dissociated silane. They concluded that the abundance of atomic hydrogen in the gas phase is crucial for the breakup of ammonia and incorporation of N in the film.

Deposition of device-quality SiN_x thin films with ultra high deposition rate in the HWCVD method using SiH_4/NH_3 gas mixtures was studied by Verlaan *et al.*[43] They discovered that the gas flow ratio and the deposition pressure had influence on the N/Si ratio in the deposited films. High flows of SiH_4 increased the rate of Si deposition, while a higher process pressure greatly enhanced the efficiency of NH_3 decomposition. By combining high SiH_4 flows with high deposition pressures, the deposition rate was increased to a very high value of 7 nm/s for device-quality SiN_x films.

Mahan *et al.*[44] studied the structure of SiN_x thin films deposited by the HWCVD technique using SiH_4 and NH_3 gas mixtures and the effect of H_2 dilution to the gas mixtures. They found that the H_2 dilution did not change the basic film structure but did increase the efficiency of NH_3 dissociation in the gas phase. The authors also found that the H_2 dilution caused a reduction in the amount of N-H bonding in the SiN_x films and that the content of N atoms in the films increased significantly with H_2 dilution for a given NH_3/SiH_4 gas flow ratio. Wang *et al.*[45] have shown that near perfect conformal coverage of high-quality a-SiN_x films can be deposited by HWCVD using SiH_4, NH_3 and H_2 gases. They found that adding H_2 to the processing significantly enhanced the SiN_x films properties and also greatly increased the N content in the film. It is believed that hydrogen dilution plays a role for the conformal deposition of silicon nitride film.

Ansari *et al.*[46] also studied the HWCVD of SiN_x thin films using SiH_4 and NH_3 and the effect of H_2 dilution. They found a sharp decrease in the decomposition efficiency of NH_3 with the introduction of SiH_4. A recovery of the decomposition efficiency of NH_3 was found by the addition of H_2 when the NH_3 pressure was low. At higher NH_3 pressures, the decomposition efficiency showed a minor dependence on the H_2 partial

pressures. The recovery of the NH_3 decomposition was attributed to the reactivation of the filament surface by the H atoms produced by the catalytic decomposition of H_2. The suppression effect on the NH_3 dissociation efficiency with the presence of SiH_4 has been demonstrated by several research groups.[47, 48] This is consistent with the fact that a high gas flow ratio of NH_3 to SiH_4 is typically required under practical deposition conditions to obtain stoichiometric Si_3N_4 films.

1.2.4.2 HWCVD of SiN_x Films Using Chlorosilanes ($SiH_{4-x}Cl_x$, x = 1-4) and Ammonia Mixtures

Silicon nitride films have been fabricated using SiH_4 and NH_3 as source gases for the deposition. The use of SiH_4 is known to suppress the dissociation of NH_3, and thus, a high gas flow rate ratio of NH_3 to SiH_4 is needed. The use of chlorosilanes and ammonia as source gases were therefore explored to investigate the effect of chlorosilanes on ammonia decomposition, and to test their use for the fabrication of SiN_x films. There is no literature on HWCVD of SiN_x thin films using chlorosilanes and ammonia. The literature studies discussed in this Section mainly concern SiN_x film deposition using other CVD methods.

Chu *et al*.[49] deposited amorphous SiN_x films on silicon substrate in a gas flow system by amonolysis of silicon tetrachloride, as represented in Equation (1-1), or nitridation of silane with ammonia, as shown in Equation (1-2), on heated substrate surfaces.

$$3SiCl_4 + 4NH_3 \longrightarrow Si_3N_4 + 12HCl \qquad (1\text{-}1)$$

$$3SiH_4 + 2N_2 \longrightarrow Si_3N_4 + 6H_2 \qquad (1\text{-}2)$$

They found that the amonolysis reaction is complicated by the formation of ammonium chloride and polymerization of the silicon diimide ($Si(NH)_2$) intermediate, as shown in Equation (1-3) and (1-4). They also found that the substrate temperature during the deposition process have the most significant influence on the properties of the deposited SiN_x films, such as density, refractive index, and infrared absorption.[49]

$$SiCl_4 + 6NH_3 \longrightarrow Si(NH)_2 + 4NH_4Cl \quad (1\text{-}3)$$

$$6[Si(NH)_2]_x \xrightarrow[-2NH_3]{400\ ^oC} 2[Si_3(NH)_3N_2]_x \xrightarrow[-NH_3]{600\ ^oC} 3[Si_2(NH)_3N_2]_x \xrightarrow[-NH_3]{1250\ ^oC} 2\text{-}Si_3N_4 \quad (1\text{-}4)$$

Grieco *et al.*[50] reported the deposition of silicon nitride films on silicon substrate by the reaction between silicon tetrachloride and ammonia in the temperature range of 550 – 1250 ^oC. They also observed a white powdery (NH_4Cl) material formed on the upper and lower portions inside of the reactor wall. The dielectric strength was found to be independent of the film thickness and the dielectric constant was found to be in a range of 7 - 8. The authors concluded that the deposited SiN_x films can be used as protective coatings.

From the investigation by various research groups, it can be seen that the use of SiH_4/NH_3 or $SiH_{4-x}Cl_x$ (x=1-4)/NH_3 mixture as source gases to fabricate SiN_x thin films is complicated and leads to the formation of other by-products. Therefore, alternative single-source precursors that are non-corrosive and non-pyrophoric are needed for the fabrication of SiN_x thin films.

1.2.4.3 HWCVD of SiN_x and SiC_yN_z Thin Films using N-containing Dimethylamino-substituted Organosilicon Molecules

The characteristics of an "ideal" CVD precursor include 1) adequate volatility to achieve acceptable growth rates at moderate temperatures; 2) stability so that decomposition does not occur during evaporation; 3) sufficiently large temperature "window" between evaporation and decomposition for film deposition; 4) high chemical purity,[51] 5) good compatibility with co-precursors during the growth of complex materials; 6) readily manufactured in high yield at a low cost; and 7) non-hazardous or with a low hazard risk.[52] Although these characteristics are common for most CVD precursors, sometimes the precise precursor requirements can depend on the specific nature of the CVD process.

Among the many organosilicon compounds that have been explored in the fabrication of SiN_x and SiC_yN_z thin films, the N-containing organosilicon molecules, especially those that contain dimethylamino substituents, are potentially promising. Two types of dimethylamino-substituted organosilicon molecules, *i.e.*, dimethylamino-substituted silanes and dimethylamino-substituted methylsilanes, have been used. Figure 1-2 shows some molecules in each of the two categories that have been reported in the literature.

(a) Dimethylamino-substituted silane

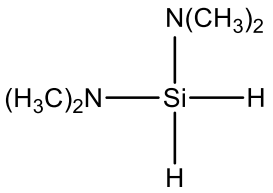

bis(dimethylamino)silane

BDMAS

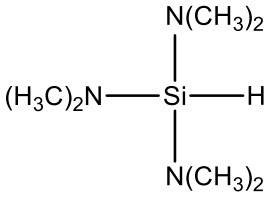

tris(dimethylamino)silane

TriDMAS

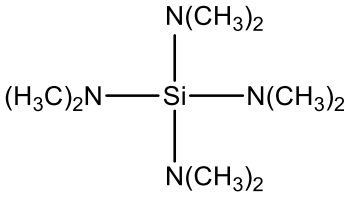

tetrakis(dimethylamino)silane

TDMAS

(b) Dimethylamino-substituted methylsilane

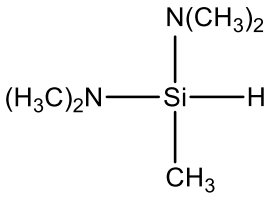

bis(dimethylamino)methylsilane

BDMAMS

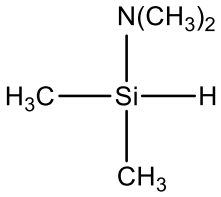

(dimethylamino)dimethylsilane

DMADMS

Figure 1-2: Two types of N-containing organosilicon molecules that contain dimethylamino substituents. (a) dimethylamino-substituted silanes, and (b) dimethylamino-substituted methylsilanes

There is no literature on the use of N-containing dimethylamino-substituted organosilicon molecules as precursors to deposit SiN_x or SiC_yN_z films in HWCVD processes. The SiN_x or SiC_yN_z films deposition using N-containing dimethylamino substituted organosilicon molecules described in this Section involves the use of other CVD methods.

Wrobel *et al.*[53] have used tris(dimethylamino)silane (TrDMAS), one of the dimethylamino-substituted silane molecules, as a single-source precursor to deposit SiC_yN_z films using remote microwave plasma CVD (RP-CVD) technique. They showed a substrate temperature dependence of the film growth rate, implying that RP-CVD is an adsorption-controlled process. They observed that an increase of the substrate temperature from 30 ^oC to 400 ^oC causes elimination of organic moieties (*e.g.,* trimethylamine groups) from the film and the formation of Si-C and Si-C network structure. From their results, the deposited SiC_yN_z films seem to be suitable for protective coating of metal surfaces to increase their wear strength.

Dimethylamino-substituted methylsilane molecules were also studied by Wrobel and coworkers. They explored (dimethylamino)dimethylsilane (DMADMS)[54] and bis(dimethylamino)methylsilane (BDMAMS)[55] as single-source precursors in RP-CVD to deposit SiC_yN_z thin films. With DMADMS as the single-source precursor, they found that, at low substrate temperatures (T_s) of 30 $^oC < T_s < 100$ ^oC, the film was limited by the desorption of the film-forming precursors, whereas at high substrate temperatures of 100 $^oC < T_s < 400$ ^oC, the film growth was independent of the substrate temperature and became a mass-transport limited process. The substrate temperature also played a major role in determining the chemical composition and structure of the SiC_yN_z films. Increasing the substrate temperature led to the elimination of organic moieties ($Si\text{-}CH_3$ groups) and crosslinking via the formation of the Si-C and Si-N networks. Using BDMAMS as the precursor gas, they demonstrated a clear relationship between the physical and mechanical properties of the investigated SiC_yN_z film and their chemical composition and structure, controlled by the substrate temperature.

1.2.4.4 HWCVD of SiC_yN_z Thin Films using N-containing Methyl-substituted Disilazane Molecules

The use of N-containing organosilicon compounds that do not contain dimethylamino substituents, such as hexamethyldisilazanes and tetramethyldisilazanes, has attracted interest as these compounds, containing Si, N and C, can serve as a single-source precursor for SiC_yN_z films. Hexamethyldisilazane (HMDSZ), which has no Si-H bonds[56] and tetramethyldisilazanes (TMDSZ), which consists of two Si-H bonds[57] are film-forming source gases. Methyl-substituted disilazane molecules have been used to deposit SiC_yN_z thin films in HWCVD as well as other CVD method. Addition of NH_3 to methyl-substituted disilazane molecules has been to control the composition of the SiC_yN_z thin films.[58, 59]

1,1,1,3,3,3-Hexamethyldisilazane (HMDSZ) was first described in a U.S. patent in 1970 by Collins and Devers as photoresist adhesion promoter for semiconductor applications.[60] HMDSZ has promising properties: it is non-explosive, non-pyrophoric, and non-corrosive. It also has a moderate vapor pressure of 13.8 Torr at the room temperature of 25 ^oC[61] and a boiling point of 125 ^oC. Therefore, it is an excellent alternative to the conventionally used precursor mixtures containing either pyrophoric silane or corrosive chlorosilanes.

Rahman *et al*.[62] studied SiC_yN_z films deposited by the HWCVD technique using HMDSZ and NH_3 as source gases. They found that SiC_yN_z deposited by HMDSZ only had high oxygen content and this happened after the wafer had been introduced outside the chamber after deposition. They observed that SiC_yN_z films containing low-oxygen content could be obtained using HMDSZ with the addition of NH_3. In addition, the amount of nitrogen is directly related to the properties of the films. The highest nitrogen

content in SiC_yN_z films showed highest density, widest band gap, and lowest refractive index.

Izumi *et al.*[59] showed that SiC_yN_z films could be deposited by employing the HWCVD technique with HMDSZ as precursor gas. From their results, they observed that the deposited film was composed of Si, C, and N when only HMDSZ was used as the source gas, and therefore SiC_yN_z films could be deposited using only HMDSZ as a source gas. They found that the composition of the deposited SiC_yN_z films could be controlled by changing the flow rate of NH_3 added to the HMDSZ/NH_3 mixtures.

Other than HWCVD, the RP-CVD method has also been explored to deposit SiC_yN_z films using N-containing methyl-substituted disilazanes molecules. For example, Belmahi *et al.*[63] obtained SiC_yN_z thin films with RP-CVD using H_2/N_2/Ar/HMDSZ as source gas mixtures. They found that introduction of a small amount of N_2 drastically changed the film composition from SiC_x:H like films to SiN_x:H like films. The optical constants of the SiC_yN_z films can be tuned over a wide domain, thus making this process attractive for applications in photovoltaic and anti-reflective coatings. Bulou *et al.*[64] studied the optical constants of the SiC_yN_z thin films deposited by H_2/N_2/Ar/HMDSZ using RP-CVD. They also found that the RP-CVD method with H_2/N_2/Ar/HMDSZ is a versatile process that allowed the growth of SiC_yN_z thin films with adjustable composition and optical properties. They observed that by controlling the amount of Si-C and Si-N bonds, thin films changing from SiC_x:H like to SiN_x:H like could be synthesized. The bandgap and the refractive index can be tuned over a wide range of values, making it suitable for applications that require thin films with tunable optical parameters.

1.3 Gas-Phase Chemistry in Hot-wire Chemical Vapor Deposition

An extensive research on HWCVD has been focused on the deposition and characteristics of the films by investigating the growth mechanism, structure, surface morphology, element compositions, and chemical bonds. Nonetheless, film growth is induced by chemical species produced from direct decomposition of source gases on the filament and/or from secondary gas-phase reactions. The properties and quality of the deposited films are governed by these gas-phase precursors species. Hence, it is important to identify the gas-phase chemical species for a better understanding of the HWCVD processes.

1.3.1 Detecting the Gas-Phase Reaction Products in HWCVD

In HWCVD, the source gases are decomposed on a heated filament, resulting in the formation of reactive radicals, which are difficult to detect because their fast loss rate leads to a small density compared to that of their molecular precursors. A technique designed to detect these radicals should be an in-situ, real-time method that is highly sensitive to the target radicals and exhibit good sensitivity in distinguishing the real signal from large background signals. In general, the detection techniques can be divided into three principal categories: electron-in-ion-out, photon-in-photon-out, and photon-in-ion-out.[65]

In electron-in-ion-out, the species of interest are ionized by high-energy electron bombardment. The conventional 70 eV electron ionization (EI) is an example of electron-in-ion-out category. It is considered a universal ionization method since it can ionize almost all compounds. However, the conventional 70 eV electron ionization is not suitable for detection of radicals from molecular dissociation since high-energy electrons cause significant fragmentation of parent molecules, creating large fragmentation signals

that conceal weak radical signals. Therefore, identification of radicals produced from the decomposition of molecules become difficult and generally not achieved. To compensate for this limitation in the 70 eV EI, an alternative technique called threshold ionization mass spectroscopy (TIMS) can be used.[27] In TIMS, the electron energy is lowered to just above the radical ionization energy but below the appearance energy of its parent precursor. In this way, ions detected by mass spectrometry are only produced from radicals. One of the disadvantages of TIMS is its laborious calibration process and long data acquisition time.[65] Laser induced fluorescence (LIF)[66] and cavity ring down spectroscopy (CRDS)[67] belong to the photon-in-photon-out category. In the technique of LIF, a laser light is tuned so that its frequency matches that of an absorption line in the atom or molecule of interest. The absorption of the laser photons by this species produces an electronically excited state which then fluoresces.[68] In the CRDS technique, an optical cavity is formed with two highly reflective mirrors around the region of interest. Usually a pulsed laser light tuned to a particular energy enters the cavity through one mirror; upon hitting the second mirror, the majority of the radiation is reflected back, but a certain percentage leaks out of the cavity and is detected.[65, 69] Although both techniques have high sensitivity, only one species can be detected at a time and any photon emission from sources other than the target species can interfere with the detection process.

Photon-in-ion-out employs a laser instead of energetic electrons to ionize the radicals, followed by a mass spectrometer to collect and detect ions. An obvious advantage of photon-in-ion-out is fast-speed data acquisition, making it more suitable for real-time detection and time-resolved study. The energy spread (linewidth) of the laser radiation is also narrow. The photon-in-ion-out process can be classified into two categories, *i.e.*,

resonant enhanced multi-photon ionization (REMPI) and single photon ionization (SPI). REMPI uses one or more photons to excite the target species to an excited state, followed by absorption of an additional photon or multiple photons to reach above the ionization threshold. REMPI is a species-specific technique.[70]. While this is an advantage for providing detailed quantum state information, it also has negative consequence in that the excitation wavelength must be changed to measure different species. Thus, it is not suitable for the analysis of a complex unknown HWCVD system. SPI uses a single photon of significant energy to ionize the target radical, but low enough to avoid fragmentation for most species. SPI can detect multiple species at one time.[71] Therefore, SPI technique is the best choice for studying the gas-phase chemistry in a HWCVD process.

1.3.2 Gas-phase Chemistry in HWCVD of Hydrogenated Silicon Thin Films

In spite of the fact that knowledge of the a-Si:H film properties deposited by HWCVD using SiH_4 has been achieved, details of gas-phase chemistry in the process have received less attention although it is important in developing a comprehensive deposition model and in controlling film properties.

Doyle *et al*.[27] have studied the HWCVD processes of a-Si:H using SiH_4 as a source gas by using mass spectrometric technique. They employed a threshold ionization technique to ionize free radicals selectively. According to their results, the main products at the heated W surface are Si and H atoms when SiH_4 was used as the precursor gas. Matsumura's group also produced high-quality silicon films at high pressures where secondary gas-phase reactions are expected to be predominant.[28] Although radical detection was not performed in this early study, the group proposed that SiH_3 was a likely

precursor for quality film growth under these conditions.[28] Nozaki and coworkers have also demonstrated that atomic Si is the main precursor for film growth with SiH_4 by monitoring the gas-phase radical species in HWCVD using LIF. From their results, SiH radicals were also detected, but the production rate of this species is two order of magnitude lower than that of Si atoms.[66]

Duan *et al.*[72] have performed an experimental study for the direct detection of desorbed species from the hot filament. They detected Si, SiH_3, and Si_2H_6 as the major silicon-containing gas-phase species identified by SPI during hot-wire activation of the SiH_4 precursor. In the study of the catalytic decomposition of SiH_4 on a hot filament using vacuum ultraviolet SPI mass spectrometry under collision-free conditions by Tange *et al.*,[73] it was found that Si atoms were the main species desorbed from the W filament. H atoms were also detected as direct desorbed species from the filament by using the REMPI method combined with time-of-flight mass spectrometry. The authors detected Si_2H_6, Si_2H_4 and Si_2 as products of gas-phase reactions of the desorbed radicals (Si and H atoms) at high pressures. Umemoto *et al*. has shown that atomic Si is the major product from the cracking of SiH_4 on heated W surfaces by employing laser spectroscopic and mass spectrometric techniques.[67]

1.3.3 Gas-phase Chemistry in HWCVD of Diamond Thin Films

Ashfold and coworkers used molecular beam mass spectrometry to obtain quantitative measurements of stable hydrocarbon species under different filament growth conditions for diamond coatings using hot-filament CVD.[74] They found that, regardless of the hydrocarbon feedstock gases used, at filament temperatures between 2000 - 2100

K, the hydrocarbon feedstock gases are converted so that CH_4 is the dominant hydrocarbon species produced. They also discovered that, at filament temperatures near or above the optimum for diamond growth (~ 2400 K), the relative concentration of various stable hydrocarbon species present in the gas mixture and the way the concentration vary with temperature are insensitive to the choice of hydrocarbon feedstock gas.[75]

In studying the gas-phase chemistry during hot-filament CVD of diamond films using CH_4/H_2 and C_2H_2/H_2 gas mixtures, Wu *et al*.[76] demonstrated that, at high filament temperatures above 1900 ^oC, the gas compositions was independent of hydrocarbons feedstock gas used. Thus, the growth rate of diamond films are largely insensitive to the hydrocarbon feedstock gas used. This observation is largely consistent with those by Ashfold *et al*.[74]

1.3.4 Gas-phase Chemistry in HWCVD of SiC Thin Films

More recently, the Shi group has studied the gas-phase reactions chemistry of a series of organosilicon compounds containing direct Si-C bonds. These molecules include tetramethylsilane (TMS),[24] trimethylsilane (TriMS),[77, 78] dimethylsilane (DMS)[79] and monomethylsilane (MMS)[80] as single-source precursors in a HWCVD for the preparation of SiC films. They have shown that free-radical short chain reactions dominate the HWCVD chemistry, whereas silylene/silene species contributions are minor, when TMS and TriMS are used as precursor gases.[24, 77] They also observed that, with an increasing number of Si-H bond in DMS, the silylene and silene chemistry becomes dominant at low filament temperature ($\leq$ 1200 ^oC). The free-radical reactions only become prevailing

when the filament temperature is increased to ≥ 1500 °C.[79] With a further increase in the number of Si-H bonds in MMS, the gas-phase chemistry was exclusively dominated by the reactions involving the methylsilylene intermediate. The free-radical and silene intermediates do not play a role in the gas-phase chemistry of MMS in a HWCVD reactor.[80] The observed change in the literature from C-rich to Si-rich materials in the deposition of SiC thin films as the number of Si-H bond in the precursor gas is increased[38] is explained by the change in the dominant gas-phase intermediate from methyl radical to silylene/silene species when moving from TMS to MMS.

The Shi group has also explored the gas-phase reaction chemistry with cyclic mono- or di-silacyclobutanes. From their studies of three monosilacyclobutane molecules, silacyclobutane (SCB),[81] 1-methylsilacyclobutane (MSCB),[82] and 1,1-dimethylsilacyclobutane (DMSCB),[83] they found that two common decomposition routes existed to form ethene/(methyl-substituted) silenes through cycloreversion and propene/(methyl-substituted)silylenes via a ring-opening reaction initiated by a 1,2-H shift. An additional decomposition route also existed to form methyl radical when MSCB and DMSCB were used as single-source precursors. Of the three molecules, they found that SCB produced the greatest amount of propene, whereas DMSCB produced the least, suggesting that the presence of Si-H bonds favours propene formation. The gas-phase chemistry of SCB was dominated by the insertion and π-type addition reactions of various silylene and silene intermediates. A competition between free-radical chain reaction and silene cyclodimerization was predominant in the gas-phase reaction chemistry of MSCB, whereas formation of 1,1,3,3-tetramethyl-1,3-disilacyclobutane (TMDSCB) was dominant when DMSCB was used. For the disilacyclobutane molecules,

1,3-disilacyclobutane (DSCB)[84] and TMDSCB[85] were studied. They found that DSCB decomposed on the filament to produce H_2 molecules and the secondary gas-phase reactions were dominated by the formation of 1,3-disilacyclobut-1-ylidene. A short free-radical chain reaction was the main mechanism in the reactor setup when TMDSCB was used. They observed that exocyclic bond cleavages played a vital role in the decomposition/reaction chemistry of disilacyclobutanes and ring-opening reactions are more important in monosilacyclobutanes.

1.3.5 Gas-phase Chemistry in HWCVD of SiN_x Thin Films using SiH_4/NH_3 Mixtures

Shi and coworkers[86, 87] examined the gas-phase reaction products produced in the HWCVD reaction chamber using SiH_4, NH_3, and SiH_4/NH_3 mixtures. They employed laser ionization time-of-flight mass spectrometric techniques to detect species produced in the gas phase. In their studies, both vacuum ultraviolet (VUV) laser SPI [47]and laser induced electron impact ionization (LIEI)[47, 87] were used. Using VUV SPI coupled with mass spectrometry, they observed the formation of H_2 and N_2 gases from NH_3 decomposition on the W filament. For the decomposition of SiH_4 on the hot W filament, H_2, Si_2H_6, and Si_3H_8 were observed as the main products. When mixtures containing SiH_4 and NH_3 were used as source gases, they found that NH_3 dissociation on the filament was suppressed by the presence of SiH_4. The SiH_4 chemistry in the reactor was dominant when equal amount of SiH_4 and NH_3 were used. They demonstrated that the extent to which the NH_3 decomposition was suppressed was enhanced with more SiH_4 molecules in the system. Shi and coworkers continued to study the application of LIEI to the deposition chemistry in the HWCVD process with SiH_4/NH_3 mixtures.[79] They showed

that species with ionization energy (IE) below 10.5 eV, such as Si_2H_6, Si_3H_8, and NH_3, exhibited stronger peaks in the mass spectra recorded under SPI conditions, whereas species with IEs above 10.5 eV, such as H_2, N_2, and He, were only weakly visible under the same conditions. They observed that species with IEs above 10.5 eV were significantly enhanced with the LIEI source. With the LIEI source coexisted with the SPI source due to the 118 nm VUV light, both the parent ions with enhanced intensity from VUV SPI and their "fingerprint" fragmentation ions from LIEI were achieved. The suppression of NH_3 decomposition by SiH_4 and the predominance of SiH_4 chemistry were confirmed using the LIEI source.

In 2009, Eustergering *et al*.[86] reported the formation of aminosilane in the HWCVD process using SiH_4/NH_3 mixtures. It was found that when the SiH_4 and NH_3 were present in equal amount, the formation of disilane and trisilane dominated. Increasing the amount of NH_3 in the mixture caused a change in the reaction pathway from disilane and trisilane production towards aminosilane formation. It was shown that the H-atoms in the aminosilane species came solely from NH_3 with the use of deuterated ammonia (ND_3). The amount of NH_2 radicals produced in the process played a vital role in the competition between the two pathways. Specifically, the formation of disilane and trisilane species was favored in the presence of insufficient NH_2 species, since the SiH_3 radicals produced from the SiH_4 decomposition reacted with each other rather than with NH_3. The formation of aminosilane was favored with high NH_2 densities. The extent of suppression of the NH_3 decomposition by SiH_4 was reduced when high NH_3 content was used.

Similar studies were reported by Umemoto *et al*.[88] The authors found that the decomposition efficiency of NH_3 on the filament surfaces decreases sharply by the

introduction of SiH_4. According to their results, 50 times more NH_3 compared to SiH_4 must be introduced to fabricate stoichiometric Si_3N_4 films. The suppression effect of SiH_4 presence in the mixture on the NH_3 dissociation efficiency has also been demonstrated by these authors. This explains why a high flow ratio of NH_3 to SiH_4 is needed under the practical deposition conditions to fabricate stocihiometric Si_3N_4 films.

1.3.6 Gas-phase Chemistry in HWCVD of SiN_x and SiC_yN_z Thin Films using Methyl-Substituted Disilazanes

Morimoto *et al.*[61] reported the decomposition of 1,1,1,3,3,3-hexamethyldisilazane (HMDSZ) on a tungsten filament in the process of HWCVD. They employed a laser ionization mass spectrometric technique to detect the gas-phase species. They observed the mass peaks at m/z 74 and 89 when the filament was turned on at 2000 K. The peaks at m/z 74 and 89 were assigned to trimethylsilane ($HSi(CH_3)_3$) and trimethylsilylamine ($(CH_3)_3SiNH_2$), respectively. From their results, the peaks at m/z 74 and 89 were observed in both low- and high-pressure conditions, suggesting that the Si-N bond dissociation took place on the filament surfaces to produce $Si(CH_3)_3$ and $(CH_3)_3SiNH$ as primary products. They attributed the formation of $HSi(CH_3)_3$ and $(CH_3)_3SiNH_2$ to the surface reactions of $Si(CH_3)_3$ and $(CH_3)_3SiNH$ on chamber walls. According to their density functional theory calculations, the bond energy of Si-N (434 kJ/mol) is higher than that of Si-C (338 kJ/mol). Nevertheless, the Si-N bond seemed to dissociate more efficiently than Si-C bonds, which was attributed to the steric hindrance for the Si-C bond cleavage. They also infer that $(CH_3)_3SiNH$ is one of the main precursors of the deposited SiN_x or SiC_yN_z films.

Yoshimura *et al.*[89] studied the fragment ions produced from HMDSZ in a freeman-type ion source with hot-tungsten wire. They employed a low-energy mass-selected ion beam system to analyze these fragment ions. The observed C^+, N^+, CH_3^+, CH_4^+, Si^+, $SiCH_5^+$, $SiC_3H_9^+$, $Si_2NCH_4^+$, $Si_2NC_2H_6^+$, $Si_2NC_2H_6^+$, $Si_2NC_2H_7^+$, $Si_2NC_2H_6^+$, $Si_2NC_5H_{16}^+$ as the dominant fragment ions. They found that the ion production strongly depended on the W temperature. Fragmentation ability was less effective at low W temperatures, but when the temperature was significantly increased, small fragments were produced. $SiCH_5^+$ ion obtained by the mass-selected fragment ion was irradiated on a Si substrate and analysis of the substrate showed a clear SiC_yN_z film deposition.

1.4 Objectives of This Thesis

This present study was carried out as an effort to expand knowledge of gas-phase chemistry in HWCVD with organosilicon molecules (e.g., methyl-substituted silanes and cyclic silacyclobutanes) for SiC film formation to N-containing organosilicon molecules for SiN_x or SiC_yN_z film production. In this regard, the gas-phase chemistry of 1,1,1,3,3,3-hexamethyldisilazane (HMDSZ), a methyl-substituted disilazane molecule, in the HWCVD process, is presented in this thesis. Methyl-substituted disilazane molecules, as potential single-source precursors for SiC_yN_z thin films using HWCVD, are carriers of Si-N-C units, which may readily be incorporated into the film network. In pursuance of gaining a better understanding of HWCVD for the growth of or SiC_yN_z thin films using HMDSZ as a precursor gas, it is important to identify the gas-phase reactive species produced in the process. In this thesis, the primary decomposition of HMDSZ on the hot W or Ta filament was detected under collision-free conditions (operating pressure 1×10^{-5} Torr) using a 118 nm VUV laser SPI source coupled with time-of-flight (TOF)mass

spectrometer. This helps to detect and understand the primary decomposition reaction pathways for HMDSZ on the two metal surfaces. The secondary reactions in the gas phase were examined by the same ionization source using a HWCVD reactor, which has a relatively higher pressure of 12 Torr. Deuterated isotopomers, including bis(trimethylsilyl)-N-deuterioamine (HMDSZ-d1) and 1,1,13,3,3-hexa(deuteratedmethyl)disilazane (HMDSZ-d18), were used to help with the assignment of mass peaks. The experimental study on the reaction chemistry was compared to the theoretical calculations of the gas-phase decomposition of HMDSZ performed in this work to understand the role that metal filaments played in the dissociation of HMDSZ. The theoretical investigation was performed using *ab initio* calculations of both the concerted and stepwise decomposition of HMDSZ along with the homolytic cleavages of S-C, Si-N, and N-H in the gas phase.

With regard to the layout of this thesis, introduction and background information relevant to this work is provided in Chapter 1. Experimental details and computational methods used in this work are provided in Chapter 2. Decomposition of HMDSZ over tungsten and tantalum filaments are provided in Chapter 3. In addition, theoretical calculations of the gas-phase decomposition of HMDSZ are also presented in Chapter 3. In Chapter 4, the gas-phase chemistry of HMDSZ in a HWCVD reactor is provided. Conclusion and future work are presented in Chapter 5.

Chapter Two: Experimental Details and Computational Methods

To examine the products from the primary decomposition of 1,1,1,3,3,3-hexamethyldisilazane (HMDSZ) on the hot metal filament and from the secondary gas-phase reaction processes in the HWCVD reactor, a laser ionization technique coupled with time-of-flight mass spectrometry (TOF MS) was employed.[24]

2.1 Vacuum Ultraviolet Single-photon Ionization Time-of-flight Mass Spectrometry

A schematic of the experimental setup of the vacuum ultraviolet (VUV) single photon ionization (SPI) time-of-flight (TOF) mass spectrometer used to study the gas-phase chemistry of HMDSZ molecule in HWCVD is illustrated in Figure 2-1. Briefly, the apparatus consists of a HWCVD source, a laser ionization source, and a linear TOF mass spectrometer (R.M. Jordan). A comprehensive description of the apparatus can be found elsewhere.[24] The main ionization chamber is a six-way stainless steel cross (10-inch diameter). The top port of the cross is coupled with the flight tube (1 m length) of the TOF mass spectrometer, while the bottom port is connected to a diffusion pump (VHS-6, Varian) through a gate valve. An Ar/Xe gas cell, where the 118 nm VUV laser radiation is generated, is attached to the left port of the cross. A quartz window is placed in the center of the flange mounted onto the right port to avoid electron emission as a result of the laser beam striking on the metal surface. The port at the back is connected to a mechanical pump which acts as both the roughing pump for the chamber and the backing pump for the diffusion pump, while the port in the front is connected with the HWCVD source, which will be described in detail below.

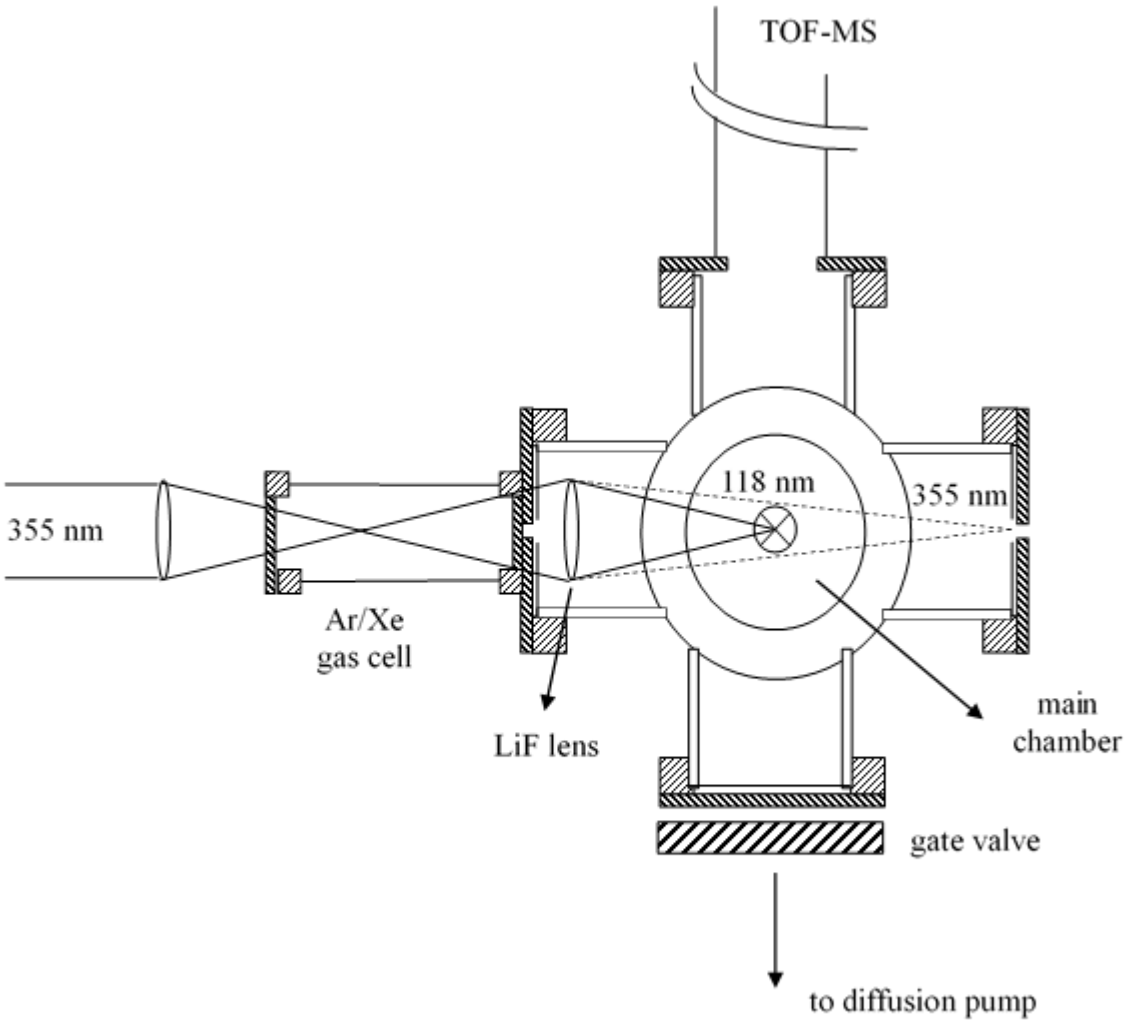

Figure 2-1: A schematic of the experimental setup for the VUV SPI/TOF mass spectrometer.[26]

2.2 HWCVD Sources

To detect the products from the primary decomposition of the gaseous precursors formed directly from the hot metal filament surfaces and from the secondary gas-phase reactions, two different setups, *i.e.*, a collision-free setup and a reaction chamber setup, were used as HWCVD sources.

2.2.1 A Collision-Free Setup to Detect Decomposition Species on the Filament

Chemical species produced directly from the hot filament were detected using the collision-free setup. A tungsten (W) or tantalum (Ta) filament (10 cm length, 0.5 cm diameter) was placed directly in the main chamber through two copper feedthroughs in this setup as shown in Figure 2-2. The filament was resistively heated by a DC power supply and its temperature was measured by a two-color pyrometer (Chino Works) through an IR-grade quartz window.

In addition, a stainless-steel plate of 18 cm in diameter with a hole in the center (D = 1 cm) was placed between the filament and the ion optics of the TOF mass spectrometer as a shield to prevent electrons generated from the hot filament from interfering with electric fields in the ion optics of the TOF-MS. A ¼ inch stainless steel tube through which source gases were introduced was positioned such that its outlet was 5 cm from the filament. The base pressures in the main chamber and the TOF tube were maintained at ~ 1.4×10^{-7} Torr and ~ 1.9×10^{-8} Torr, respectively, by diffusion pump and turbo pump. The operating pressure during the experiment was 1.0×10^{-5} Torr in the main chamber and 1.0×10^{-6} Torr in the tube, respectively. Under this experimental condition, a collision-free condition was maintained, consequently, the secondary gas-phase reactions were avoided.

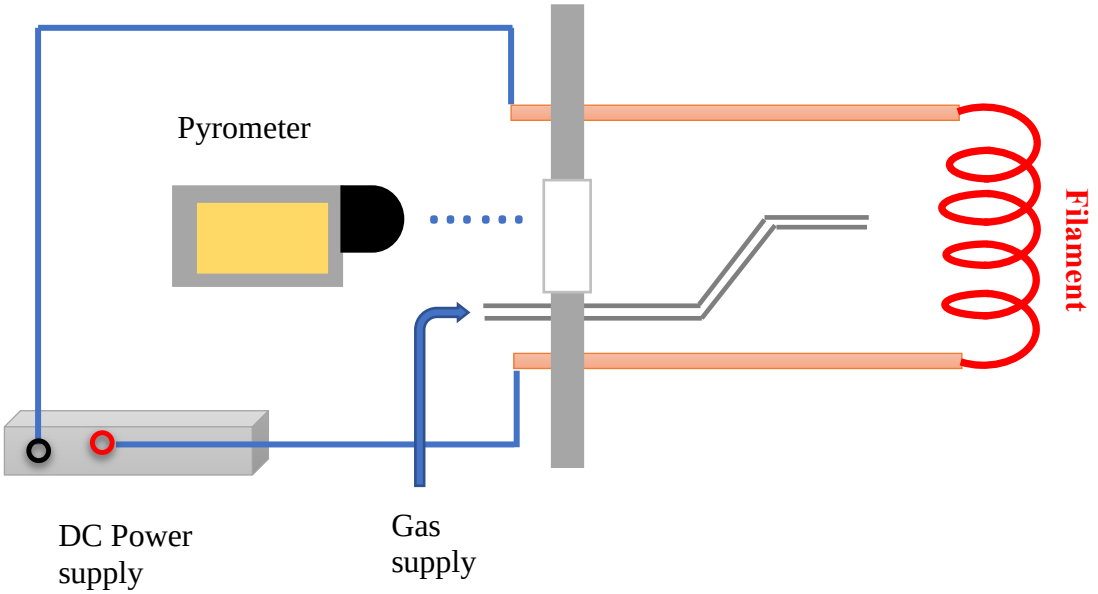

Figure 2-2: A collision-free HWCVD source for detection of direct hot-wire decomposition products. (Adapted with permission from American Chemical Society, Account of Chemical Research journal published by American Chemical Society)

2.2.2 A HWCVD Reactor Setup to Detect Species from Secondary Gas-phase Reactions

For the detection of chemical species formed from the secondary gas-phase reactions, a HWCVD reactor, made of a cylindrical tube of an inner diameter of 15 cm, was attached to the main chamber. The reactor and the main chamber were connected through a pin-hole (0.15 mm diameter) drilled in the bottom plate of the reactor as shown in Figure 2-3. The distance between the filament and the pin-hole was set at 5 cm. This is the typical distance between the filament and the substrate for the thin film deposition. The pressure in the reactor was maintained at 12 Torr using a mass flow controller (MKS, 1179A) and was monitored by a capacitance manometer (MKS Baratron, type 626A).

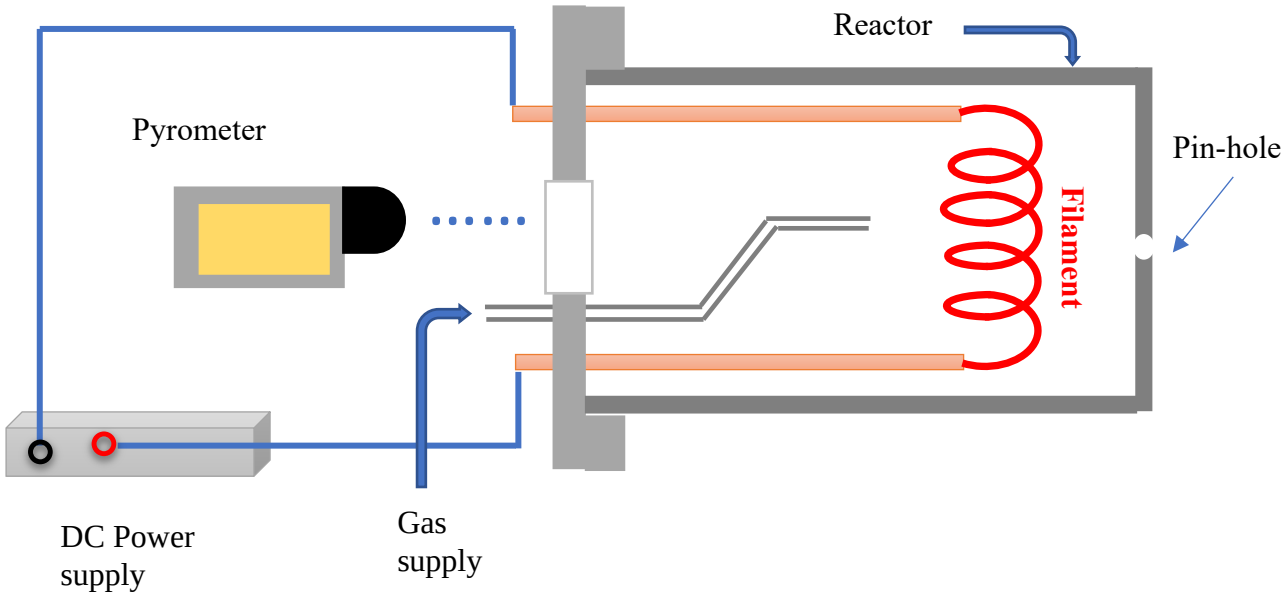

Figure 2-3: A HWCVD reactor for detection of gas-phase reaction products (Adapted with permission from American Chemical Society, Account of Chemical Research journal published by American Chemical Society)

Secondary gas-phase reactions are expected to occur under this relatively high pressure in the reactor. The products of these reactions were sampled through the pin-hole into the main chamber and the gas stream exiting the reactor formed an effusive molecular beam. As mentioned above, the operating pressures in the main chamber and the flight tube were maintained at 1.0×10^{-5} Torr and 1.0×10^{-6} Torr, respectively. Under the low pressure in the main chamber, it is expected that all further gas-phase reactions cease, hence, the detected species by TOF-MS constitute those from the gas-phase reactions in the HWCVD reactor. The TOF mass spectra were collected at different filament temperatures ranging from 900 to 2000 ^{o}C with an increment of 100 ^{o} C. At each temperature, a mass spectrum was recorded every five minutes for one hour.

2.3 Vacuum ultraviolet (VUV) Laser Single-Photon Ionization (SPI) Source

The gas-phase species from the hot-wire decomposition and the secondary reactions in the experiments were ionized by a VUV SPI source. SPI uses a single photon of sufficient energy to ionize the target species, but low enough to avoid fragmentation for most species. SPI can detect multiple species at one time, as long as their ionization energies are below the photon energy.[71] In this work, a 118 nm laser radiation (10.5 eV), produced by non-resonant frequency tripling of 355 nm UV output from a commercial Nd-YAG laser (Spectra-Physics, LAB-170-10) operating at a 10 Hz repetitive rate, was used to ionize species directly from the hot-wire decomposition and from the secondary gas-phase reactions. The 355 nm output was attenuated to a constant energy of 25 mJ per pulse by the combination of a half-wave plate and Glan laser polarizer. The laser was then focused into the Ar/Xe gas cell by a quartz lens (f = 20 cm). The gas cell was filled with 210 Torr of 10:1 Ar:Xe gas mixture (> 99.5%, Praxair). This pressure was found to be the optimum pressure to produce the maximum intensity of VUV radiation.[90, 91]

A lithium fluoride (LiF) lens was inserted into the optical path after the gas cell to focus the 118 nm VUV light directly into the center of the space between the repeller plate and extraction grid in the TOF ion optics, while the 355 nm UV beam is caused to diverge away from the 118 nm beam after passing through the lens due to the different refractive indices of the LiF lens for 118 nm and 355 nm light, as illustrated in the Figure 2-4. Multiphoton ionization by the 355 nm UV light is thus minimized.

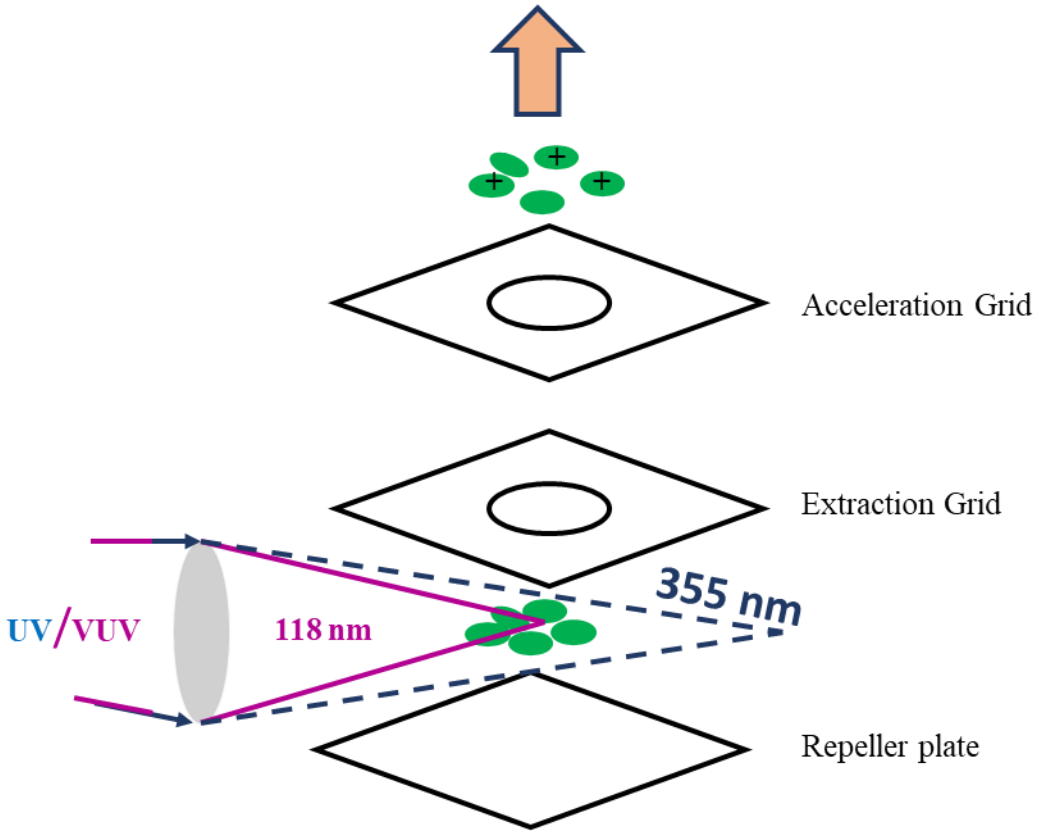

Figure 2-4: A schematic diagram of the single photon ionization (SPI) source (Adapted with permission from American Chemical Society, Account of Chemical Research journal published by American Chemical Society)

2.4 Time-of-flight Mass Spectra Collection

In this work, the TOF mass spectrometer used is of Wiley-McLaren design.[92] The design consists of an ionization region with modest electric field strength and an acceleration region with significantly stronger field strength. As illustrated in Figure 2-5, partition of these regions is defined by three metal plates: the repeller plate, the extraction grid, and the acceleration grid. The ionization region and the acceleration region experience field strength of E_s and $E_{d,}$ respectively. The drift region of length D is field

free. The distance between the repeller plate and extraction is S_o, and the one between extraction grid and the acceleration is d.

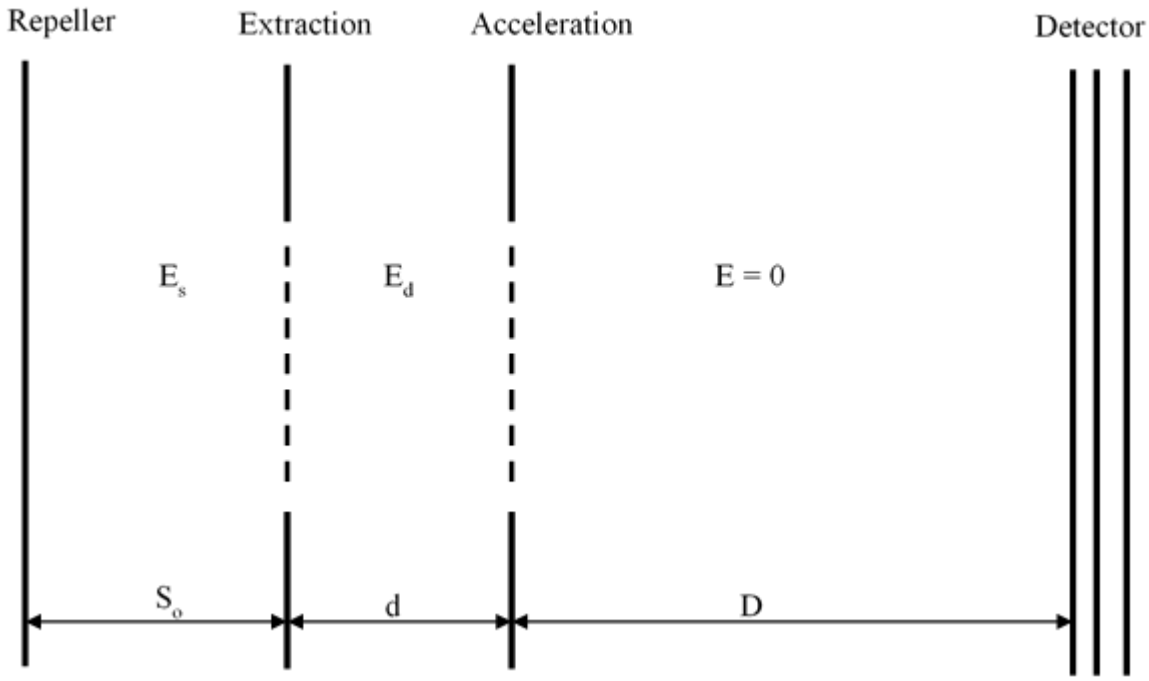

Figure 2-5: A schematic diagram of the Wiley-McLaren TOF mass spectrometer with a two-stage ion extraction optics configuration

Wiley and McLaren have shown that the location at which maximum resolution can be obtained is described by Equation (2-1).[92]

$$D = 2s_o k_o^{3/2}\left(1 - \frac{1}{k_o + k_o^{1/2}s}\frac{d}{s_o}\right) \qquad (2\text{-}1)$$

Where k_o is defined by

$$k_o = \frac{s_o + dE_d}{s_o E_d} \tag{2-2}$$

The values for E_s and E_d must be determined experimentally. The drift region D was fixed at 1 m. The distance between plates was 1.27 cm for both E_s and E_d regions. In this work the optimal values were found to be at E_s = 196 V cm^{-1} and E_d = 2182 V cm^{-1}, which corresponds to a repeller voltage of 3020 V and an extraction grid voltage of 2771 V. The acceleration grid is grounded. Ions produced from the VUV SPI source were detected by a microchannel plate (MCP) detector at the end of the flight tube by first extracting the ion from the ionization region by the electric field between the repeller plate and extraction grid and then accelerated into the field-free drift region of the TOF MS. Signals were pre-amplified using a pre-amplifier (Stanford Research Systems, SR 445A) and displayed on a 300 MHz digital oscilloscope (Tektronics, TDS 3032B).

Signals were averaged over 512 laser pulses before being saved into a computer using E-scope. The TOF Mass spectra collected initially from the computer were in the format of signal intensity versus time-of-flight. A conversion from the time-of-flight values to mass-to-charge ratio (m/z) was obtained by using chemical(s) with known m/z values and their corresponding time-of-flight. The calibration was achieved by fitting the known data to the following Equation (2-3).

$$\left(m/z\right)^{1/2} = At + B \tag{2-3}$$

where A and B are the slope and y-intercept from the linear fit, respectively.

Under collision-free conditions, the filament was etched between each run of the experiments by heating the filament to 2000 ^oC for two hours using 10% of H_2 in He

mixture under a total pressure of 1×10^{-5} Torr. This procedure ensures the cleanness of the filament surface. Three runs of 0.9 % HMDSZ/He were studied at a filament temperature range of 900 - 2400 ^{o} C at an increment of 100 ^{o}C.

2.5 Synthesis of bis(trimethylsilyl)-N-deuterioamine

To confirm the mechanism proposed for the primary decomposition and secondary gas-phase reactions of HMDSZ, two isotopomers, *i.e*., bis(trimethylsilyl)-N-deuterioamine (HMDSZ-d1, $(CH_3)_3SiNDSi(CH_3)_3$) and 1,1,1,3,3,3-hexa(deuterated methyl)disilazane (HMDSZ-d18,$(CD_3)_3SiNHSi(CD_3)_3$), were used. HMDSZ-d18 was purchased from CDN isotopes (> 98 %) and used without further purification. The HMDSZ-d1 isotopomer is not commercially available. It was synthesized following the method described by Sauer et al,[93] where trimethylchlorosilane (TMCS) reacted with deuterated ammonia.

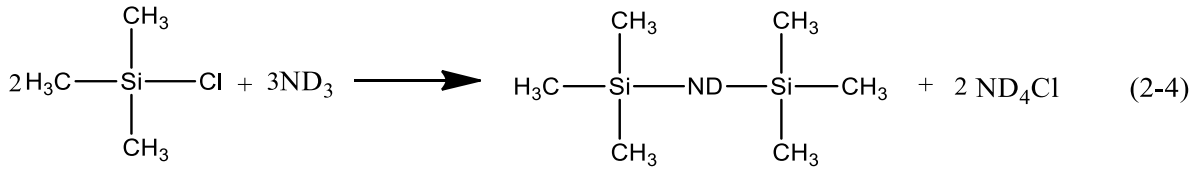

(2-4)

Specifically, a solution of 24 ml of trimethylchlorosilane (≥ 98.0 %, Sigma Aldrich) in 60 ml of anhydrous ether (≥ 99.0 %, VWR) was placed in 100 ml round-bottom flask. The round bottom flask was placed in a pressurized vessel with an inlet tube connected to deuterated ammonia (ND_3) cylinder. The pressurized vessel was mounted on hot plate at 45 ^{o}C with a stirring speed of 500 rpm. Ammonia was introduced under a pressure of 80 psi. The system was heated for three hours and allowed to stir overnight. A white precipitate (NH_4Cl) was observed after the reaction. The white precipitate was allowed to

settle, and the solution was decanted and filtered. The filtrate was then distilled in a mineral oil bath to remove the ether from the combined extracts, giving 5.799 g of HMDSZ-d1 (38% yield). The experimental apparatus for the synthesis is shown in Figure 2-6.

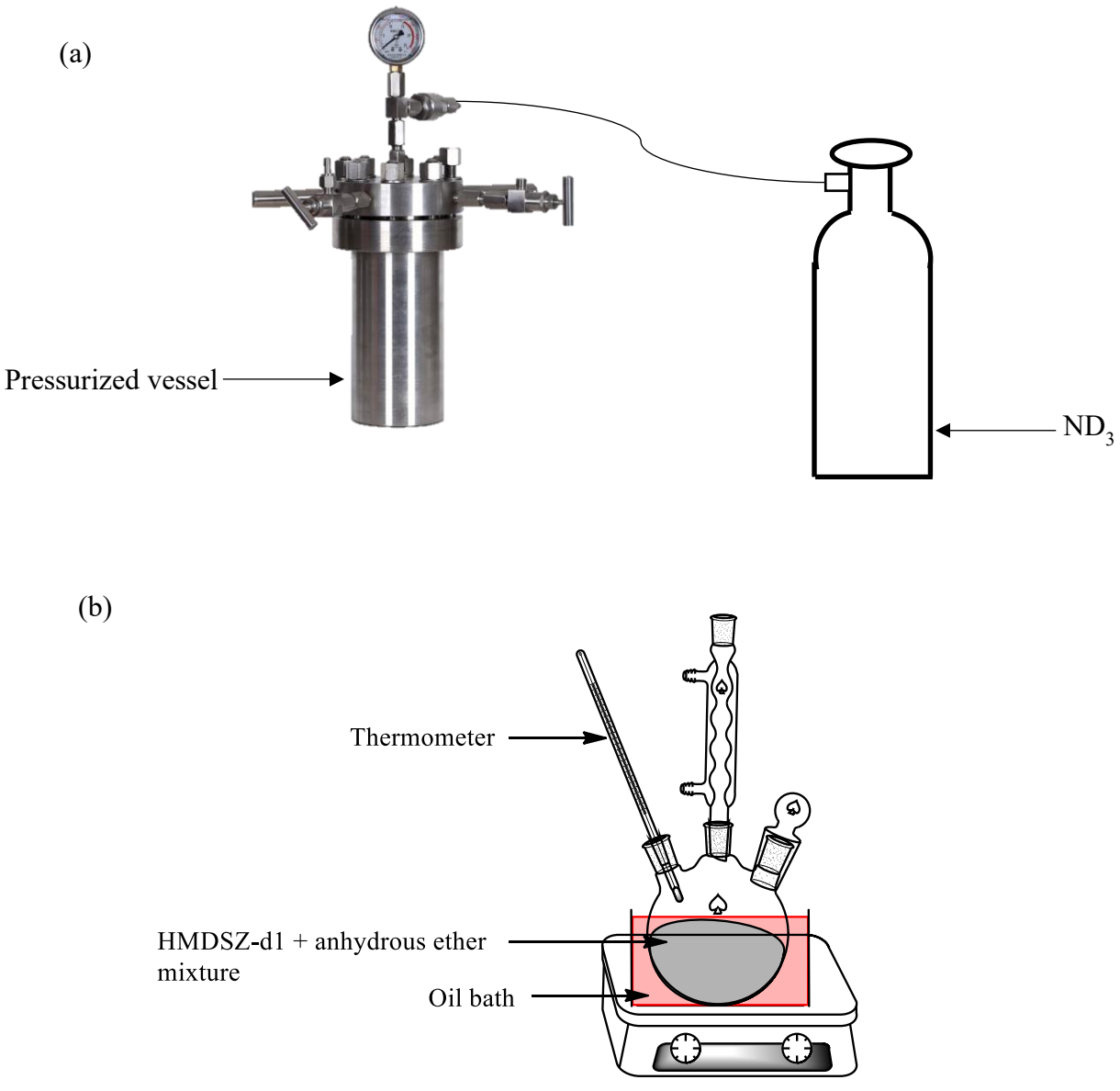

Figure 2-6: Reaction setup to synthesize HMDSZ-d_1 including (a) pressurization of reaction mixture (b) distillation to obtain HMDSZ-d1

2.6 Sample Preparation and Introduction

1,1,1,3,3,3-hexamethyldisilazane (HMDSZ) (≥ 99 %, Sigma Aldrich) was used in this work without further purification. Diluted gaseous samples of HMDSZ was prepared by mixing their room-temperature vapor with helium (99.999%, Praxair) after degassing their liquid sample through several cycles of 'freeze-pump-thaw'. For example, 0.9% HMDSZ in He was prepared by first introducing 14 Torr of HMDSZ vapor into a 2.25 L stainless steel cylinder, followed by balancing the pressure to 200 kPa with helium. To confirm the proposed mechanism, 0.9% HMDSZ-d18, and 0.9% HMDSZ-d1 mixtures were also prepared in a 2.25 L sample cylinder. Prior to each preparation, the introduction manifold was pumped for at least one hour. The introduction manifold was then purged with high-pressure helium for at least three times.

Due to the moisture-sensitive nature of HMDSZ, a protocol of transferring HMDSZ into our liquid sample holder has been developed to avoid its exposure to air. For this, the sample holder and the cannula were washed with acetone thoroughly for three times to clean it from any previously used chemicals. The sample holder and the cannula were baked at 120 ^{o}C for one hour to remove any moisture and allowed to cool down to room temperature. The sample holder was capped immediately and closed firmly. The chemical was transferred into the sample holder via cannula transfer after the sample holder has been pumped to a vacuum and purged with argon. The pumping and argon filling were repeated at least twice with each lasting for ten minutes. At this point, the chemical is transferred to the holder which is now filled with argon as shown in Figure 2-7.

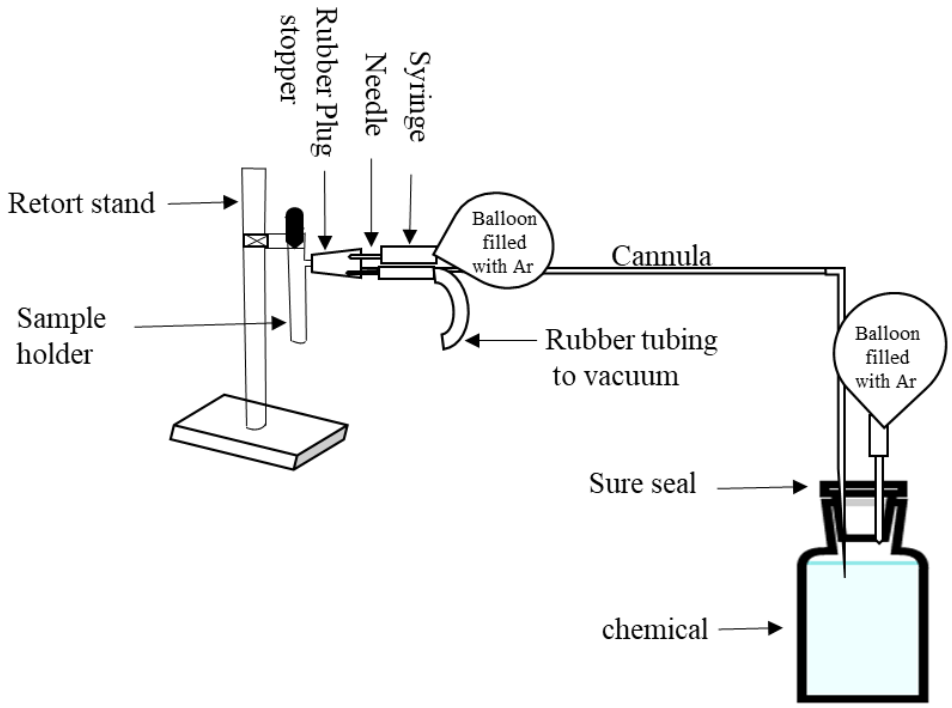

Figure 2-7: A schematic of the setup for transferring chemical into sample holder

2.7 Computational Methods

In this thesis, *ab initio* calculations were performed to study the homolytic, stepwise and concerted decomposition pathways of HMDSZ. For the theoretical calculations in this work, the density functional theory (DFT) method with the Becke, 3-parameter, Lee-Yang-Parr (B3LYP) functionals [94, 95] and the coupled cluster method with single, double and perturbative triple excitations (CCSD(T))[96] were used. The B3LYP hybrid functional has emanated as a good compromise between computational cost, coverage and accuracy of results.[97] This functional provides good results in predicting the structures of silylamines.[98, 99] CCSD(T) is a 'golden method' and elegant approach to computing single point energies. Geometry optimization and vibrational frequency calculations of the minimum-energy structures of the reactants, intermediates, and products involved in

this study were performed at the B3LYP/6-311++G(d,p) level of theory. All intermediates involved in this work were minima in their singlet state unless stated otherwise. The transition states were located by performing a TS search followed by geometry optimization and vibration frequency calculation. All the TSs were confirmed to have only one imaginary frequency as per the criteria. The hard-to-find TSs were located by exploring the potential energy surface (PES) along the expected reaction coordinate, which was followed by TS optimization for the highest point at the PES.

Each TS was verified by performing intrinsic reactions coordinate (IRC) to confirm that it connects the two desired minima. Single-point energies (SPE) were calculated at the CCSD(T)/6-311++G(d,p) level of theory. The full notation for the calculation method used in this work is thus CCSD(T)/6-311++G(d,p)//B3LYP/6-311++G(d,p). Zero-point energies (ZPE) were determined at the B3LYP/6-311++G(d,p) level of theory and were scaled by a factor of 0.9806, as proposed by Scott and Radom.[100] The enthalpies at 298 K (H_{298}) were obtained by adding the quantity (H_{298}-H_0) to the enthalpies at 0 K (H_0). The quantity (H_{298}-H_0) was calculated by subtracting the unscaled ZPE from the thermal correction to enthalpy. Gibbs free energies at 298 K (G_{298}) were obtained in a similar way using thermal correction to the Gibbs free energy. Entropy at 298 K (S_{298}) was computed from values of enthalpy and Gibbs free energy at 298 K. The activation enthalpy ($\Delta H^{\ddagger}$) and activation Gibbs free energy ($\Delta G^{\ddagger}$) were determined by computing the difference between the $H^{\ddagger}$ or $G^{\ddagger}$ for the reactant and those of the transition state. The activation entropies ($\Delta S^{\ddagger}$) was computed by dividing the quantity ($\Delta H^{\ddagger}$-$\Delta G^{\ddagger}$) by temperature. The reaction enthalpies (ΔH), reaction Gibbs free energies (ΔG), and reaction entropies (ΔS)

were determined similarly using *H*, *G*, and *S* of the reactants and products. All computations in this work were performed using Gaussian 16 program.[101]

Chapter Three: Decomposition of 1,1,1,3,3,3-Hexamethyldisilazane on Hot Tungsten and Tantalum Surfaces

3.1 Motivation

1,1,1,3,3,3-Hexamethyldisilazane (HMDSZ), a methyl-substituted disilazane molecule, has been used extensively as a single-source precursor in various CVD processes to form silicon carbonitride (SiC_yN_z) thin films.[102-108] As mentioned in Chapter 1, HMDSZ has been used as a source gas in HWCVD to fabricate SiC_yN_z.[61, 89] Among the two methyl-substituted disilazanes (HMDSZ and tetramethyldisilazne, TMDSZ), TMDSZ has been found to have higher deposition rate compared to HMDSZ. The higher deposition rate is attributed to the presence of Si-H bonds in the structure of TMDSZ. Also, addition of NH_3 (as source of nitrogen) to methyl-substituted disilazane molecules controls the composition of the deposited SiC_yN_z thin film. Despite these studies, radical formation and detection of gas-phase chemical species with HMDSZ have received less attention. Stelzner *et al.*[109] detected $(CH_3)_3SiNH\dot{S}i(CH_3)_2$ and $\dot{C}H_3$ as the two primary products from the first fragmentation step in plasma-enhanced CVD of silicon carbonitride thin films using HMDSZ as the single-source precursor. The activation energy for the methyl production was not determined in their work.

Recently, the Shi group has explored the gas-phase reaction chemistry of two-types of organosilicon molecules, namely open-chain alkylsilanes and four-membered-ring (di)silacylcobutanes.[110] The formation of methyl radical has been found to be the common step in the primary decomposition of methyl-substituted silanes[111] and methyl-substituted (di)silacylcobutanes[82, 83, 85] on the W or Ta filaments. The activation energy has been determined for the methyl formation in all the above-mentioned precursors. The

role of methyl radical in the deposition of SiC_yN_z thin films is uncertain, but previous studies in the Shi group on the gas-phase reaction chemistry using organosilicon compounds[24, 83, 85, 112] in HWCVD have shown that the formation of methyl radical from hot-wire decomposition initiates a short chain reaction in the gas phase.

Recently, Shi and coworkers[113] studied the catalytic dissociation of tris(dimethylamino)silane ($(N(CH_3)_2)_3SiH$), a dimethylamino-substituted silane molecule, on hot W and Ta filaments. They observed the formation of methyl radical using the 10.5 eV VUV laser SPI mass spectrometry, suggesting the dissociation of N-CH_3 bond on the hot filaments. The authors determined the activation energy for the production of methyl radical to be in the range of 47.4 ± 6.7 to 81.0 ± 9.9 kJ mol^{-1}, depending on the filament material and temperature. Tris(dimethylamino)silane is a N-containing organosilicon molecule lacking a direct Si-C bond. It will be interesting to examine a N-containing organosilicon molecule that has a direct Si-C bond, such as HMDSZ.

As a base, the use of only HMDSZ as source gas was examined experimentally in this work using HWCVD sources to identify the gas-phase species responsible for the SiC_yN_z film growth. In this Chapter, a systematic study on the decomposition chemistry of HMDSZ on W and Ta filament surfaces is reported. The decomposition products were detected with the 118 nm (10.5 eV) VUV laser SPI coupled with time-of-flight mass spectrometer (TOF MS). The operating pressure was maintained at 1×10^{-5} Torr to ensure collision-free conditions to allow the detection of species produced directly form hot-wire decomposition of HMDSZ. The intensity profile of any decomposition product at different temperatures were explored for the study of the effect of filament temperature on their production. From the Arrhenius plot in the temperature-dependent rise of these

products, the apparent activation energies could be determined. The effect of filament material on the decomposition chemistry was also examined. A theoretical investigation using *ab initio* calculations of the concerted and stepwise decomposition of HMDSZ along with the homolytic cleavage of Si-C bond were also explored. The results obtained from the experimental study were compared with those determined theoretically.

3.2 Room-temperature VUV Single-photon Ionization Mass Spectra of HMDSZ

HMDSZ is extremely sensitive to moisture and care needs to be taken in handling the chemical. The room-temperature mass spectrum of HMDSZ after using the developed protocol of transferring moisture-sensitive chemicals as shown in Section 2.6, was recorded using SPI with the VUV photon of 10.5 eV (λ = 118 nm) when the filament was off. As shown in Figure 3-1, the mass spectrum is dominated by a photofragment ion peak at m/z 146 ($C_5H_{16}Si_2N^{+\cdot}$, base peak) and the parent ion peak at m/z 161 (34.8 ± 6.2% to the base peak). The isotope peaks of the parent ion at m/z 161 originating the ^{29}Si, ^{30}Si, and ^{13}C were observed at 162 (22.2 ± 4.4%) and 163 (9.8 ± 3.5%), respectively. The percentage intensities of the isotope peaks are relative to the parent ion intensity at m/z 161. Other main peaks are observed from Figure 3-1 at m/z 4, 74 and 89, with the peak at m/z 4 from He^+. From the enlarged mass spectrum shown in the inset, other weak peaks can also be seen at m/z 75, 90, 108, and 110.

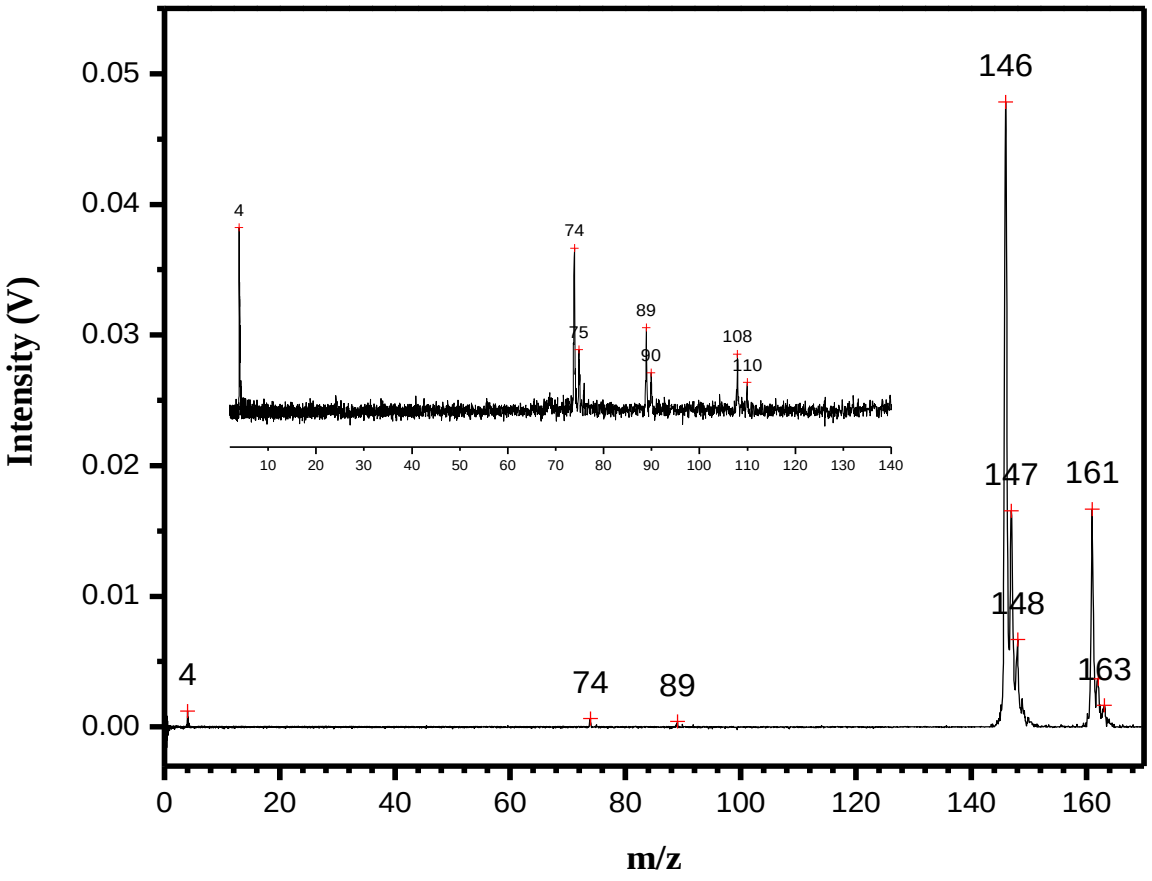

Figure 3-1: Room-temperature 10.5 eV single-photon ionization TOF mass spectrum of 0.9 % HMDSZ/He. The inset is an enlarged picture in the mass region of 0-140 amu

Tamas *et al.*[114] reported the mass spectrometric study of electron impact-induced fragmentation of HMDSZ. They showed that the primary fragmentation pathway was the loss of CH_3 radical, leading to the formation of $(CH_3)_3SiNHSi(CH_3)_2^{+\cdot}$ with m/z 146 From this ion, the main process of further fragmentation is the elimination of methane molecule to form a fragment ion of $CH_3)_2Si\text{-}N{=}Si(CH_3)_2^{+\cdot}$ with m/z 130. They found that the $CH_3)_2Si\text{-}N{=}Si(CH_3)_2^{+\cdot}$ (m/z 130) arising from this process was stable and its fragmentation only took place weakly which involved the elimination of NH_3 to form a

fragment ion of $C_4H_9Si_2^{+\cdot}$ at m/z 113. Figure 3-2 shows a 70 eV mass spectrum from NIST Chemistry WebBook, which showed the fragment ion peaks at m/z 146, 130, and 73. A comparison of the 10.5 eV SPI mass spectrum shown in Figure 3-1 and the 70-eV EI mass spectrum in Figure 3-2 showed that the parent ion (m/z 161) intensity was significantly enhanced using 10.5 eV SPI. Furthermore, only the main fragment ion of $(CH_3)_3SiNHSi(CH_3)_2^{+\cdot}$ (m/z 146) was observed in Figure 3-1, with all other known fragment ions from HMDSZ absent. The above two observations provides support that 10.5 eV VUV SPI is a "soft" ionization source.[115, 116]

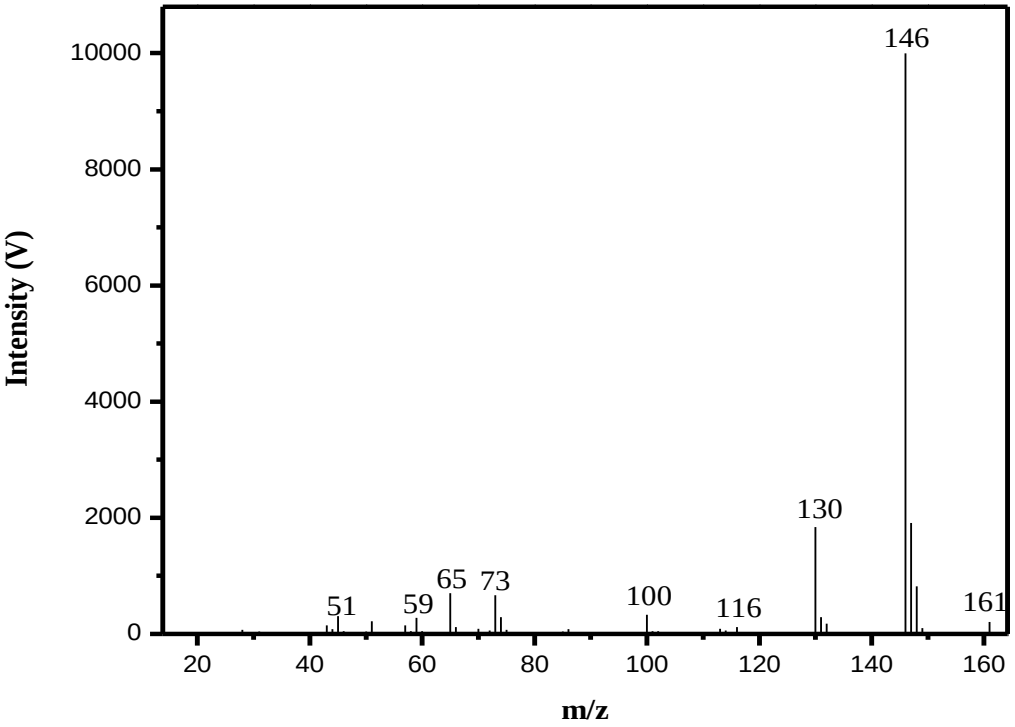

Figure 3-2: Room-temperature 70 eV mass spectrum of HMDSZ showing the main fragment peaks (Adapted from NIST Chemistry WebBook)

The two weak peaks at m/z 74 and 89 in Figure 3-1 were believed to come from the hydrolysis products of HMDSZ. Gas chromatography-mass spectrometry (GC-MS)

analysis of contaminated HMDSZ samples exposed to the air showed the existence of both hexamethyldisiloxane (HMDSO) and trimethylsilanol (TriMSO) (See Appendix A). HMDSO and TriMSO are the products of HMDSZ with water, as illustrated in Equations (3-1) and (3-2).

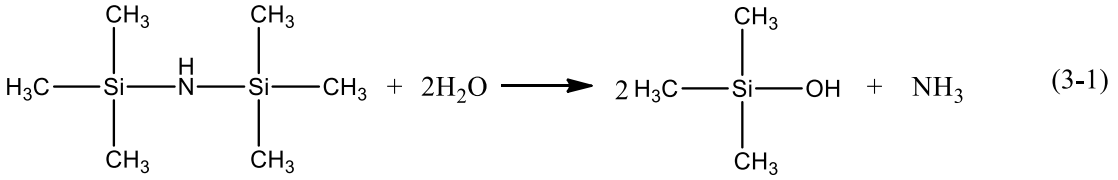

HMDSZ

trimethylsilanol (TriMSO)
(90 amu)

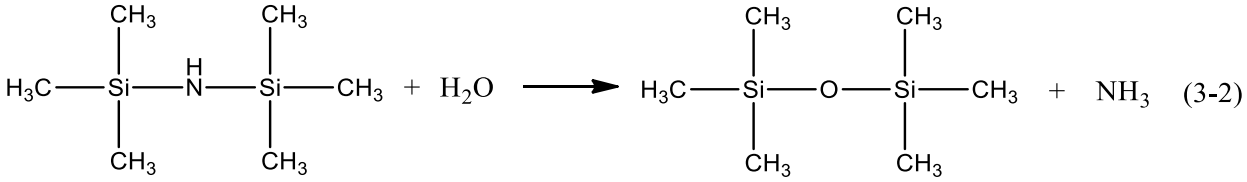

HMDSZ

hexamethyldisiloxane (HMDSO)
(162 amu)

Figure 3-3 shows a room-temperature mass spectrum of HMDSZ with contamination of hydrolysis products recorded with the 10.5 eV SPI source. The mass peak from HMDSO are represented by its molecular ion peak at m/z 162 and the fragment ion peak at m/z 147. These two peaks overlap with the isotope peaks of the molecular ion of HMDSZ and its fragment ion at m/z 146. Therefore, an increased intensity ratio of I(m/z 147)/I(m/z 146) and I(m/z 162)/I(m/z 161) is a strong indication that HMDSO (from the reaction of HMDSZ and H_2O) is present. According to the theoretical calculations, the

isotopic contributions from m/z 147 and 162 to the ones at m/z 146 and 161 from HMDSZ are 16.5% and 17.6%, respectively. The TOF mass spectrum of hydrolyzed HMDSZ using the 10.5 eV VUV SPI showed an increase in the intensity ratio of I(m/z 147)/I(m/z 146) and I(m/z 162)/I(m/z 161) to 81.0% and 41.1%, respectively.

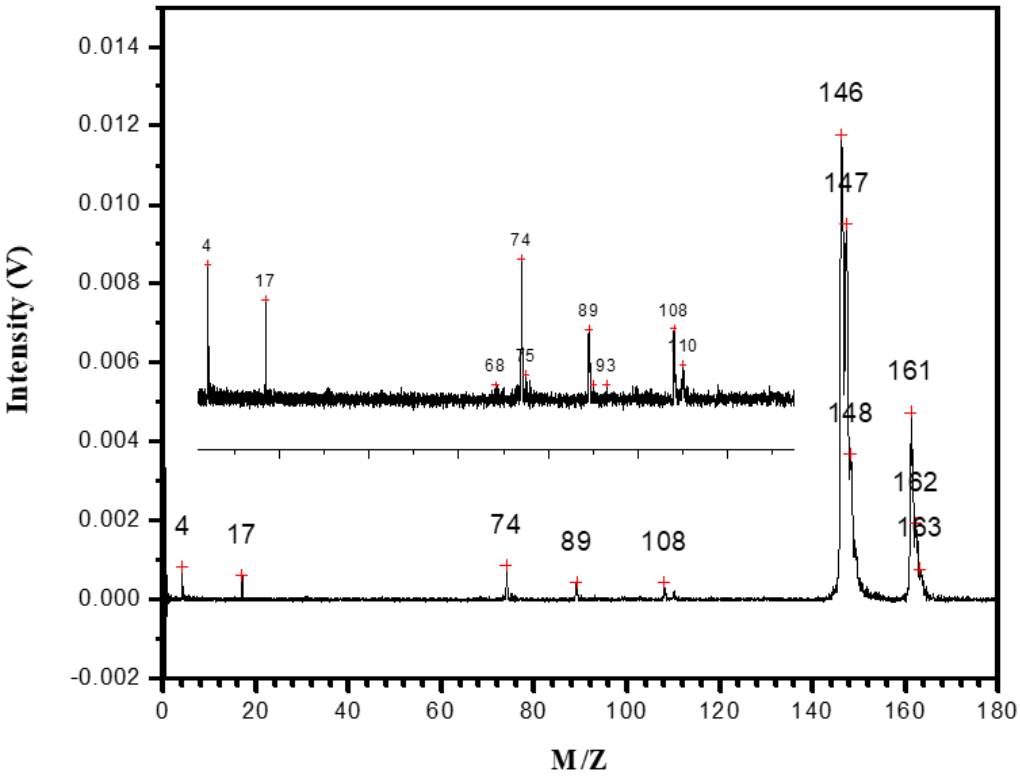

Figure 3-3: Room-temperature 10.5 eV single-photon ionization TOF mass spectrum of 0.9 % HMDSZ/He with contamination of hydrolysis products. The inset is an enlarged picture in the mass region of 0-140 amu

In addition, the peaks at m/z 17, 74, and 89 are also found to come with the formation of HMDSO as shown in Figure 3-3. The peak at m/z 89 is attributed to trimethylamine ($(CH_3)_3SiNH_2^+$), formed from the partial hydrolysis of HMDSZ as shown in Equation (3-3). The peak at m/z 74 ($(CH_3)_2SiNH_2^+$) is believed to be a photofragment ion from the

peak at m/z 89. Peak at m/z 17 is from NH_3, the other product from the hydrolysis of HMDSZ. The peaks at m/z 108 and 110 have not been assigned yet.

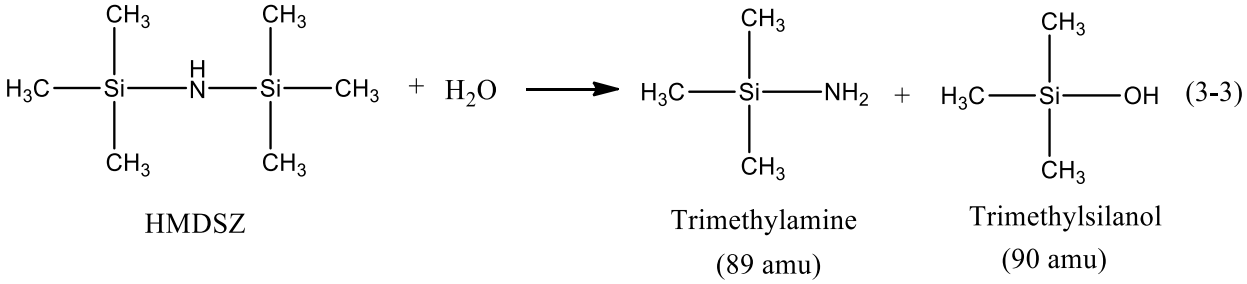

(3-3)

3.3 Primary Decomposition of HMDSZ on W

To examine the primary decomposition products of HMDSZ on W filaments, mass spectra were collected at different W filament temperatures ranging from 900 - 2400 ^{o}C at an increment of 100 ^{o}C for a mixture of HMDSZ/He. Figure 3-4 shows the mass spectra in the mass region of 2-28 amu for the temperature range of 1200 – 2400 ^{o}C. As can be seen from Figure 3-4, mass peak at m/z 15 was very weak at low filament temperatures and started to show increases in intensity with increasing filament temperature at high filament temperatures. The peak at m/z 15 should come from the methyl radical, produced by the breakage of Si-CH_3 bond connection in the HMDSZ molecule. In Figure 3-5 (a) and (b), the distribution of the bare intensity and the normalised intensity of $^{+}CH_3$ as a function of filament temperature for HMDSZ is shown respectively. The normalised intensity is achieved by multiplying the intensity of $^{+}CH_3$ at one specific temperature by the ratio of the intensity of the parent ion peak at room temperature to that at the same temperature. The $^{+}CH_3$ radical intensity is relatively constant from 900 ^{o}C to 1700 ^{o}C,and shows an increase from 1800 ^{o}C. The intensity keeps increasing with temperature to 2400 ^{o}C, the highest temperature tested in this

work. This increase in intensity indicates that a decomposition path exists to cleave the Si-CH_3 bond on the W filament. This observation further confirms that HMDSZ, a methyl-substituted disilazane molecule, decomposes on heated W filament to produce methyl radicals as shown in the Equation (3-4). This is in good agreement with the results from the work of Stelzner *et al.*[109] who detected $(CH_3)_3SiNHSi(CH_3)_2$ and CH_3 as the two primary products from the first fragmentation step in plasma-enhanced CVD of silicon carbonitride thin films using HMDSZ as the single-source precursor.

$$((CH_3)_3Si)_2NH \longrightarrow (CH_3)_3SiNH\dot{S}i(CH_3)_2 + \dot{C}H_3 \qquad (3\text{-}3)$$

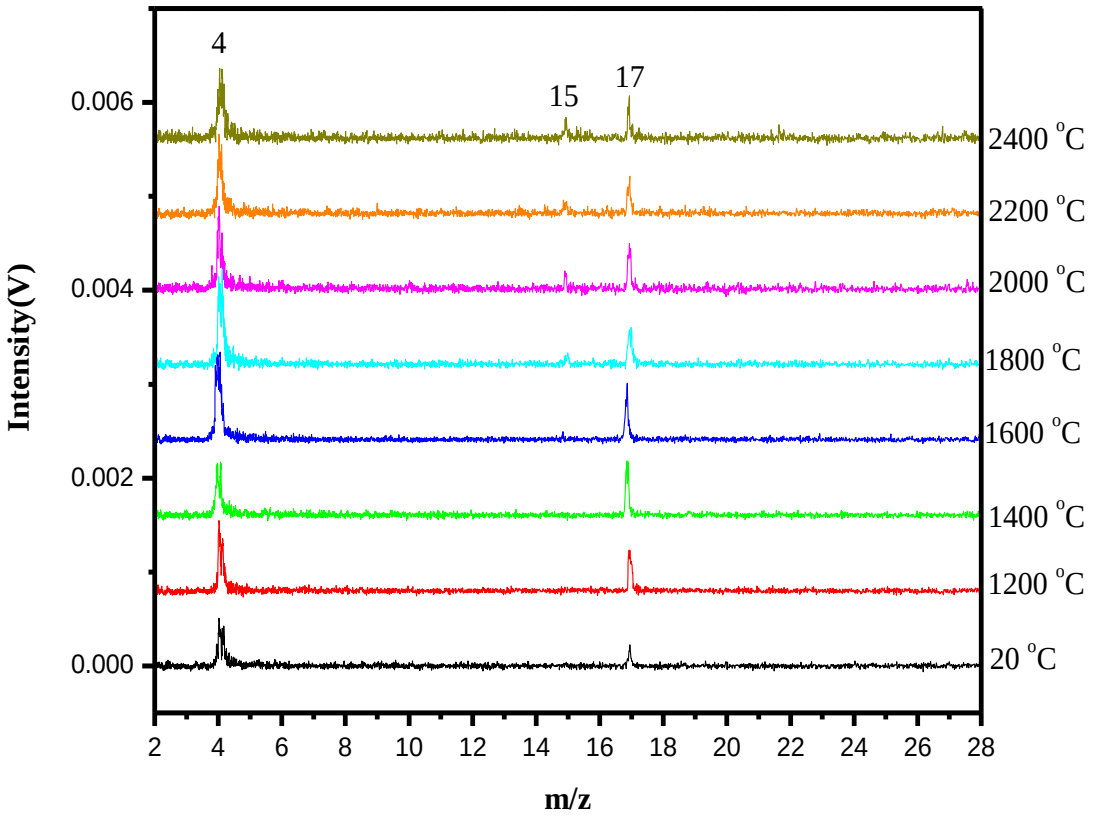

Figure 3-4: 10.5 eV single-photon ionization TOF mass spectra of HMDSZ in the mass region of 2-28 amu with W filament temperatures in the range 1200-2400 ºC at a chamber pressure of 1× 10^{-5} Torr. Room-temperature mass spectrum is also shown for comparison.

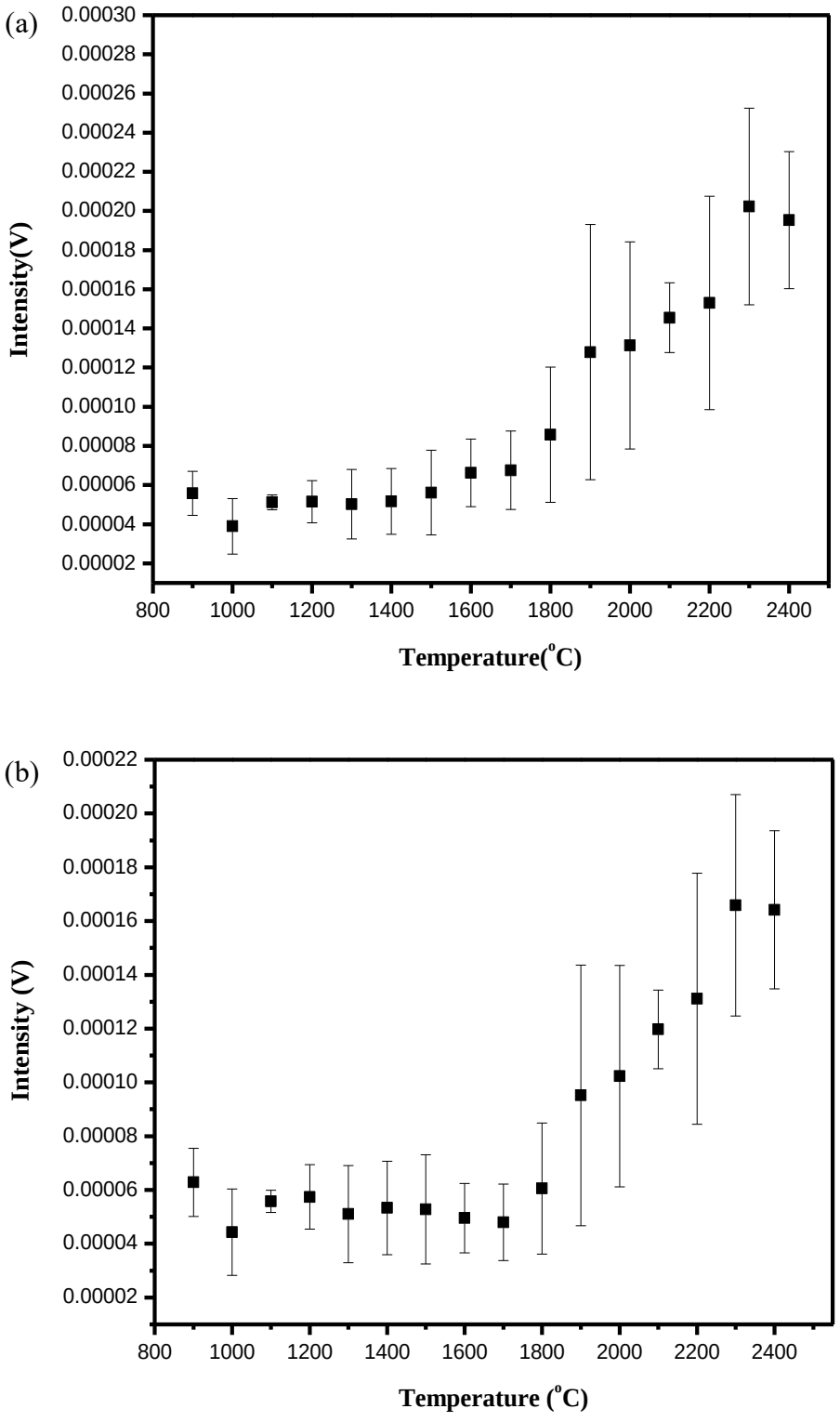

Figure 3-5: The peak intensity of (a) bare intensity of peak m/z 15 (CH_3^+), and (b) normalised intensity of peak m/z 15 (CH_3^+) as a function of filament temperature for HMDSZ on W filament at a chamber pressure of 1×10^{-5} Torr

As shown in Figure 3-5, the intensity of the methyl radical increases with increase in filament temperature in the range of 1800 - 2400 ^{o} C. This indicates that the formation of methyl radicals from the decomposition of HMDSZ on W filament is controlled by surface reactions at filament temperatures ranging from 1800 to 2400 ^{o}C. Unlike HMDSZ, tris(dimethylanino)silane[113] and other organosilicon molecules not containing N atoms, such as methyl-substituted (di)silanes[111, 117] and silacyclobutanes,[82, 83] show transition from surface reaction to mass transport regime.

The formation of methyl radical from HMDSZ follows Arrhenius behavior in the region where there is a monotonic increase. The apparent activation energy (E_a^{app}) for the formation of methyl radical was determined to be 71.2 ± 9.1 kJ/mol in the temperature range of 1700 - 2400 ^{o}C. A comparison of the determined E_a^{app} value with the energy for the homolytic cleavage of Si-CH_3 bond in HMDSZ from the theoretical calculations will be discussed later on in this Chapter.

The peak at m/z 17 (NH_3) was observed under collision-free conditions when the filament is off. The intensity ratio of m/z 17 to m/z 161 (parent ion) revealed no obvious increase with increase in temperature as shown in Figure 3-6. Therefore, it is believed that there is no contribution to the peak intensity of NH_3 from the decomposition of the HMDSZ molecule.

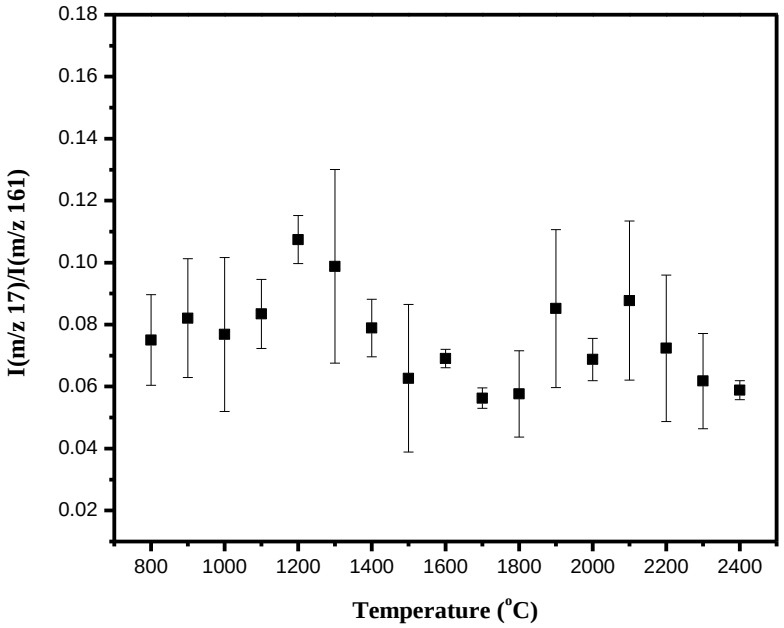

Figure 3-6: The intensity ratio of I(m/z 17)/I(m/z 161) for 0.9 %HMDSZ/He as a function of filament temperature in the range of 900 – 2400 º C. Note that the room-temperature (20 ºC) intensity was represented by the data point at 800 ºC in the figure to avoid a large empty space between 20 ºC and 900 ºC.

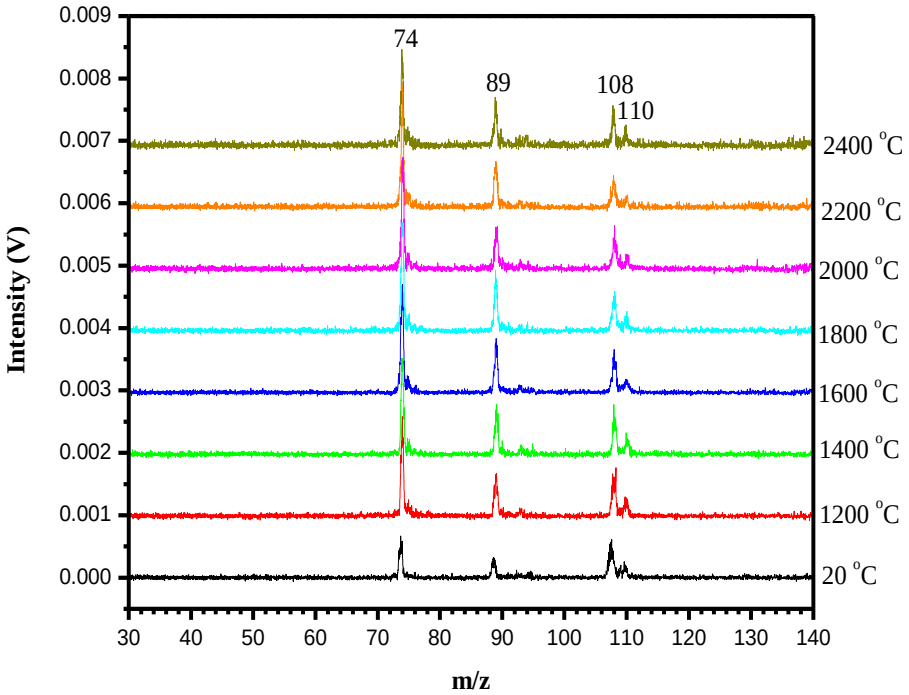

Figure 3-7: 10.5 eV single-photon ionization TOF mass spectra of HMDSZ in the mass region of 26-140 amu with W filament temperatures in the range 1200-2400 ºC at a chamber pressure of 1× 10^{-5} Torr

Figure 3-7 shows the mass spectra in the mass regions of 30 – 140 amu recorded after the filament was turned on at the temperatures of 1200 – 2400 ºC. No new mass peaks were observed in this region when the filament was turned on. In their work on the mass spectrometric studies of HWCVD processes with both HMDSZ and TrDMAS, Morimoto *et al*.[61] showed the appearance of the two peaks at m/z 74 and 89 after heating the tungsten catalyzer. They attributed these two peaks to $HSi(CH_3)_3^+$ and $(CH_3)_3SiNH_2^+$, respectively, which was produced by the surface reactions of $Si(CH_3)_3$ and $(CH_3)_3SiNH$ on chamber walls. This suggests that Si-N bond dissociation takes place on the filament surfaces to produce $Si(CH_3)_3$ and $(CH_3)_3SiNH$, although the bond dissociation energy of Si-C (338 kJ/mol) is lower than Si-N (434 kJ/mol).[61] In our experiment, the two peaks at m/z 74 and 89 were observed when the filament was off. the intensity ratios of the mass peaks at 74 and 89 to that of the parent HMDSZ ion at m/z 161 versus the filament temperatures are shown in Figure 3-8 (a) and (b), respectively. The intensity ratios did not show an obvious increase with filament temperature, indicating no contribution from the decomposition of the parent HMDSZ molecule to these two peak intensities. This suggests that no chemical species with mass of 74 amu and 89 amu, respectively, was produced from the dissociation of HMDSZ on the W filament surfaces under our experimental conditions.

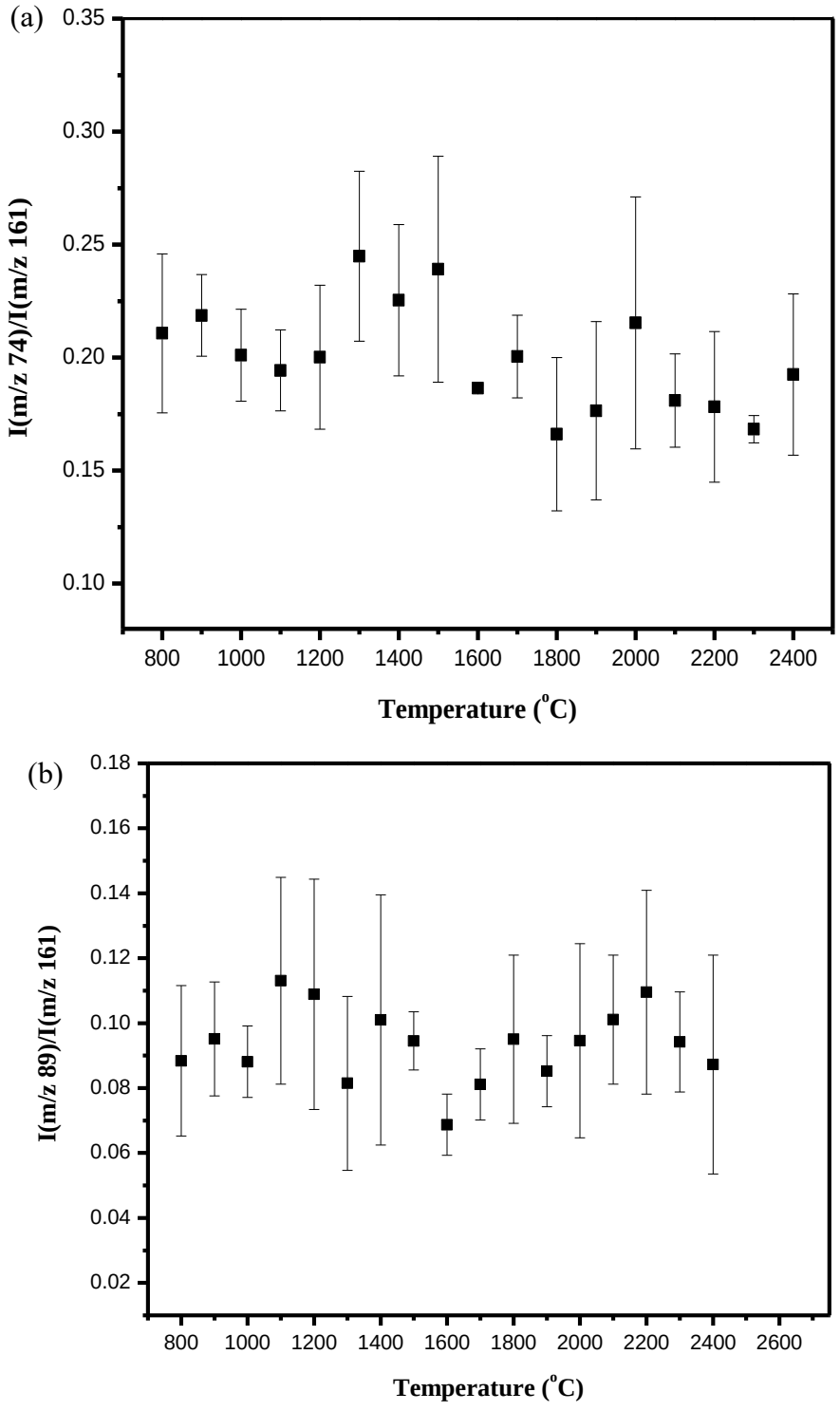

Figure 3-8: The intensity ratio of (a) I(m/z 74)/I(m/z 161), and (b) I(m/z 89)/I(m/z 161) for 0.9%HMDSZ/He as a function of filament temperature in the range of 900 – 2400 º C. Note that the room-temperature (20 ºC) intensity was represented by the data point at 800 ºC in the figure to avoid a large empty space between 20 ºC and 900 ºC.

3.4. Experiments with 1,1,1,3,3,3-hexa(deuteratedmethyl)disilazane (HMDSZ-d18) on W

In order to better understand the decomposition of HMDSZ on W and to help assign the mass peaks, experiments with the deuterated isotopomer, 1,1,1,3,3,3-hexa(deuteratedmethyl)disilazane, (HMDSZ-d18), were carried out using 10.5 eV SPI TOF MS. The room-temperature TOF mass spectrum of HMDSZ-d18 is shown in Figure 3-9, which is dominated by the peaks at m/z 161 and 179. Compared to the room-temperature mass spectrum of HMDSZ in Figure 3-1, it is clear that the mass peaks at m/z 146 and 161 are shifted to 161 and 179, respectively, when HMDSZ is replaced by HMDSZ-d18. The dominance of these two peaks is also preserved. The weak peaks at m/z 80 and 98 are the corresponding peaks for the ones at m/z 74 and 89, respectively, as appeared in Figure 3-1, the usual mass peaks that accompany the hydrolysis of HMDSZ.

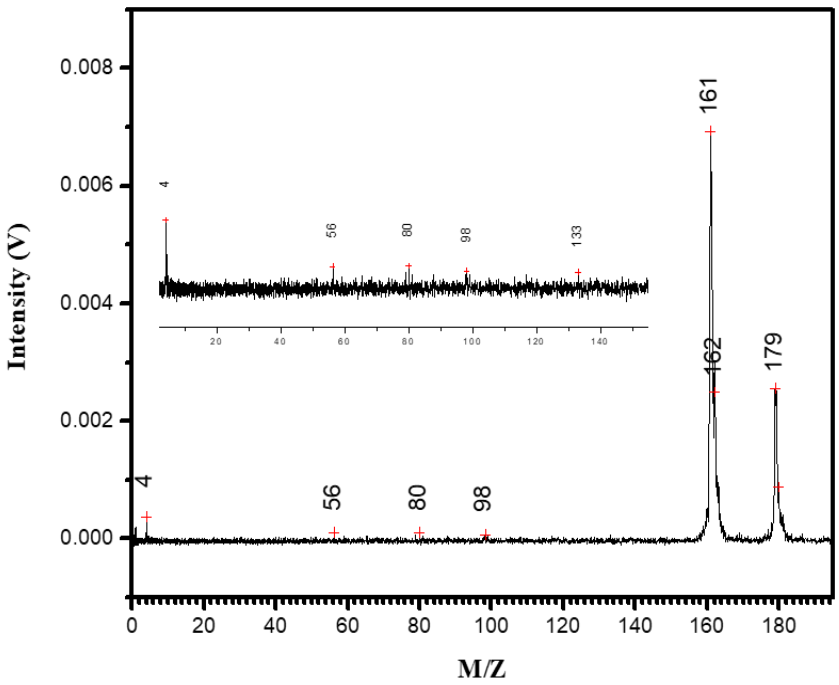

Figure 3-9: Room-temperature 10.5 eV single-photon ionization TOF mass spectrum of 0.9%HMDSZ-d_{18}/He. The inset is an enlarged picture in the mass region of 0-140 amu

Figure 3-10 shows the mass spectra for HMDSZ-d_{18} after the filament was turned on. A careful examination of the mass spectra in the low mass region revealed no presence of the peak at m/z 18 (CD_3), which is the corresponding peak at m/z 15 (CH_3) in HMDSZ. The formation of peak at 17 (NH_3), which is the by-product of the hydrolysis of HMDSZ, was observed. The observation of peak at m/z 17 with HMDSZ-d18 confirms its origin from the hydrolysis of HMDSZ since the formation of NH_3 involves the reaction of the N-H bond in HMDSZ with the hydrogen atoms in H_2O. The absence of a peak at m/z 18 (CD_3) could be due to the weak intensity as the intensity of the parent ion (HMDSZ-d_{18}) is also weak. The peaks at m/z 133 and 139, appeared after the filament was turned on when HMDSZ-d18 was used, and believed to be produced in-situ in the presence of the filament.

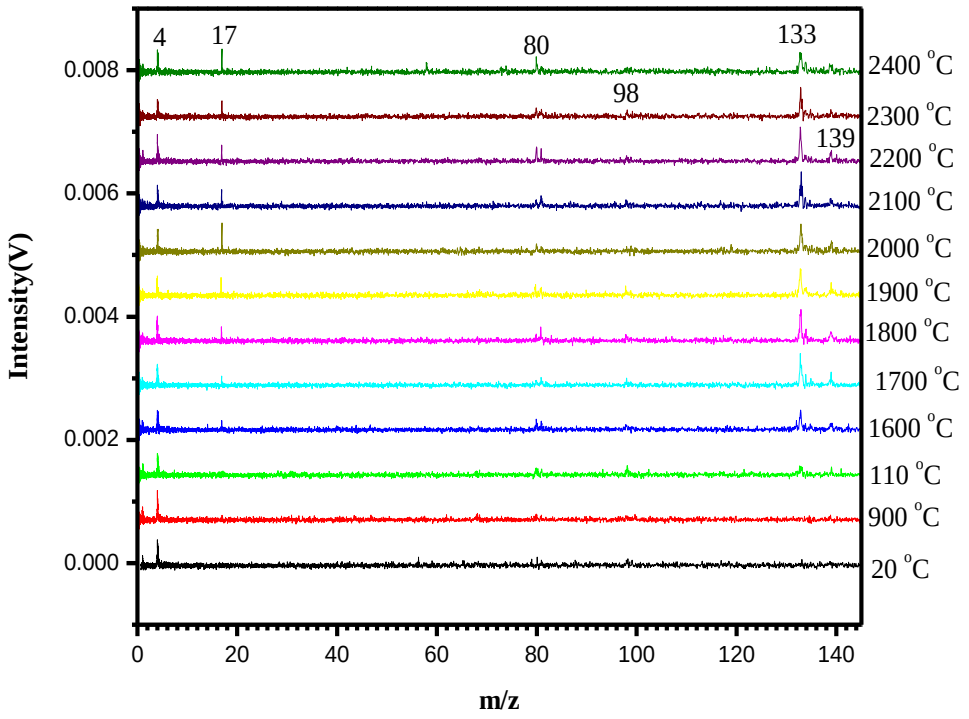

Figure 3-10: 10.5 eV VUV SPI TOF mass spectra of 0.9% HMDSZ-d_{18}/He in the mass region of 0-150 amu with W filament temperature in the range of 900 - 2000 ºC at a chamber pressure of 1× 10^{-5} Torr. Room-temperature mass spectrum is also shown for comparison.

3.5 Primary Decomposition on Ta

The mass spectra of HMDSZ after turning on a Ta filament were collected at different temperatures ranging from 900 - 2400 ^{o}C at an increment of 100 ^{o}C. The normalised intensity distribution of peak at m/z 15 as a function of filament temperature for HMDSZ is shown in Figure 3-11. The normalised intensity is achieved as described earlier. An increase in the $^{+}CH_3$ radical intensity was observed in the temperature range of 1700 - 2400 ^{o}C, which indicates that a decomposition path exists to cleave the Si-CH_3 bond on the Ta filament, producing methyl radicals.

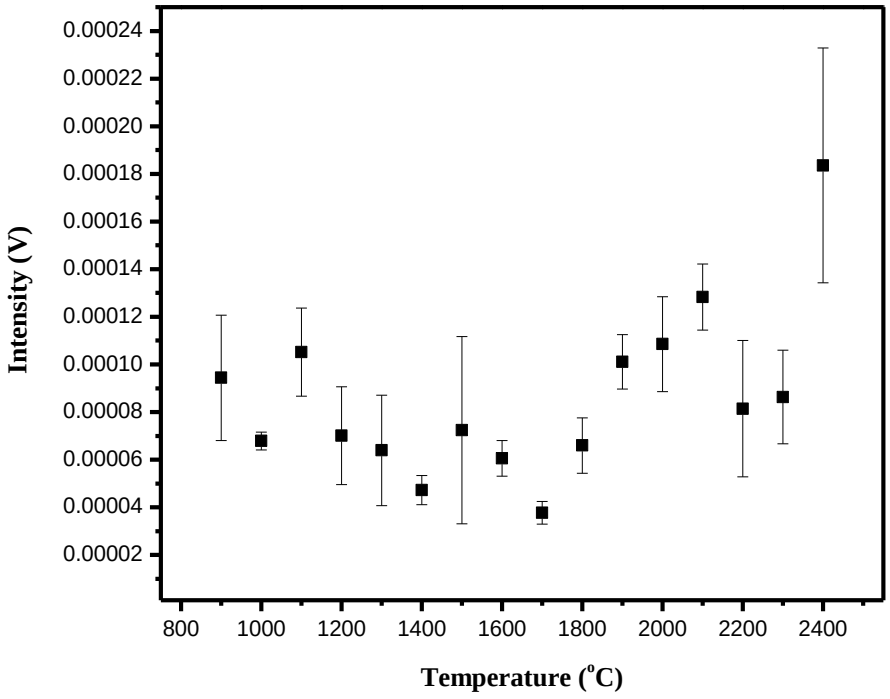

Figure 3-11: The normalised peak intensity of m/z 15 (CH_3^+) as a function of filament temperature for HMDSZ on Ta filament at a chamber pressure of 1× 10^{-5} Torr.

The apparent activation energy for the formation of methyl radical was also determined using Ta filament. The average apparent activation energy (E_a^{app}) was

determined to be 76.7 ± 8.1kJmol^{-1} in a temperature range of 1600 - 1900 ^{o}C. A comparison of the determined E_a^{app} value using Ta filament with the energy for the homolytic cleavage of Si-CH_3 bond in HMDSZ from the theoretical calculations will be discussed later on in this Chapter.

The filament material used in HWCVD process is believed to play an important role in the decomposition of the source gas.[118] Toukabri *et al*. observed that the temperature at which the gas-phase chemistry was active for MMS[80] and DMS[79] decomposition on W and Ta were different. However, the gas-phase chemistry of the two precursors were not affected by W or Ta materials. The decomposition of HMDSZ molecules were studied on two filaments, W and Ta, to understand the effect of filament material. The methyl radical intensities from the primary decomposition of HMDSZ were compared using these two filaments. The normalised intensity of the methyl radicals as a function of the filament temperature for both W and Ta showed Arrhenius behavior. The temperature profile of methyl radical for HMDSZ for both W (1700-2400 ^{o}C) and Ta (1600-1900 ^{o}C) shows an increase with increase in filament temperature. This suggest that the methyl radical formation on both W and Ta follows the same mechanism as described earlier. With Ta, the temperature range (1600-1900 ^{o}C) was narrower compared to that of W (1700-2400 ^{o}C).

The average E_a^{app} was determined to be 71.2 ± 9.1 kJ/mol for W filament which is comparable to that of Ta filament (76.7 ± 8.1 kJ/mol). This shows that, W and Ta exhibit similar apparent activation energies for methyl radical production. Although the binding energies of CH_3-W or CH_3-Ta are unknown, several groups have studied the binding energies of CH_3 with various other transition metal surfaces such as Cu(111), Ni(111),

Pd(111), Pt(111), Rh(111), Ru(001), Ir(111), and Au(111).[119-121] The binding energies of these transition metals and CH_3 are in the range of 112 - 238 $kJmol^{-1}$, which is higher than the activation energies determined in our work. From Lin and Bent's[122] studies on the thermal decomposition of CH_3I on Cu(111) surface, there are two pathways to form methyl radical. The first pathway is to generate free methyl radicals in the gas-phase with I bound simultaneously to the Cu surface, and the second is formation of bound CH_3 group and I to the Cu surface followed by their desorption. This indicates that the methyl radicals are ejected from the filament surfaces and follows the first pathway as described by Bent and coworkers.

3.6 Theoretical Study on the Decomposition Chemistry of HMDSZ

In order to understand the role that metal filaments play in the dissociation processes of HMDSZ, an *ab initio* calculation of various decomposition pathways of HMDSZ in the gas phase was performed. To the best of our knowledge, there have been no reports on a systematic study on the decomposition of HMDSZ using *ab initio* calculations. As stated in Section 2.7, all geometry optimization and vibrational frequency calculations were carried out at the B3LYP/6-311++G(d,p) level of theory and single-point energies of optimized geometries were calculated using CCSD(T) with the basis set of 6-311++G(d,p). Scheme 3-1 illustrates both the concerted and stepwise pathways for the decomposition of HMDSZ studied in this work.

3.6.1 Homolytic cleavage of various bonds in HMDSZ

As the first step for the theoretical study of the decomposition pathways of HMDSZ, the homolytic bond cleavages of the various bonds in HMDSZ, including Si-C, Si-N, and N-H bonds, were examined as shown in Scheme 3-1. A homolytic cleavage results in the

formation of free radicals. In route SR-1a, the Si-C bond cleavage leads to the formation of (trimethylsilylamino)dimethylsilyl radical (I1) and CH_3 radical (I2). The Si-N bond cleavage in route SR-2a leads to the formation of trimethylsilyl radical (I3) and trimethylsilylamino radical (I4). In route SR-3a, the N-H bond cleaves to form H radical (I5) and hexamethyldisilazyl radical (I6). Typically, homolytic cleavages proceed with no energy barrier, *i.e.*, no transition states exist for homolytic bond cleavage processes.[84, 113, 123-125] The optimized geometries of HMDSZ, I1, I3, I4, and I6 are illustrated in Figure 3-12. The typical bond length for Si-C, Si-N, and N-H bond in the optimized geometry of HMDSZ is 1.888 Å, 1.753 Å, and 1.013 Å, respectively. The optimized geometry of HMDSZ calculated in this work at B3LYP/6-311++G(d,p) level is in good agreement with a previous *ab initio* study by Fleischer and McKean.[126] However, our results for HMDSZ are in much better agreement with the previously reported structure by experimental electron diffraction study by Fjeldberg *et al.*[127] For example, the Si-N bond length of 1.753 Å in the B3LYP/6-311++G(d,p) structure is very close to the experimental result of 1.738 ± 0.005 Å. The calculated Si-C bond length at B3LYP/6-311++G(d,p) level at 1.888 Å agrees well with the experimental results of 1.876 ± 0.001 Å. The Si-C bond lengths (1.896 Å) in I1 was slightly elongated compared to that in HMDSZ (1.887 Å) after the homolytic cleavage of Si-C in HMDSZ. The Si-C bond lengths in I3 also saw a slight increase, whereas those in I4 and I6 were very close to that of HMDSZ. The Si-N bond length in I1 and I4 showed a slight increase in bond, whereas that of I6 showed a slight decrease as compared to HMDSZ.

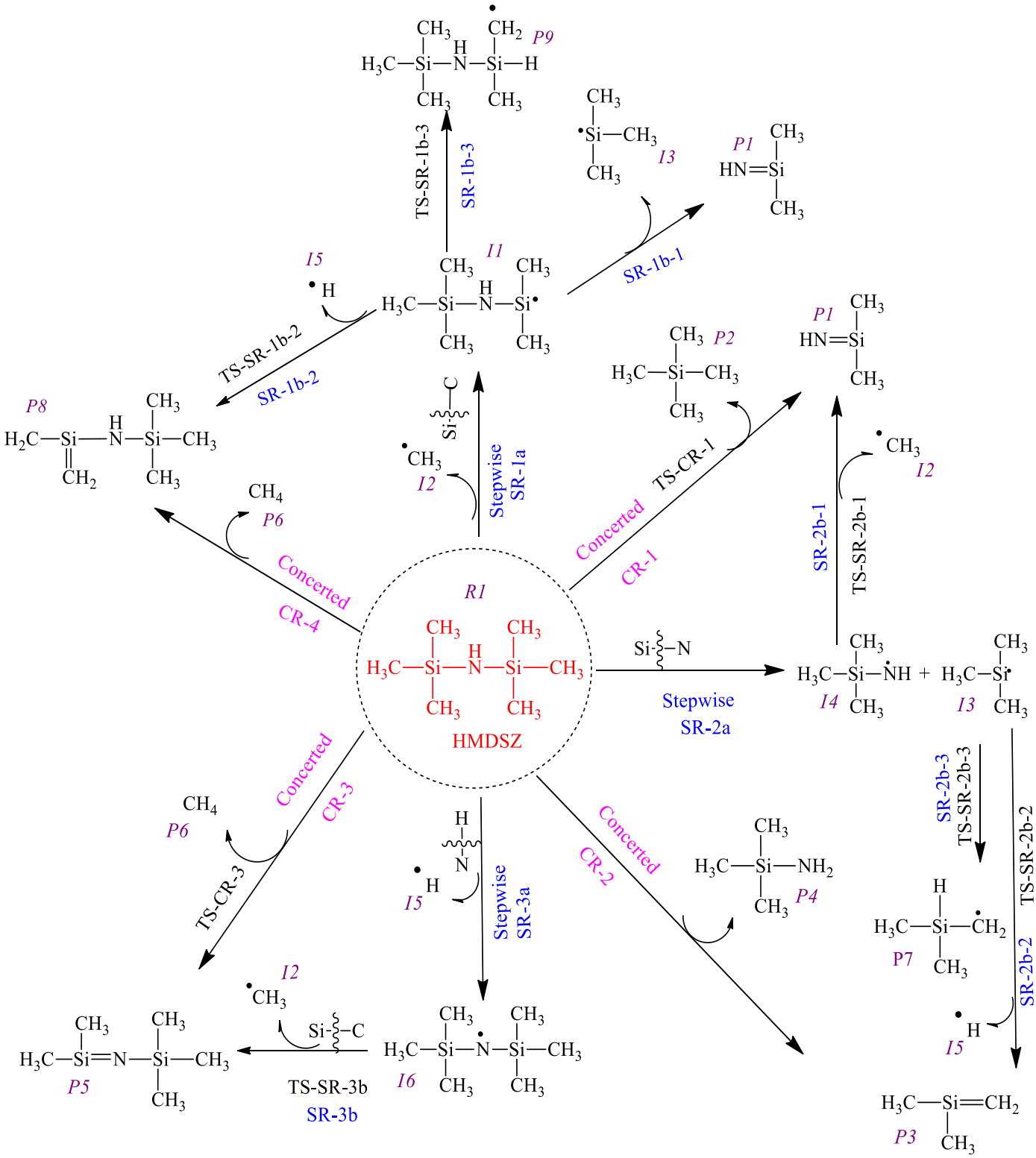

Scheme 3-1: Stepwise and concerted routes for the decomposition of hexamethyldisilazane

(a) Hexamethyldisilazane

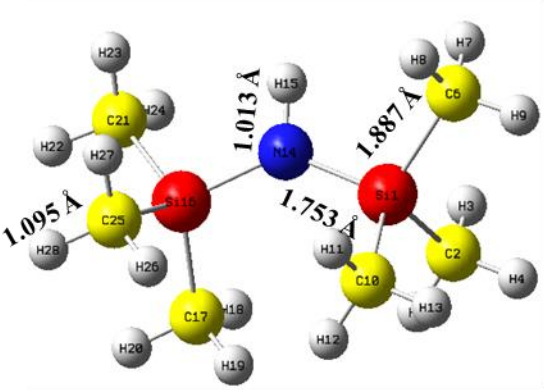

(b) (Trimethylsilylamino)dimethylsilyl radical (I1)

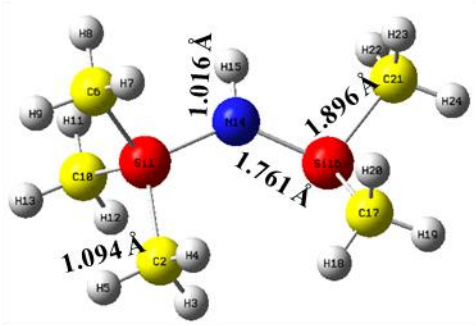

(c) Trimethylsilyl radical (I3)

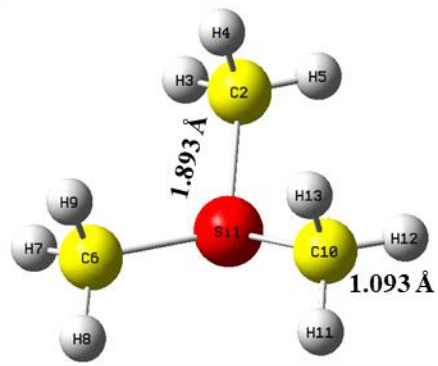

(d) Trimethylsilylamino radical (I4)

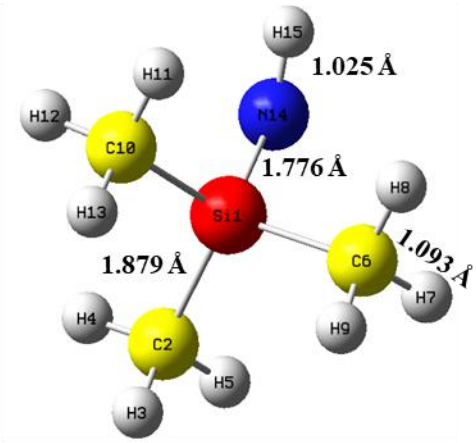

(e) Hexamethyldisilazyl radical (I6)

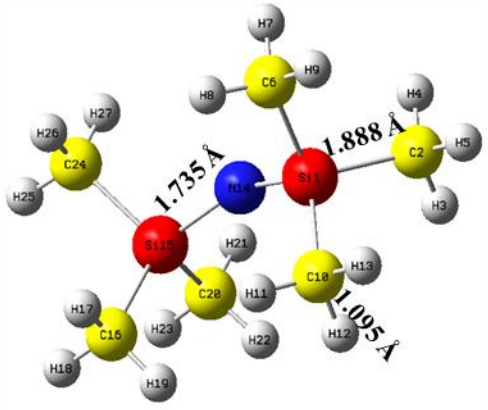

Figure 3-12: Optimized geometries of (a) hexamethyldisilazane (HMDSZ), (b) (trimethylsilylamino)dimethylsilyl radical (I1), (c) trimethylsilyl radical (I3), (d) trimethylsilylamino radical (I4), and (e) hexamethyldisilazyl radical (I6)

The energy-level diagram for all three homolytic bond cleavage processes, *i.e.*, SR-1a, SR-2a, and SR-3a, is shown in Figure 3-13.

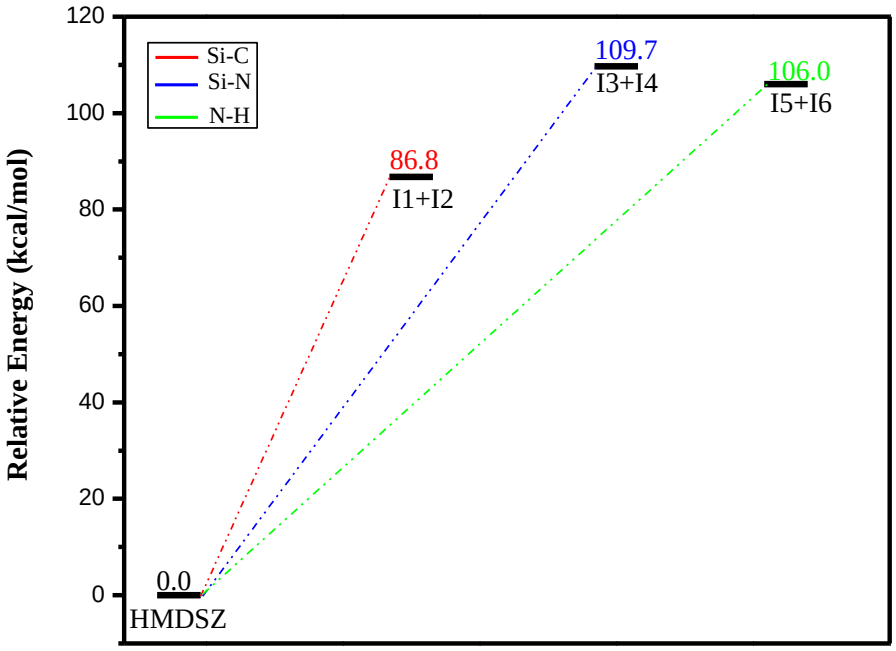

Figure 3-13: Energy-level diagram for the homolytic bond cleavages of HMDSZ. Energy values represent the relative enthalpies in kcal/mol at 0 K (ZPE correction included).

The reaction enthalpies for the homolytic cleavages of Si-C bond, Si-N bond, and N-H bond were determined to be 86.8 kcal/mol (*i.e.*, 363.2 kJ/mol), 109.7 kcal/mol (*i.e.*, 459.0 kJ/mol), and 106.0 kcal/mol (*i.e.*, 443.5 kJ/mol), respectively. From our experimental study of the decomposition of HMDSZ on W and Ta filaments, the activation energies for the production of CH_3 were determined to be 71.2 ± 9.1 kJ/mol and 76.7 ± 8.1kJ/mol, respectively. These values are much lower than the theoretically determined value of 86.8 kcal/mol (*i.e.*, 363.2 kJ/mol) for the Si-C bond cleavage in HMDSZ. This clearly suggests that the dissociation of HMDSZ on both W and Ta

filaments is a catalytic process and the metal wires serve as the catalyst in the cracking of HMDSZ molecules. Toukabri *et al.*[111] studied the formation of methyl radicals from the decomposition of methyl-substituted silanes. In their studies, the Si-C bonds in these molecules cleave to form methyl radicals and the obtained activation energy values for the methyl radical formation were in the range of 51.1 - 84.7 kJ/mol. In a similar effort, Badran *et al.*[125] also studied the gas-phase reactions of 1-methylsilacyclobutane in HWCVD. They observed that the exocyclic Si-CH_3 bond cleaves to form methyl radical and the obtained experimental activation energy of 46.7 kJ/mol was much lower than the theoretically determined value of 361 kJ/mol at the CCSD(T)/6-311++G(3d,2p)//MP2/6-311++G(d,p) level of theory.[125] The results obtained from this work on HMDSZ are in good agreement with those obtained from previous studies on hot wire decomposition of organosilicon molecules containing direct Si-C bonds.

3.6.2 Concerted Decomposition routes

The possible concerted routes for the decomposition of HMDSZ were then explored. From this, four concerted decomposition routes were identified as shown in Scheme 3-1. They lead to the formation of 1,1-dimethyl silanimine (P1) and tetramethylsilane (P2) in the concerted CR-1 route, 1,1-dimethylsilene (P3) and trimethylsilylamine (P4) in the CR-2 route, (trimethylsilyl)dimethylsilanimine (P5) and methane (P6) in the concerted CR-3 route, and 1-trimethylsilylamino-1-methylsilene (P8) and methane (P6) in the concerted CR-4 route.

3.6.2.1 Concerted Decomposition Route (CR-1) for the Formation of 1,1-Dimethyl silanimine (P1) and Tetramethylsilane (P2)

The first concerted decomposition route, denoted as CR-1, is a 1,3-methyl shift from one Si to another Si to produce 1,1-dimethylsilanimine (P1) and tetramethylsilane (P2). The transition state for this route, which is labeled as TS-CR-1, has been located at the B3LYP/6-311++G(d,p) level of theory. The single imaginary frequency for the TS was 308.2*i* cm^{-1}. The intrinsic reaction coordinate (IRC) path of the TS-CR-1 confirms that it connect to both P1 and P2 at the two minima. The optimized geometries of TS-CR-1 and the two products (P1 and P2) are shown in Figure 3-14.

(a) TS-CR-1

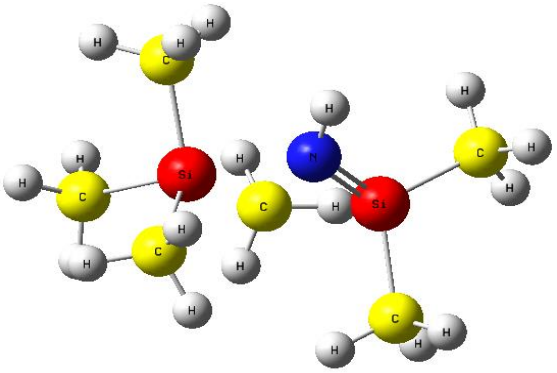

(b) 1,1-Dimethylsilanimine (P1)

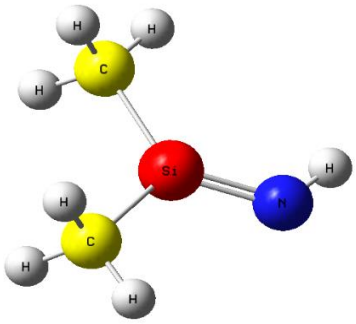

(c) Tetramethylsilane (P2)

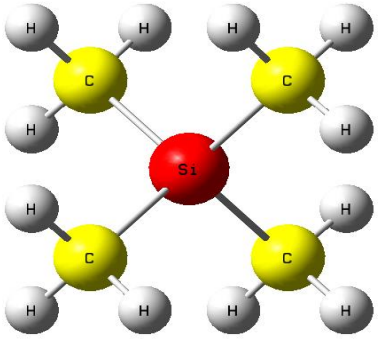

Figure 3-14: Optimized geometries of (a) TS-CR-1, (b) 1,1-dimethylsilanimine (P1), and (c) tetramethylsilane (P2) involved in the concerted 1,3 methyl-shift for the formation of P1 and P2 in the CR-1 route

3.6.2.2 Concerted Decomposition Route (CR-2) for the Formation of 1,1-Dimethylsilene (P3) and Trimethylsilylamine (P4)

The second concerted pathway, denoted as CR-2, concerns a 1,3-H shift from C to N to form 1,1-dimethylsilene (P3) and trimethylsilylamine (P4). The transition state for this concerted route, labeled as TS-CR-2, was also successfully found at the B3LYP/6-311++G(d,p) level of theory. The single imaginary frequency for TS-CR-2 was 1216.9*i* cm^{-1}. The IRC path of the TS-CR-2 confirms that it connects to both P3 and P4 at the two minima. Figure 3-15 illustrate the optimized geometries of TS-CR-2, P3, and P4.

(a) TS-CR-2

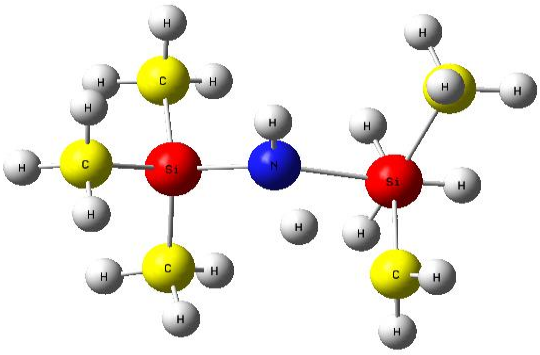

(b) 1,1-Dimethylsilene (P3)

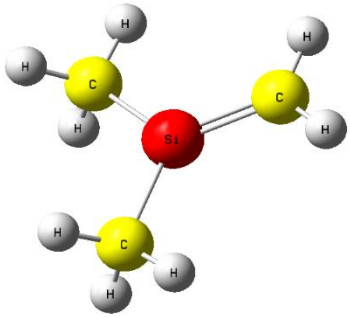

(c) Trimethylsilylamine (P4)

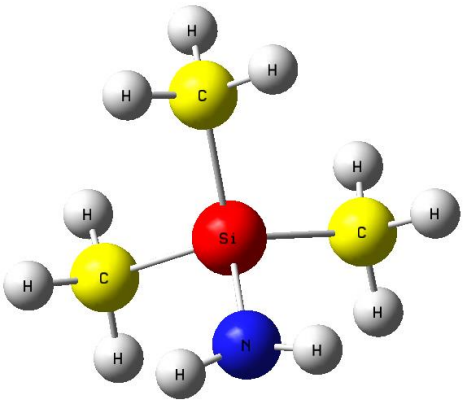

Figure 3-15: Optimized geometries of (a) TS-CR-2, (b) 1,1-dimethylsilene (P3), and trimethylsilylamine (P4) involved in the concerted 1,3 H-shift for the formation of P3 and P4 in the CR-2 route

3.6.2.3 Concerted Elimination of Methane (P6) for the Formation of (Trimethylsilyl)dimethylsilanimine (P5)

The third concerted pathway (CR-3) is the first of the two concerted elimination of methane (P6), which forms (trimethylsilyl)dimethylsilanimine (P5). The transition state for this route, labeled as TS-CR-3, was located at B3LYP/6-311++G(d,p) level of theory. The single imaginary frequency for TS-CR-3 at 1517.1*i* cm^{-1} corresponds to concurrent bond breaking of Si-C and N-H bonds, and subsequent bond formation between methyl and hydrogen radicals in HMDSZ, which is in agreement with the coordinate of this reaction. The IRC path of the TS-CR-3 confirms that it connects to both P5 and P6 at the two minima. The optimized geometries of TS-CR-3 and P5 are illustrated in Figure 3-16.

(a) TS-CR-3

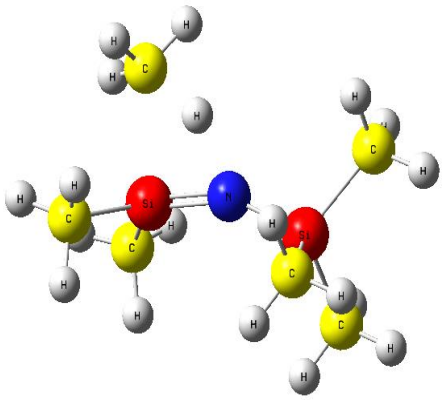

(b) (Trimethylsilyl)dimethylsilanimine (P5)

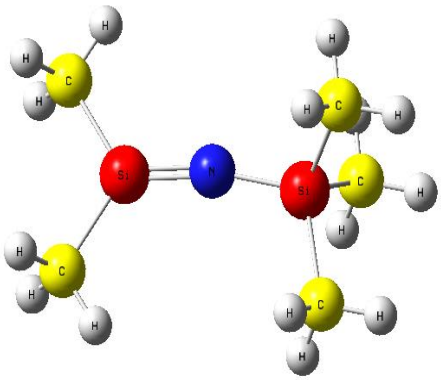

Figure 3-16: Optimized geometries of (a) TS-CR-3 and (b) (trimethylsilyl)dimethylsilanimine (P5) involved in the concerted elimination of methane for the formation of P5 in the CR-3 route

3.6.2.4 Concerted Elimination of Methane (P6) for the Formation of 1-Trimethylsilylamino-1-methylsilene (P8)

The last concerted pathway (CR-4) is the second of the two concerted elimination of methane (P6), which forms 1-trimethylsilylamino-1-methylsilene (P8). The strong single imaginary frequency (1487.97*i* cm^{-1}) for transition state of this route, labeled as TS-CR-4, corresponds to simultaneous bond breaking and forming between methyl and hydrogen readicals, to form P6 and P8 in the concerted manner. The IRC path of TS-CR-4 connects both P6 and P8 at the two minima. Figure 3-17 shows the optimized geometries of TS-CR-4 and P8.

(a) TS-CR-4 (b) 1-Trimethylsilylamino-1-methylsilene (P8)

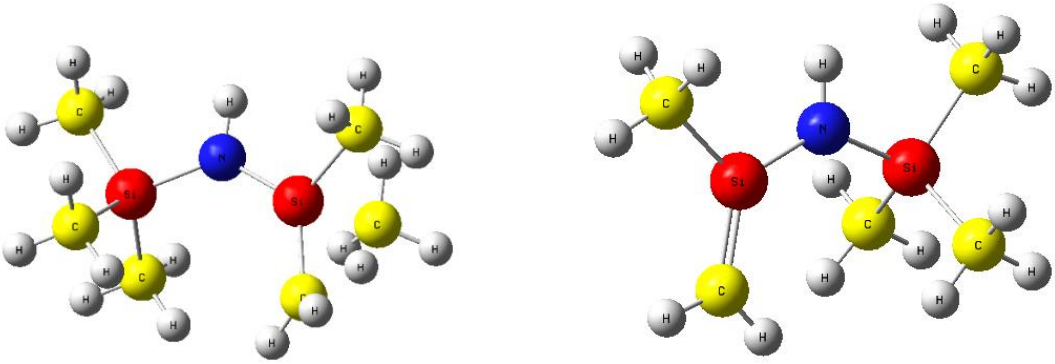

Figure 3-17: Optimized geometries of (a) TS-CR-4 and (b) 1-trimethylsilylamino-1-methylsilene (P8) involved in the concerted elimination of methane for the formation of P8 in the CR-4 route

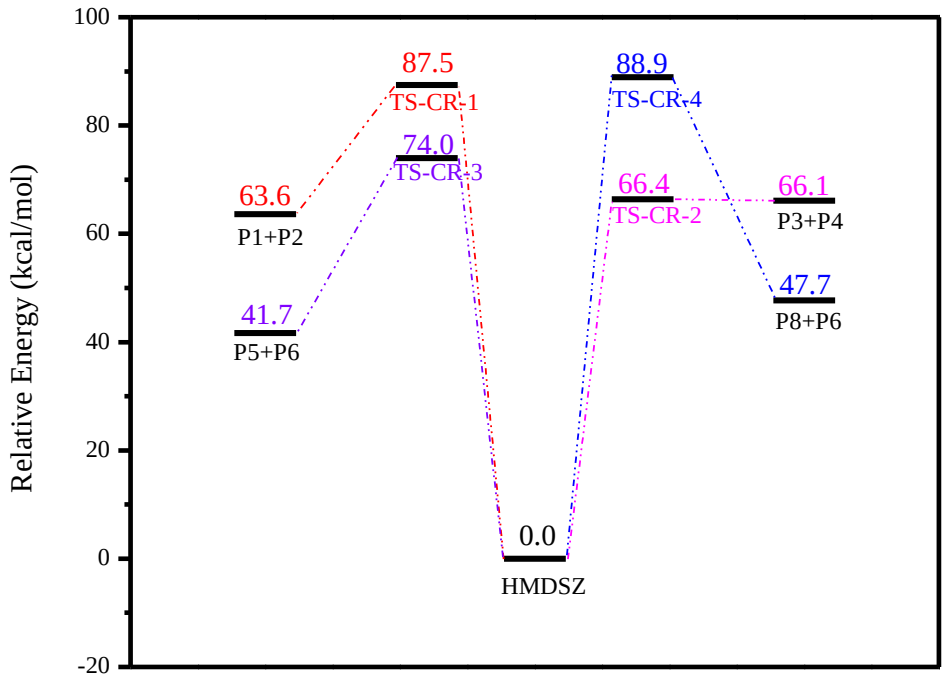

Figure 3-18: Energy-level diagram for all concerted mechanisms of HMDSZ. Energy values represent the relative enthalpies in kcal/mol at 0 K (ZPE correction included)

Figure 3-18 shows the energy-level diagram for all the four concerted pathways investigated in this work, including CR-1, CR-2, CR-3, and CR-4. All the enthalpies were calculated for 0 K at the CCSD(T)/6-311++G(d,p)//B3LYP/6-311++G(d,p) level of theory. All energy values in Figure 3-17 include the zero-point energy (ZPE) corrections. The activation enthalpy for the concerted formation of P1 and P2 in route CR-1 was determined to be 87.5 kcal/mol (*i.e.*, 366.1 kJ/mol). In route CR-2, the determined activation enthalpy for the concerted formation of P3 and P4 was 66.4 kcal/mol (*i.e.*, 277.5 kJ/mol). Both CR-3 and CR-4 routes involve the elimination of methane, with the respective formation of P5 and P8. The activation enthalpies for the formation of P5 in

CR-3 and P8 in CR-4 were calculated to be 74.0 kcal/mol (*i.e.*, 310 kJ/mol) and 88.9 kcal/mol (*i.e.*, 372.0 kJ/mol), respectively. A comparison of all the four concerted pathways studied in this work showed that the formation of P3 and P4 in route CR-2 is most energetically favourable with lowest activation enthalpy of 66.4 kcal/mol. The concerted elimination methane to form P5 (CR-3) has the second lowest activation enthalpy of 74.0 kcal/mol, whereas the other methane elimination route (CR-4) has the highest value of 88.9 kcal/mol. The remaining route, CR-1, gives the second highest activation enthalpy value.

3.6.3 Stepwise Decomposition routes

The stepwise decomposition routes of HMDSZ were also explored. For the stepwise processes, the reaction starts with the homolytic cleavage of the various bonds in HMDSZ, including Si-C, Si-N, and N-H bonds, to generate free radicals. The free radicals then undergo further decomposition to form the final products.

3.6.3.1 Stepwise Decomposition Route Initiated by the Rupture of Si-C bond

The first step in this stepwise decomposition route is the homolytic cleavage of Si-C bond, labeled as SR-1a, to generate I1 and I2, as described in Section 3.6.1. As mentioned before, this step proceeds without a TS. From I1, the elimination of trimethylsilyl radical (I3) is possible to produce 1,1-dimethylsilanimine (P1), one of the products in CR-1. This second step is labeled as SR-1b-1. This is one of the three possible pathways for the formation of P1. The elimination of H radical from I1 proceeded by the removal of H from C-H is labeled as SR-1b-2. The final product of SR-1b-2 is H radical and 1-trimethylsilylamino-1-methylsilene (P8), which is one of the products in CR-4. The H

atom from C-H can also undergo 1,2-H shift from C to Si. This step is labeled as SR-1b-3, which leads to the formation of (trimethylsilylamino)methylsilyl methyl radical (P9).

A transition state was located for SR-1b-1 by exploring the potential energy surface (PES) along the reaction coordinate in I1. The located TS, labeled as TS-SR-1b-1, has a weak imaginary frequency of 101.01*i* cm^{-1}. The imaginary frequency corresponds to the stretching of the N_{14} and Si_1 (atom numbering scheme indicated in Figure 3-19), which is in agreement with the coordinate of this reaction. The optimised TS is shown in Figure 3-19. An IRC was performed to confirm that the TS connects the desired minima. As it can be seen in Figure 3-20, a shallow minimum exists at the product side in the IRC.

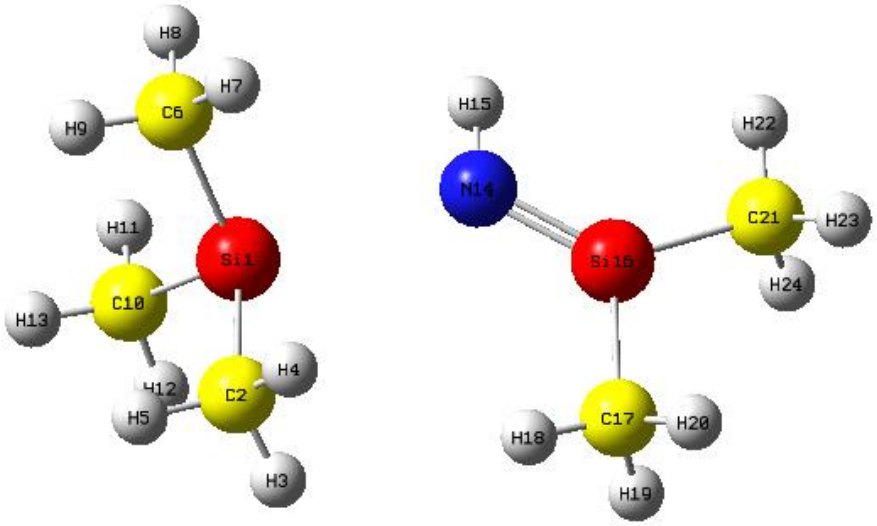

Figure 3-19: Optimized geometry of TS-SR-1b-1 involved in the elimination of trimethylsilyl radical from (trimethylsilylamino)dimethylsilyl radical (I1).

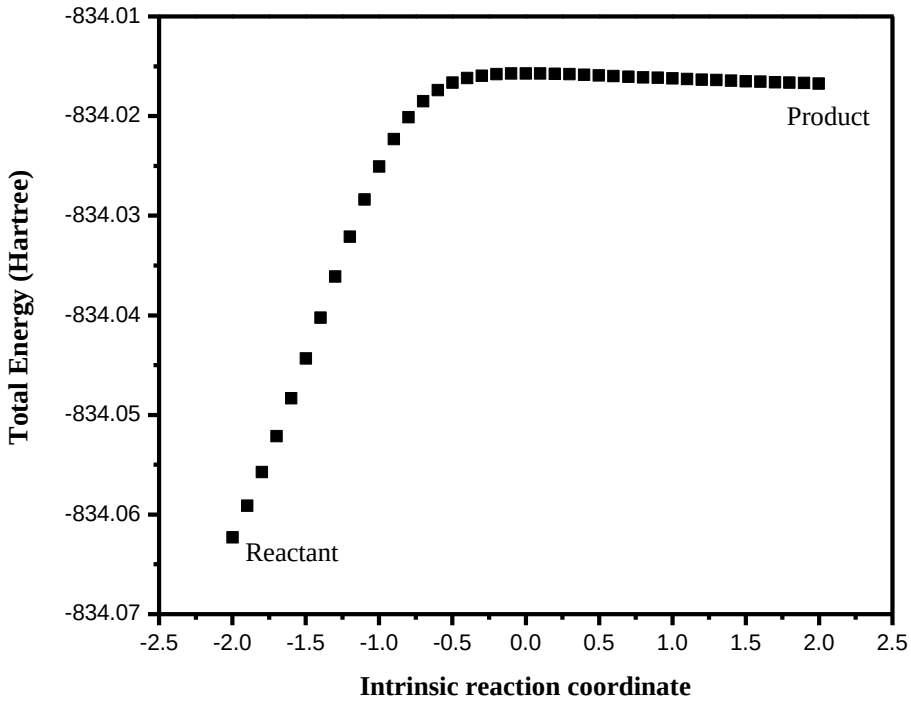

Figure 3-20: Intrinsic reaction coordinate path of TS-SR-1b-1

In an attempt to locate the transition state, TS-SR-1b-2, that connects I1 with P8 by the elimination of H atom at B3LYP/6-311++G(d,p) level of theory, the potential energy surface was explored by scanning C-H bond up to a distance of 5.5 Å as shown in Figure 3-21. Along the PES, no saddle points were located, which indicates that no transition state exists. Another attempt was made to locate the transition state, TS-SR-1b-2, by exploring the relaxed scan with 'ModRedundant'. This enables geometry relaxation around a constrained degree of freedom (bond length, angle, dihedral *etc*.) in the Gaussian program.

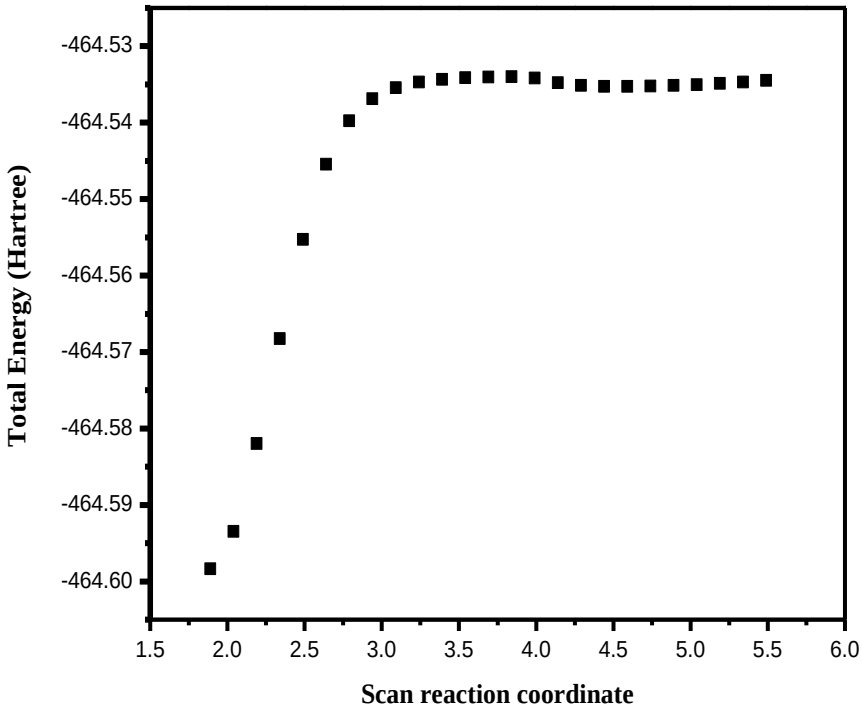

Figure 3-21: Potential energy scan of Si-C bond of I1 to a distance of 5.5 Å

A transition state was located with this approach, but an IRC performed showed that the H atom forms a bond with the Si in the silyl radical site in I1. This led to the location of a new transition state, labeled TS-SR-1b-3. The single imaginary frequency (817.25*i* cm^{-1}) of TS-SR-1b-3 corresponds to the swinging of the H_{19} between Si_{16} and C_{17} (atom numbering scheme indicated in Figure 3-19). The IRC of TS-SR-1b-3 connects I1 to P9 through a 1,2-H shift. This strongly suggests that the reactive H connected to C atom on I1 tends to form a bond with Si via a 1,2-H shift rather than leaving the radical regardless of any restrictions placed on the H-atom. The optimised geometries of the TS-SR-1b-3 and the product (P9) for SR-1b-3 are shown in Figure 3-22.

(a) TS-SR-1b-3

(b) (Trimethylsilylamino)methylsilyl methyl radical (P9)

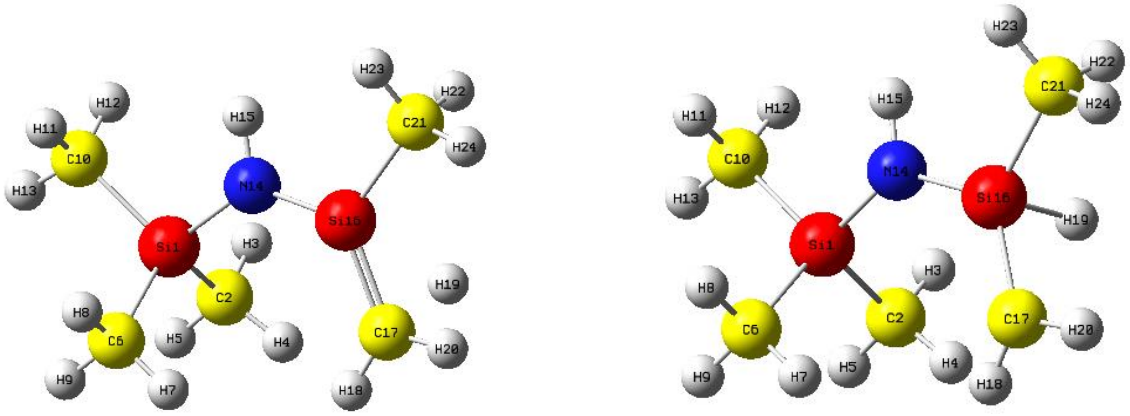

Figure 3-22: Optimized geometries of (a) TS-SR-1b-3 and (b) (Trimethylsilylamino)methylsilylmethyl radical (P9) involved in the 1,2-H shift in SR-1b-3

3.6.3.2 Stepwise Decomposition Route Initiated by the Rupture of Si-N bond

The first step in this stepwise decomposition route is the Si-N bond cleavage in SR-2a to generate I3 and I4 proceeding without TS, as described in Section 3.6.1. From I4, the elimination of methyl radical (I2) leads to the formation of 1,1-dimethylsilanimine (P1), which is one of the products in CR-1. This second step is labeled as SR-2b-1. As regards to I3, the elimination of H radical from C-H in I3 could form 1,1-dimethylsilene (P3), one of the products in CR-2. This step is labeled as SR-2b-2. The H atom from C-H in I3 can also undergo 1,2-H shift from C to Si to form dimethylsilyl methyl radical (P7), which is labeled as SR-2b-3.

The TS search for SR-2b-1 was performed by exploring the PES along the reaction coordinate of Si-C in I4. The PES scan plateaued beyond the distance of 2.8 Å and no saddle points were located along the PES, as shown in Figure 3-23. This shows that the elimination of $\bullet CH_3$ from I4 proceeds with no barrier at the B3LYP/6-311++G(d,p) level of theory. The optimization of the last point in the plateaued region as TS gave a very

weak imaginary frequency of 27.37*i* cm^{-1}, labeled as TS-2b-1x. This very small imaginary frequency corresponds to the stretching of C_6 and C_{10} as shown in Figure 3-24 which is not in agreement with the coordinate for this reaction. This further confirms that no TS exists for this route.

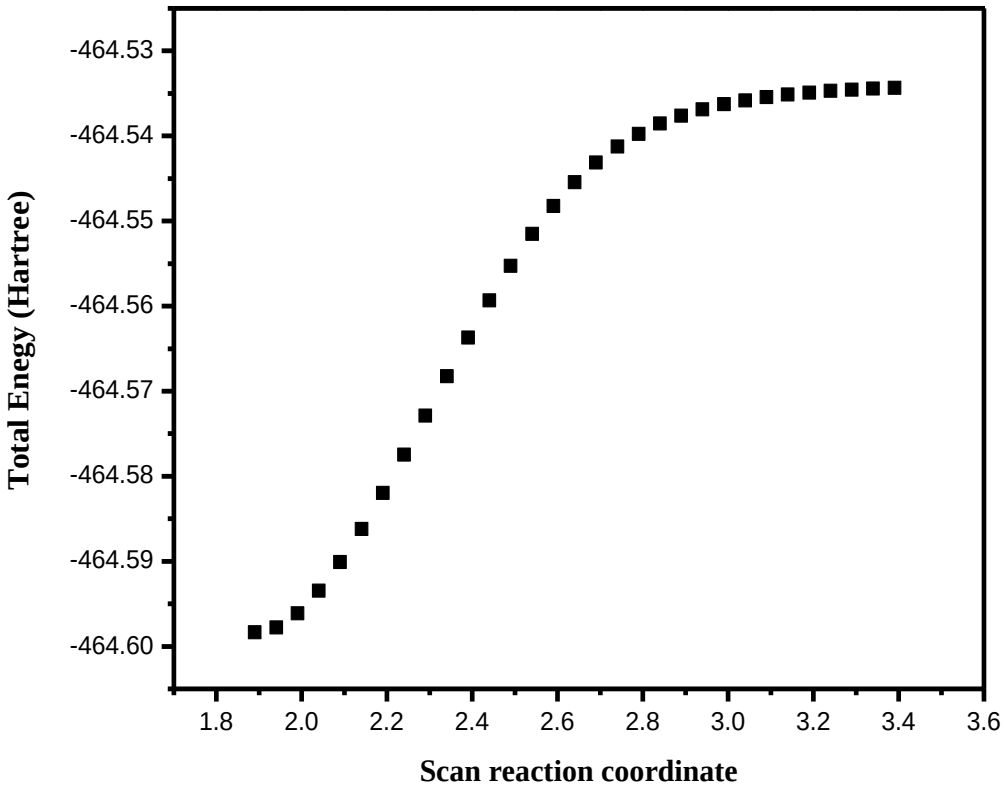

Figure 3-23: Potential energy scan of Si-C bond of I4 to a distance of 3.6 Å

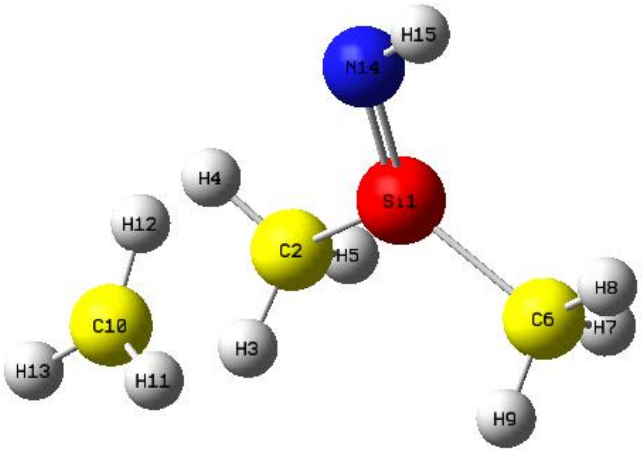

Figure 3-24: Optimized geometry of TS-SR-2b-1x from the last point of PES scan of I4 as shown in Figure 3-23

An attempt was made to locate the transition state, TS-SR-2b-2, that connects I3 with P3 by the elimination of H atom at the B3LYP/6-311++G(d,p) level of theory by exploring the potential energy surface and following the rise in energy up to a C-H distance of 6.5 Å. There was no saddle point along this PES scan, which indicates no TS for SR-2b-2. A similar approach was employed by exploring the relaxed scan with 'ModRedundant' optimization. A transition state was located with this approach, but from the analysis of the IRC of the located TS, the H atom forms a bond with Si in I3. This also led to the location of a new transition state labeled as TS-SR-2b-3. The single imaginary frequency (778.36*i* cm^{-1}) of TS-SR-2b-3 corresponds to the stretching of Si_1 and H_4, which agrees with the coordinate for this reaction. The progress of the IRC path of TS-SR-2b-3 connects I3 and P7**.** This observation is consistent with that observed in SR-1b-3. Figure 3-25 illustrates the optimized geometries of TS-SR-2b-3 and product (P7) in SR-2b-3.

(a) TS-SR-2b-3

(b) Dimethylsilylmethyl radical

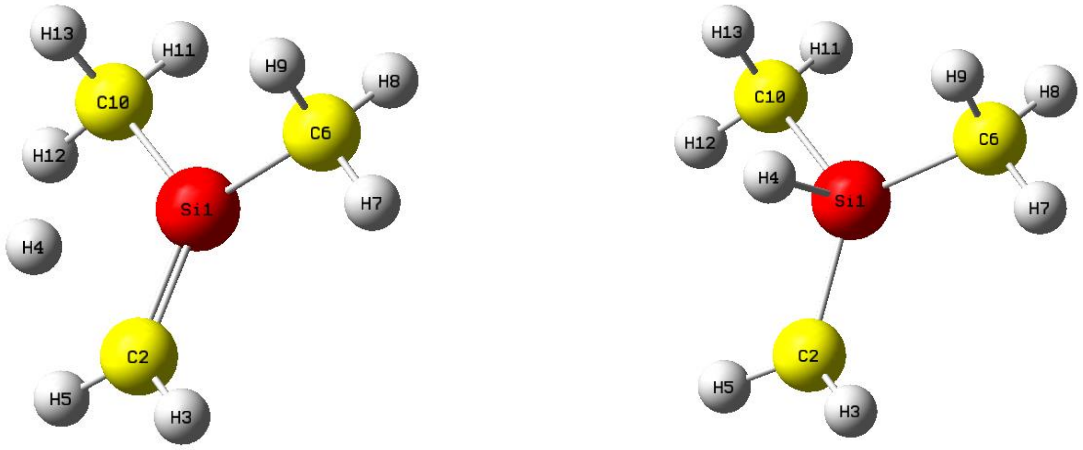

Figure 3-25 Optimized structures of (a) TS-SR-2b-3 and (b) dimethylsilylmethyl radical (P7) involved in the 1,2-H shift of I3 in SR-2b-3

3.6.3.3 Stepwise Decomposition Route Initiated by the Rupture of N-H bond

The first step in this stepwise decomposition route is the homolytic cleavage of N-H bond, labeled as SR-1a, to generate I5 and I6, as described in Section 3.6.1. As mentioned before, this step proceeds without a TS. From I6, the elimination of methyl radical (I2) is possible to produce (trimethylsilyl)dimethylsilanimine (P5), which is one of the products in CR-3. This second step is labeled as SR-3b. The TS search for SR-3b was performed by exploring the PES along the reaction coordinate of Si-C in I6. As shown in Figure 3-26, no saddle points were located on the PES and the energy plateaued beyond the distance of 3.0 Å. This shows that no TS exists for the elimination of CH_3 from I6. The optimization of the last point in the plateaued region as TS gave no imaginary frequency. This supports the point that no TS exists for SR-3b at the B3LYP/6-311++G(d,p) level of

theory. This observation is also consistent with the previous observation that there is no TS for the elimination of CH_3 from I4 in the SR-2b-1 route.

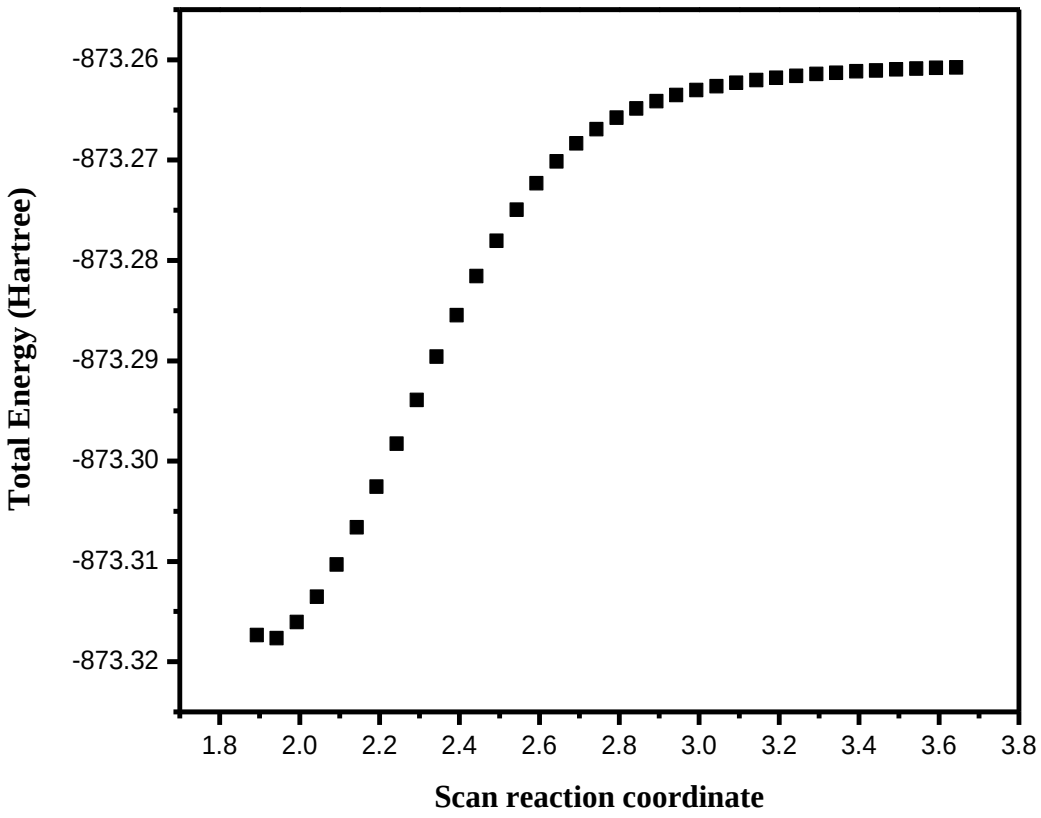

Figure 3-26: PES scanning along the reaction coordinate of Si-C bond of I6 up to a distance of 3.7 Å

To summarize, for the stepwise routes, transition states for SR-1b-1 (the elimination of trimethylsilyl (I3) from I1), SR-1b-3 (1,2-H shift in I1), SR-2b-3 (1,2-H shift in I3) were successfully located in this work. It is interesting to find that the elimination of H from the C atom attached to a Si atom in a silyl radical proceeds with no activation barrier. This is illustrated in the two routes of SR-1b-2 (elimination of H from I1) and SR-2b-2 (elimination of H from I3). In addition, it is found that the elimination of $\cdot CH_3$

radical from a methylated silylamino radical also proceeds with no transition state, as is shown in SR-2b-1 (elimination of CH_3 from I4) and SR-3b (elimination of CH_3 from I6).

Figure 3-27 shows the energy-level diagram for all the stepwise pathways as represented in Scheme 3-1. The two radicals of I1 and I2, produced from the cleavage of Si-C bond in HMDSZ, lie at an energy of 86.8 kcal/mol above HMDSZ. From this, it takes a further activation barrier of 60.6 kcal/mol (*i.e.,* 253.6 kJ/mol) and 61.3 kcal/mol (256.5 kJ/mol) to produce P1 in SR-1b-1 and P9 in SR-1b-3, respectively, from one of the radical, I1. The two radicals of I3 and I4, produced from the cleavage of Si-N bond in HMDSZ, lie at an energy of 109.7 kcal/mol above HMDSZ, from which it takes a further activation barrier of 64.0 kcal/mol (*i.e.,* 268.0 kJ/mol) to produce P7 from one of the radical, I3. The elimination of H from the C atom attached to a Si atom in a silyl radical site proceeds with no activation barrier and this is shown in route SR-1b-2 (elimination of H from I1) with reaction enthalpy of 60.1kcal/mol, and in route SR-2b-2 (elimination of H from I3) with a reaction enthalpy of 61.1kcal/mol. Also, the elimination of CH_3 radical from a methylated silylamino radical proceeds with no transition state as illustrated in SR-2b-1(elimination of CH_3 from I4) route, with a reaction enthalpy of 40.2 kcal/mol, and in SR-3b (elimination of CH_3 from I6) route with reaction enthalpy 34.9kcal/mol.

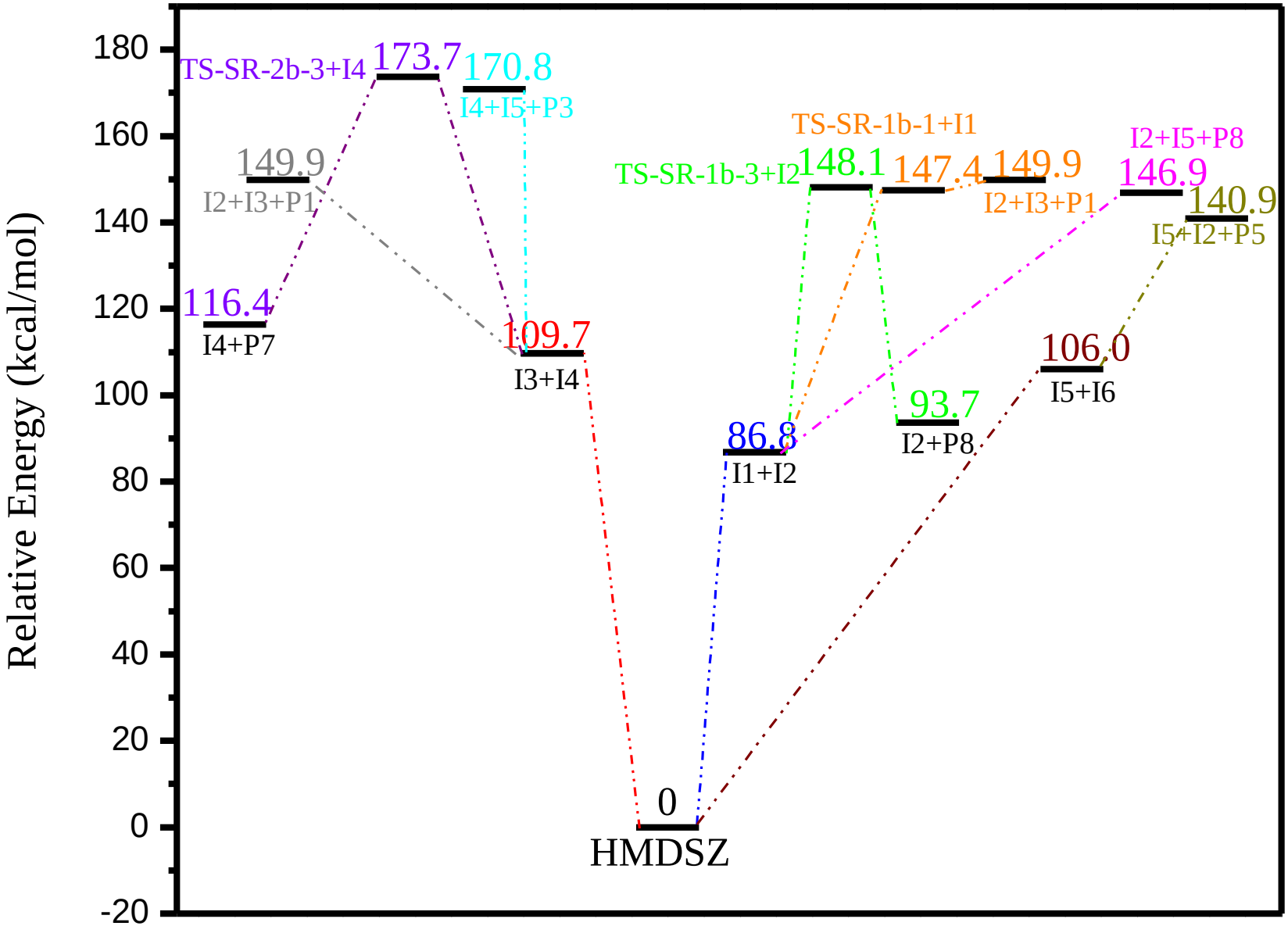

Figure 3-27: Energy-level diagram for all stepwise decomposition routes of HMDSZ. Energy values represent the relative enthalpies in kcal/mol at 0 K (ZPE correction included)

3.6.4 Reaction Kinetics and Thermochemistry

The activation enthalpies ($\Delta H_0^{\ddagger}$) and reaction enthalpies (ΔH_0) for the various decomposition pathways of HMDSZ studied in this work are listed in Table 3-1 and 3-2 respectively. The subscript 0 indicates the enthalpy values are calculated at 0 K. It is clear that the concerted 1,3-H shift from C to N atom to form P3 and P4 in the CR-2 route has the lowest activation barrier (66.4 kcal/mol) of all. This is followed closely by the concerted formation of P5 and P6 in the CR-3 route with an activation barrier of 74.0 kcal/mol. All the reaction studied in this work are endothermic in nature. A comparison of the reaction enthalpy values show that the concerted formation of P5 and P6 in the CR-3 route is the least endothermic in the concerted routes. In the stepwise routes, SR-1b-3 and SR-2b-3 involve rearrangement of H atom via 1,2-H shift from C to Si resulting in the least endothermic values for these routes. For the other reactions in the stepwise routes that do not involve rearrangement, the SR-3b route is the least endothermic.

So far, we have discussed the concerted and stepwise decomposition of HMDSZ in terms of enthalpies at 0 K. In order to understand the effect of temperature on the reaction kinetics and thermochemistry, we computed the kinetic ($\Delta H^{\ddagger}_{298}$, $\Delta G^{\ddagger}_{298}$, $\Delta S^{\ddagger}_{298}$) and thermochemical ($\Delta H_{298}$, ΔG_{298}, ΔS_{298}) parameters at the room temperature of 298 K to examine the effect of temperature change on the activation and reaction enthalpy ($\Delta H^{\ddagger}$, ΔH), entropy ($\Delta S^{\ddagger}$, ΔS), and Gibbs free energy ($\Delta G^{\ddagger}$, ΔG). Tables 3-1 and 3-2 summarise the thermochemical and kinetic parameters obtained at 298 K. The negative entropy of activation found in some of the decomposition routes is counter-intuitive, since a positive entropy of activation is typical for a decomposition reaction. The negative $\Delta S^{\ddagger}$ obtained in this work could be attributed to the simultaneous bond breaking and bond formation in

the concerted routes. As regards to Gibbs free energies of activations, it is found that the enthalpy term is the major contributor by comparing the $\Delta H^{\ddagger}_{298}$ and $T\Delta S^{\ddagger}_{298}$ values. The reaction entropy (ΔS_{298}) was always positive in Table 3-2. This is ascribed to the fact that two different species are formed as products in the overall reactions of the decomposition of HMDSZ. The observed increase in the difference between ΔG_{298} and ΔH_{298} indicates that the reaction entropy started to contribute more to the Gibbs free energy. It is expected that further increase in temperature will increase the contribution from the reaction entropy to ΔG.

Table 3-1: Activation enthalpies, entropies and Gibbs free energies for the various decomposition pathways of HMDSZ

Concerted	$\Delta H^{\ddagger}_{0}$(kcal/mol)	$\Delta H^{\ddagger}_{298}$(kcal/mol)	$\Delta G^{\ddagger}_{298}$(kcal/mol)	$T\Delta S^{\ddagger}_{298}$(kcal/mol)
TS-CR-1	87.5	87.1	88.7	-1.6
TS-CR-2	66.4	66.1	66.8	-0.7
TS-CR-3	74.0	74.1	73.1	1.1
TS-CR-4	88.9	88.9	89.3	-0.4
Stepwise				
TS-SR-1b-1	60.6	61.0	59.0	2.0
TS-SR-1b-3	61.3	61.5	61.6	-0.1
TS-SR-2b-3	64.0	64.2	64.0	0.2

Table 3-2: The reaction enthalpies, entropies and Gibbs free energies for the various decomposition pathways of HMDSZ

Concerted	ΔH_0(kcal/mol)	ΔH_{298}(kcal/mol)	ΔG_{298}(kcal/mol)	$T\Delta S_{298}$(kcal/mol)
CR-1	63.6	63.7	53.2	10.5
CR-2	66.1	66.4	54.7	11.7
CR-3	41.7	42.8	30.9	11.9
CR-4	47.7	48.5	38.6	9.9
Stepwise				
SR-1b-1	63.1	63.4	52.0	11.4
SR-1b-2	60.1	61.4	54.4	7.0
SR-1b-3	6.9	7.0	7.0	0.0
SR-2b-1	40.2	41.2	31.0	10.2
SR-2b-2	61.2	62.3	55.0	7.3
SR-2b-3	6.7	6.9	5.7	1.2
SR-3b	35.0	36.2	25.0	11.2

3.7 Summary

The primary decomposition of HMDSZ on hot W and Ta filaments under the collision-free conditions was investigated in this work. The species produced directly from the hot-wire decomposition were ionized using an SPI source with a VUV wavelength of 118 nm (photon energy of 10.5 eV) coupled with TOF MS. The SPI is designed to detect multiple species at one time, as long as their ionization energies are below 10.5 eV. This technique is very useful for probing a system that contains a large number of reactive species. In principle, information on all the species with IE < 10.5 eV can be obtained in each laser shot.

Methyl radicals were produced on the heated W and Ta filaments during the study of the decomposition of HMDSZ. The intensity of the methyl radicals increased with an increase in filament temperature for both filaments. The increase in intensity for the methyl radical production was observed at high temperatures. The average apparent activation energies (E_a^{app}) determined for methyl radicals on both W and Ta were 71.2 ± 9.1 $kJmol^{-1}$ and 76.74 ± 8.1 $kJmol^{-1}$ respectively. This indicates that W and Ta exhibit similar apparent activation energy for methyl radical production. The binding energy of CH_3 and other various transition metal surfaces are in the range of 112 - 238 kJ/mol, which is higher than the E_a^{app} determined for both W (71.2 ± 9.1 kJ/mol) and Ta (76.7 ± 8.1 kJ/mol) in this work,, indicating that the CH_3 radicals are ejected from the filament surfaces. HMDSZ is moisture sensitive and reacts with H_2O to form HMDSO and TriMSO. The peaks at m/z 17, 74, and 89 are products from the hydrolysis of HMDSZ and were not produced from the hot-wire decomposition as shown by Morimoto *et al.*

An *ab initio* calculation of the various decomposition pathways of HMDSZ in the gas phase was performed. The concerted and stepwise decomposition pathways were explored using the CCSD(T)/6-311++G(d,p)//B3LYP/6-311++G(d,p) level of theory. From the theoretical calculations, the determined reaction enthalpy for the production of CH_3 via homolytic cleavage of Si-C bond in HMDSZ was determined to be 86.8 kcal/mol (*i.e.,* 363.2 kJ/mol). This value is much higher than the experimentally determined values of 71.2 ± 9.1 $kJmol^{-1}$ and 76.7 ± 8.1 $kJmol^{-1}$ for W and Ta, respectively. This suggests that the dissociation of HMDSZ on both W and Ta filaments is a catalytic process and the metal wires serve as the catalyst in the cracking of HMDSZ molecules.

In the theoretical calculations, four possible concerted routes for the decomposition of HMDSZ were explored, including the formation of 1,1-dimethyl silanimine (P1) and tetramethylsilane (P2) in CR-1, 1,1-dimethylsilene (P3) and trimethylsilylamine (P4) in CR-2, and the elimination of CH_4 to form (trimethylsilyl)dimethylsilanimine (P5) in CR-3 and 1-trimethylsilylamino-1-methylsilene (P8) in CR-4. The transition states for all four concerted routes were successfully located. A comparison of all the four concerted pathways studied in this work showed that the formation of P3 and P4 in route CR-2 is most energetically favourable with the lowest activation enthalpy of 66.4 kcal/mol. In the stepwise routes, three transition states were successfully located, including TS-SR-1b-1 (for the elimination of trimethylsilyl (I3) from I1), TS-SR-1b-3 (for 1,2-H shift in I1), and TS-SR-2b-3 (for 1,2-H shift in I3). It has been shown that the elimination of H from the C atom attached to a Si atom in a silyl radical proceeds with no activation barrier. This is illustrated in the two routes of SR-1b-2 (elimination of H from I1) and SR-2b-2 (elimination of H from I3). The elimination of CH_3 radical from a methylated silylamino

radical also proceeds with no transition state, as is shown in SR-2b-1 (elimination of CH_3 from I4) and SR-3b (elimination of CH_3 from I6).

Chapter Four: Gas-phase Reaction Chemistry of 1,1,1,3,3,3-Hexamethyldisilazane in a Hot-wire Chemical Vapor Deposition Reactor

4.1 Motivation

1,1,1,3,3,3-Hexamethyldisilazane (HMDSZ) has been widely used as the source gas in chemical vapor deposition (CVD) of silicon carbonitride (SiC_yN_z) thin films.[56, 102-105, 107, 108, 128, 129] Fainer *et al.*[56] investigated the properties of thin films obtained by remote plasma enhanced CVD from HMDSZ or its mixture with NH_3 as source gases in the temperature range of 373 - 773 K. They observed the formation of polycrystalline hexagonal Si_3N_4 and polycrystalline SiC phases when pure HMDSZ was used as the source gas. Addition of NH_3 to the gas mixture resulted in a change in the chemical composition and structure of the deposited film by the disappearance of C-bonding to silicon. They showed that the SiC_yN_z films containing considerable amount of C in the form of a polycrystalline SiC phase worsened its dielectric properties, whereas SiN_x:H films containing no C had dielectric properties close to the films grown from $SiH_4 + NH_3$ gas mixtures. The authors observed that an increase in substrate temperature favored the formation of hexagonal silicon nitride.

In a similar effort, Guruvenket *et al.*[128] studied the atmospheric-pressure plasma-enhanced CVD of amorphous SiC_yN_z:H films using HMDSZ and N_2 as the source and reactive gases, respectively. The reactive gas is activated in the afterglow region of the plasma, which reacts with the source gas to activate it. They also found that the substrate temperature played a crucial role in controlling the structure and chemical composition of SiC_yN_z films. It was observed that organic moieties such as Si-CH_3 groups were eliminated by increasing the substrate temperature, which led to the formation of films exhibiting ceramic-like features of Si-C, Si-N, and SiCN bonds. At low substrate

temperatures (25 – 250 ^{o} C), the film thickness decreased with increasing substrate temperature, indicating that the film growth mechanism is surface-reaction controlled. An increase in the film thickness was observed at high temperatures (250 – 450 ^{o} C), which showed that the film growth mechanism is mass-transport controlled.

Saloum *et al.*[129] studied the structural, optical, and electrical properties of plasma deposited SiC_yN_z thin films from using HMDSZ as the source gas. The authors found that a change in the feed gas for plasma generation from rare gas (argon) to a reactive molecular gas (N_2) was accompanied with an increase of refractive index, dielectric constant, photoluminescence intensity, and a decrease in energy band gap of SiC_yN_z films. A change in the applied power for the plasma generation from 100 W to 300 W corresponded to a maximum refractive index, dielectric constant, optical absorbance, photoluminescence intensity, and a minimum energy band gap of SiC_xN_y films. They found that the deposited SiC_yN_z films exhibited high electrical resistivity which is inversely proportional to the film thickness. It was concluded that the deposited films had several applications in the optoelectronic and microelectronic devices.

The characteristics of deposited SiC_yN_z thin films from hot-wire CVD process using HMDSZ and NH_3 as source gases was studied by Neethirajan *et al.*[130] The authors found that the composition of Si, C, and N in the obtained SiC_yN_z films was influenced by the flow rate of NH_3 gas. They observed that a higher flow rate of NH_3 gas resulted in higher N and lower C content in the deposited thin films. They also found out that correlation existed between mechanical stress and substrate temperature. At the substrate temperature in the range of 275 to 325 ^{o}C, the stress changed from compressive to tensile. From their

observation, they concluded that the deposited SiC_yN_z thin films can be used for developing sensors for harsh environment.

Although HMDSZ has been used as a source gas for different CVD processes, the gas-phase chemistry involved in the generation of the actual growth precursor for the SiC_yN_z films has received less attention. As mention in Chapter 1, Morimoto *et al.*[61] and Yoshimura *et al.*[89] studied the gas-phase chemistry using HMDSZ in HWCVD. Morimoto *et al.* employed mass spectrometric techniques to detect the gas-phase species. They observed the formation of trimethylsilane and trimethylsilylamine when the filament was turned on and attributed the formation of these species to the surface reaction on the chamber walls. In their work on using low-energy mass-selected fragment ion beam with a hot tungsten wire, Yoshimura *et al.* showed that ion production strongly depended on W temperature. They observed that fragmentation was less effective at low W temperatures, but significantly increased when the W temperature was increased.

In this work, single-photon ionization (SPI) with a vacuum ultraviolet (VUV) laser wavelength of 118 nm coupled with time-of-flight mass spectrometry (TOF MS) was used to study the secondary gas-phase reactions in the HWCVD reactor. The mechanism for the formation of secondary gas-phase reaction products, that are generated from the reactions between species from the primary decomposition and the abundant HMDSZ molecules, has been explored. Experiments with deuterated isotopomers of HMDSZ, including bis(trimethylsilyl)-N-deuterioamine (HMDSZ-d_1) and 1,1,1,3,3,3-hexa(deuteratedmethyl)disilazane (HMDSZ-d_{18}), were also performed under the same experimental conditions to help understand the reaction chemistry in the HWCVD reactor.

4.2. Secondary Gas-phase Reactions of HMDSZ in a HWCVD Reactor with W Filaments

The chemical products from secondary gas-phase reactions between the primary decomposition products of HMDSZ on the filament and the parent molecules were investigated by monitoring the species exiting from a HWCVD reactor as described in Section 2.2. Mass spectra for filament temperatures ranging from 1200 - 2000 ^{o}C were recorded. For each temperature, a mass spectrum was collected every 5 minutes for 60 minutes. Temperatures lower than 1200 ^{o}C and above 2000 ^{o}C were not explored. At temperatures higher than 2000 ^{o}C, the parent mass peak and the predominant photofragment peak disappeared quickly after the filament was turned on.

Figure 4-1 shows the TOF mass spectra recorded for 12 Torr of 0.9 % HMDSZ/He sample at different filament temperatures ranging from 1200 - 2000 ^{o}C. For comparison, the room-temperature mass spectrum is also shown. As shown in Figure 4-1, the mass spectra when filament was on were still dominated by the parent ion peak (m/z 161) and its photofragment ion, i.e., (trimethylsilylamino)dimethylsilyl ion (m/z 146). However, with increasing filament temperatures, the intensities of the parent mass peaks were decreased, indicating that the parent HMDSZ molecules were decomposed on the filament and consumed in the secondary gas-phase reactions in the reactor. At the same time when the parent ion and the photofragment ion peaks decreased in intensities, a new mass peak were observed at m/z 17 in the mass regions lower than the photofragment mass (146 amu). Several new peaks were observed in the mass regions higher than the parent mass (161 amu), including those at m/z 175, 203, and 219. These are shown in Figure 4-1.

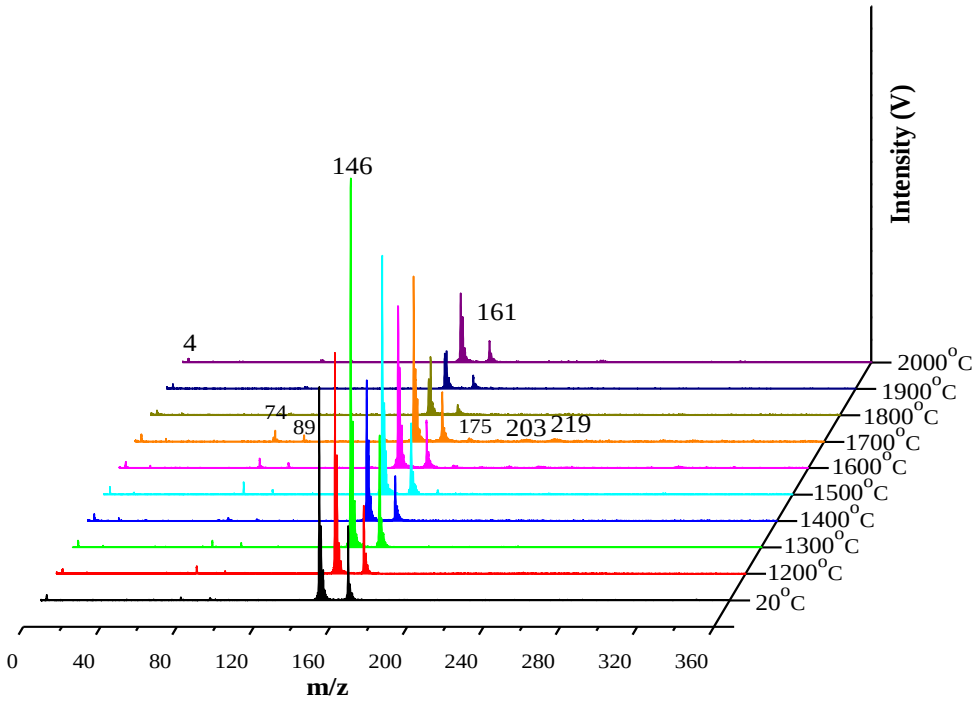

Figure 4-1: 10.5 eV VUV SPI TOF mass spectra of 12 Torr of 0.9% HMDSZ/He at W filament temperatures between 1200 ºC -2000 ºC at 60 minutes of reaction time. The spectrum at 20 ºC is recorded when the filament is off.

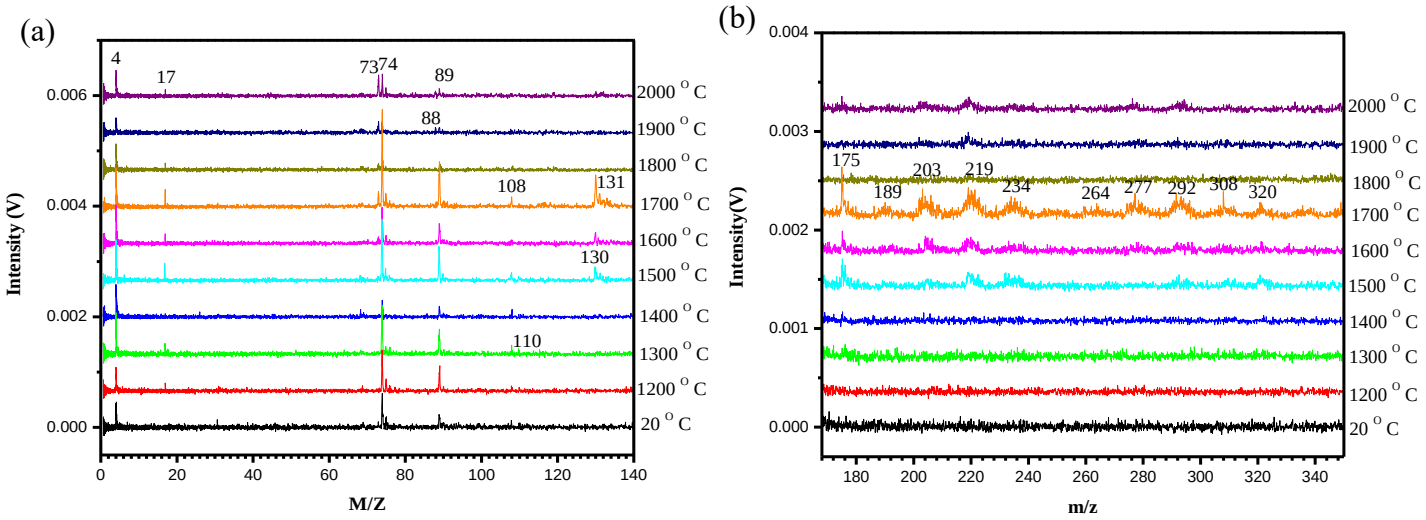

Figure 4-2: 10.5 eV VUV SPI TOF mass spectra of 12 Torr of 0.9% HMDSZ/He at W filament temperatures between 1200 ºC-2000 ºC in mass regions of (a) 2 amu and 140 amu (b) 165 amu and 360 amu at 35 minutes of reaction time.

From the enlarged mass spectra shown in Figure 4-2 (a) in the mass regions between 2 and 140 amu, new mass peaks at m/z 73, 88, 130, and 131 were also observed. Figure 4-2 (b) shows the enlarged mass spectra in the high mass regions between 170 and 350 amu. Weaker high-mass peaks at 189, 234, 264, 277, 292, 308, and 320 were observed in this region.

4.2.1 Formation of Peaks in the Mass Regions Lower Than the Photofragment Mass of 146 amu

As stated above, several new mass peaks were observed in the low mass region below 146 amu, including those at m/z 17, 73, 88, 130, and 131.

4.2.1.1 Formation of Ammonia (m/z 17)

The new peak at m/z 17 observed when the filament was turned on in the HWCVD reactor shows an increase with increase in filament temperature and filament-on time. In Figure 4-3, the intensity distributions of the peak at m/z 17 as a function of filament-on time at different filament temperatures are shown. When the filament-on time is shorter than 30 min, the intensity generally increases with increasing filament-on time at all temperatures. At a filament temperature of 1700 ^{o}C, the intensity shows a continual increase beyond 30 min for the whole duration of 1 hour, as shown in the inset in Figure 4-3. The peak at m/z 17 is assigned to NH_3. The intensity distribution of the peak at m/z 17 in Figure 4-3 suggests that NH_3 is produced in-situ in the presence of the filament in a HWCVD reactor. However, the mechanism for the formation of NH_3 (m/z 17) from HMDSZ in the process of HWCVD is not understood at the moment.

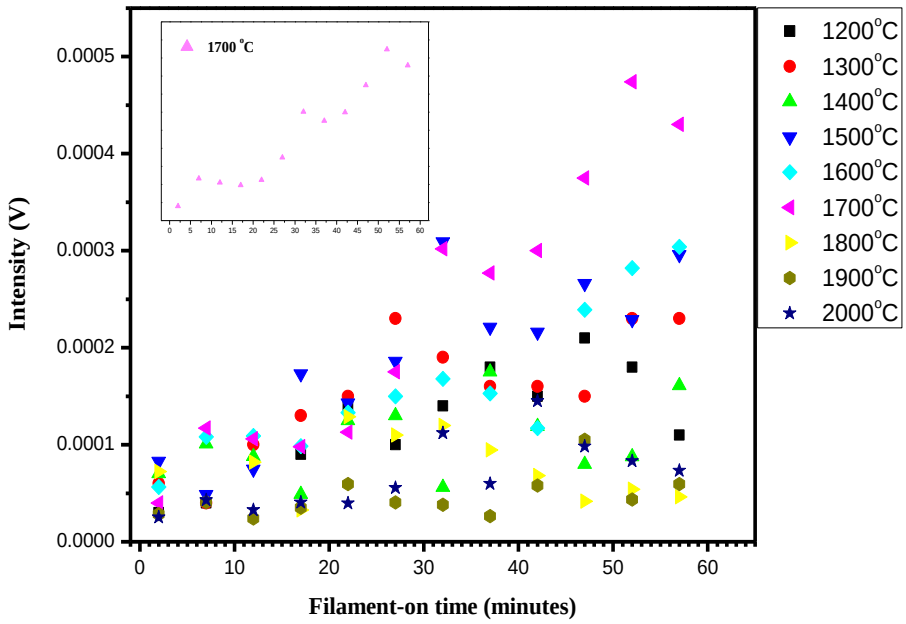

Figure 4-3: Intensity distributions of the mass peak at m/z 17 versus filament-on time at filament temperatures from 1200 - 2000 ^{o} C in a HWCVD reactor with a W filament

4.2.1.2 Formation of 1,1-Dimethylsilanimine (m/z 73)

From the enlarged mass spectra shown in Figure 4-2 (a), a new peak at m/z 73 was observed at high temperatures from 1700 ^{o}C - 2000 ^{o}C. Figure 4-4 illustrates the intensity distributions of the peak at m/z 73 as a function of temperature at different filament-on time. A general increase in the peak intensity with increase in temperature is observed for the different filament-on time.

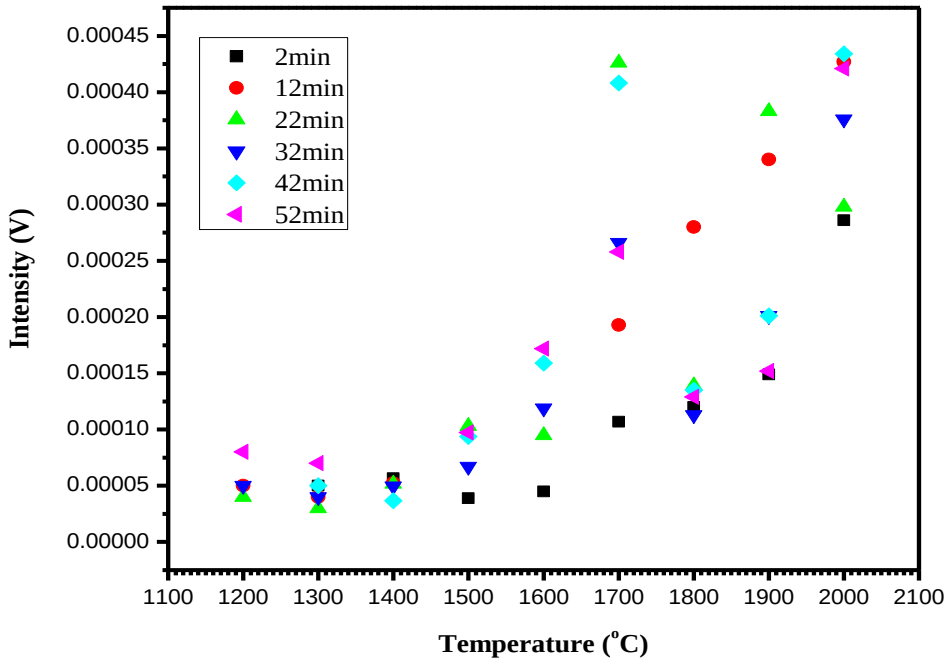

Figure 4-4: Intensity distributions of the mass peak at m/z 73 as a function of filament temperature at different reaction time in a HWCVD reactor with a W filament

Guruvenket *et al.*[128] have previously studied atmospheric-pressure plasma-enhanced CVD of SiC_yN_z using HMDSZ. N_2 was used as the reactive gas in plasma generation. They observed that the afterglow region of the plasma consisted of N species. The activated nitrogen species in the afterglow region can react with the source gas (HMDSZ) and activate them in several ways. The initiation reaction between HMDSZ and the activated N atoms was given as:

$$\dot{N} + (CH_3)_3SiNHSi(CH_3)_3 \longrightarrow 2[(CH_3)_3\dot{Si}] + NH + N \qquad (4\text{-}1)$$

The trimethylsilyl radical species formed can undergo secondary gas-phase reactions as shown in Equation (4-2).

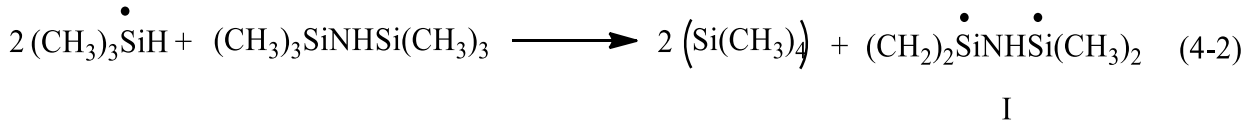

(4-2)

The biradical species, I, in Equation (4-2) may convert to 1,1-dimethylsilanimine and dimethylsilylene upon reaching the substrate, as shown in Equation (4-3).

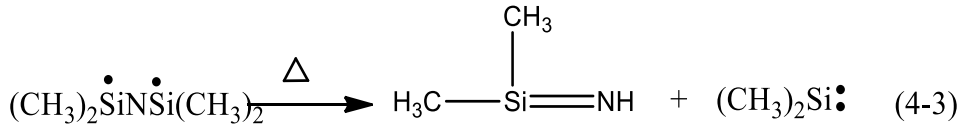

(4-3)

1,1-dimethylsilanimine

1,1-dimethylsilanimine ($HN=Si(Me)_2$) is believed to be the 'hot' intermediate, which readily undergo film-forming reactions. The authors suggested that the highly reactive species of 1,1-dimethylsilanimine contributed to film formation.[128] Other literature work on the formation of the SiC_yN_z thin films using HMDSZ[53, 109] also showed that chemical species containing a N=Si double bond were involved in the film growth. According to these, the peak observed at m/z 73 in our experiment is attributed to 1,1-dimethylsilaninime ($HN=Si(CH_3)_2$). The ionization energy (IE) of 1,1-dimethylsilaninime is unknown. However, the IE for other silanimine compounds are known. For example, the IE of silanimine, N-methylslanimine, and trimethylsilanimine ($(CH_3)N=Si(CH_3)_2$) is known to be 9.62 eV, 8.71 eV, and 7.98 eV, respectively.[131] All of them are lower than the VUV photon energy of 10.5 eV. Therefore, the IE for ($HN=Si(Me)_2$) should not be higher than 10.5 eV. This suggests that 1,1-dimethylsilaninime, once formed in the HWCVD reactor, can be ionized by the ionization laser source and detected by our TOF MS.

From the theoretical calculations discussed in Section 3.6, there are three possible routes to form 1,1-dimethylsilanimine, *i.e.*, the concerted route CR-1 to form 1,1-dimethylsilanimine (P1) and tetramethylsilane (P2), the stepwise route SR-1b-1 to form 1,1-dimethylsilanimine by the elimination of trimethylsilyl radical (I3) from (trimethylsilyamino)dimethylsilyl radical (I1), and the stepwise route SR-2b-1 by the elimination of methyl radical (I2) from trimethylsilyamino radical (I4). The calculated activation barrier for the concerted formation of P1 and P2 in CR-1 was determined to be 87.5 kcal/mol (*i.e.*, 366.1 kJ/mol). A comparison with the activation barriers of other three concerted routes, for example, the one at 66.4 kcal/mol (*i.e.*, 277.8 kJ/mol) for CR-2 for the formation of 1,1-dimethylsilene (P3) and trimethylsiylamine (P4), indicates that the CR-1 route is not the most energetically favourable concerted route.

The stepwise formation of P1 and I2 from I4 in SR-2b-1 proceeded with no barrier, however, the production of I4 and trimethylsilyl radical via a homolytic cleavage of Si-N bond requires an energy of 109.7 kcal/mol (*i.e.*, 459.0 kJ/mol). I1 and methyl radical via the homolytic cleavage of Si-C bond lies at 86.8 kcal/mol above the reactant of HMDSZ, and it takes a further activation barrier of 60.6 kcal/mol (*i.e.*, 253.55 kJ/mol) to produce P1 and I3 from I1 in SR-1b-1. Comparing all the three possible routes for the formation of 1,1-dimethylsilanimine, it is clear that the concerted formation via CR-1 is the most energetically favorable one in the gas phase, according to theoretical calculations.

On a W filament, however, it has been shown in Section 3.3 that the primary decomposition products of HMDSZ are methyl ($\dot{C}H_3$) and (trimethylsilylamino) dimethylsilyl ($(CH_3)_3SiNH\dot{S}i(CH_3)_2$, denoted as I1 in Scheme 3-1) radicals (Equation 3-3). The decomposition is catalytic with a low activation barrier. Once the

$(CH_3)_3SiNHSi(CH_3)_2$ radical (I1) is produced from the hot-wire decomposition, it can undergo further fragmentation by eliminating a trimethylsilyl radical to form 1,1-dimethylsilanimine ($HN=Si(Me)_2$) species, as represented by Equation (4-4).

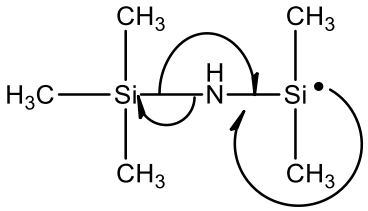

Trimethylsilylamino dimethylsiyl radical
(146 amu)

$$HN=Si(CH_3)_2 + (CH_3)_3Si^{\bullet} \quad (4\text{-}4)$$

(73 amu)

A careful examination of the mass regions lower than the photofragment mass (146 amu) shows a weak peak at m/z 88 at high temperatures of 1900 ^{o}C and 2000 ^{o}C, as shown in Figure 4-2 (a). This peak could be from tetramethylsilane (m/z 88) via the concerted formation of 1,1-dimethylsilanimine, as illustrated in route CR-1. Li *et al.*[24] showed that the room-temperature mass spectrum of tetramethylsilane recorded with a 10.5 eV VUV SPI showed a predominant photofragment ion ($Si(CH_3)_3^+$) peak at m/z 73 and the parent ions atm/z 88. The intensity ratio of the peak at m/z 73 to that at m/z 88 was determined to be 4.0:1. In our experiments with HMDSZ in a HWCVD reactor, the intensity ratios of the peak at m/z 73 to that at m/z 88 was less than 4.0:1. The intensity ratios of peak at m/z 73 to that of peak at m/z 88 was about 3.5: 1. This could be attributed to the weak intensity of peak at m/z 73 ($Si(CH_3)_3^+$) which might be embedded in peak at m/z 73 (1,1-dimethylsilanimine).

4.2.1.3 Reactions Involving Silanimines

Silanimines are known to be highly reactive and they tend to undergo dimerization easily.[132-136] Sander et *al*.[133] investigated the existence of silanimines in cryogenic matrices. They observed that in the absence of trapping agents, silanimines easily dimerized to form cyclodisilazane as shown in Equation (4-5), (where R and R'= H or CH_3).

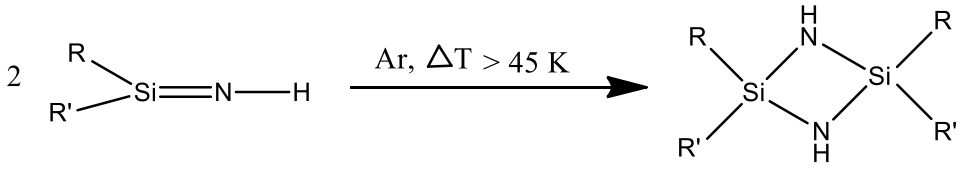

(4-5)

Letulle *et al*.[136] generated silanimines from two different source gases, *i.e.*, azasilacyclobutane and propargylic disilazane, using flash vacuum thermolysis. Using the mass spectrometric technique, they observed the formation of the cyclo-dimer of 1,1-dimethylsilanimine, which is 1,1,3,3-tetramethylcyclodisilazane (146 amu), represented by its fragment peak at m/z 131. In our experiment, 1,1-dimethylsilanimine can undergo head-to-tail cycloaddition to form 1,1,3,3-tetramethylcyclodisilazane as shown in Equation (4-6). The mass of 1,1,3,3-tetramethylcyclodisilazane (146 amu) overlaps with that of the photofragment mass peak at m/z 146 from HMDSZ. This makes it difficult to distinguish between the two masses. However, similar to what was observed by Letulle *et al.*,[136] the 1,1,3,3-tetramethylcyclodisilazane formed can lose one methyl group upon ionization by the VUV radiation. This leads to the observation of the weak peak at m/z 131 in our work.

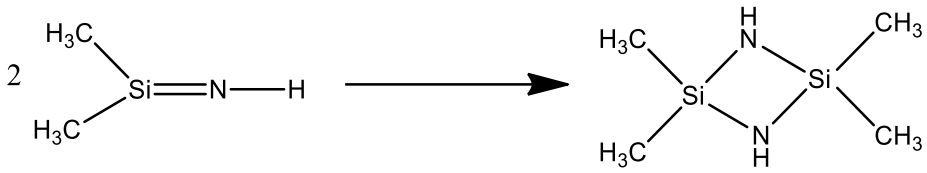

(4-6)

(1,1,3,3-tetramethylcyclodisilazane)

(146 amu)

4.2.2 Formation of Peaks in the Mass Regions Higher Than the Parent Mass of 161 amu

As stated earlier, several new mass peaks were observed in the high-mass region above 161 amu. These include the peaks at m/z 175, 189, 203, 219, 234, 264, 277, 292, 308, and 320.

4.2.2.1 Free Radical Short-Chain Reactions

As described in Section 3.3, the primary decomposition products of HMDSZ on the W filament are methyl and (trimethylsilylamino)dimethylsilyl radicals. This process serves as the initiation step in the HWCVD reactor. In the HWCVD reactor, secondary reactions of $\dot{C}H_3$ and $(CH_3)_3SiNH\dot{S}i(CH_3)_2$ radicals with the parent HMDSZ molecule are likely to occur. The primary radicals produced will react with each other or with the abundant parent molecule in the reactor chamber. It has long been known that methyl radicals can react with organosilicon molecules by abstracting the hydrogen atom attached to C atoms.[137, 138] The hydrogen abstraction by methyl radical is well known and they are found to be the main chain propagation steps in the short chain mechanisms that dominate the secondary gas-phase reactions when tetramethylsilane,[24] trimethylsilane,[77] and hexamethyldisilane[117] were used in a HWCVD reactor. The abstraction of H from C-

H bond in HMDSZ by the methyl radical is represented in Equation (4-6), which also propagates a chain reaction.

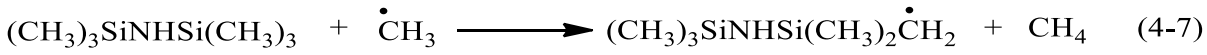

$$(CH_3)_3SiNHSi(CH_3)_3 + \dot{C}H_3 \longrightarrow (CH_3)_3SiNHSi(CH_3)_2\dot{C}H_2 + CH_4 \quad (4\text{-}7)$$

The subsequent recombination reactions between radicals produced in Equation (4-7) and the two primary radicals from Equation (3-3) terminate the short-chain reactions, leading to the formation of stable high-molecular-mass products as shown below:

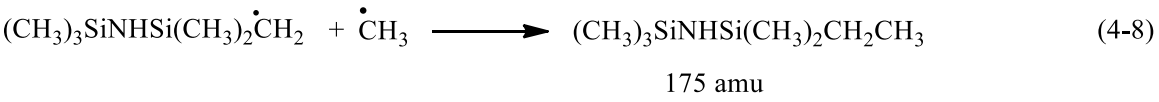

$$(CH_3)_3SiNHSi(CH_3)_2\dot{C}H_2 + \dot{C}H_3 \longrightarrow (CH_3)_3SiNHSi(CH_3)_2CH_2CH_3 \quad (4\text{-}8)$$

175 amu

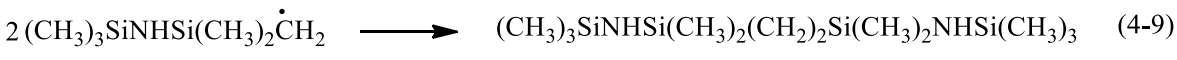

$$2\,(CH_3)_3SiNHSi(CH_3)_2\dot{C}H_2 \longrightarrow (CH_3)_3SiNHSi(CH_3)_2(CH_2)_2Si(CH_3)_2NHSi(CH_3)_3 \quad (4\text{-}9)$$

320 amu

$$2\,(CH_3)_3SiNH\dot{S}i(CH_3)_2 \longrightarrow (CH_3)_3SiNHSi(CH_3)_2Si(CH_3)_2NHSi(CH_3)_3 \quad (4\text{-}10)$$

292 amu

$$(CH_3)_3SiNHSi(CH_3)_2\dot{C}H_2 + (CH_2)_3SiNHS\dot{i}(CH_3)_2 \longrightarrow (CH_3)_3SiN(H)Si(CH_3)_2CH_2Si(CH_3)_2N(H)Si(CH_3)_3 \quad (4\text{-}11)$$

306 amu

The products from Equation (4-8), (4-9), and (4-10) seemed to be observed experimentally. The intensity of peak at m/z 175 was dominant in the high mass region. The peaks at m/z 175, 189 and 203 have a mass difference of 14 amu between the neighbouring peaks. This is because the produced species with 175 amu also has multiple CH_3 groups that contain C-H bond. Cycles of H-abstraction reaction and biradical recombination reaction lead to the formation of chemical species that has one or two additional CH_2 moiety in the products. The observation of peak at m/z 277 is a photofragment of peak at m/z 292 by losing one methyl group upon ionization by the 10.5 eV VUV photon. However, the signal of the stable product from Equation (4-6),

methane, was not observed due to its high IE of 12.6 eV, which is above the 10.5 eV used in this work. The product from Equation (4-10) with a mass of 306 amu was not observed in our mass spectra.

4.2.2.2 Other Products from Reactions Involving Silanimines

Silanimines are also known to undergo nucleophilic addition reactions as shown in Equation (4-12).[132]

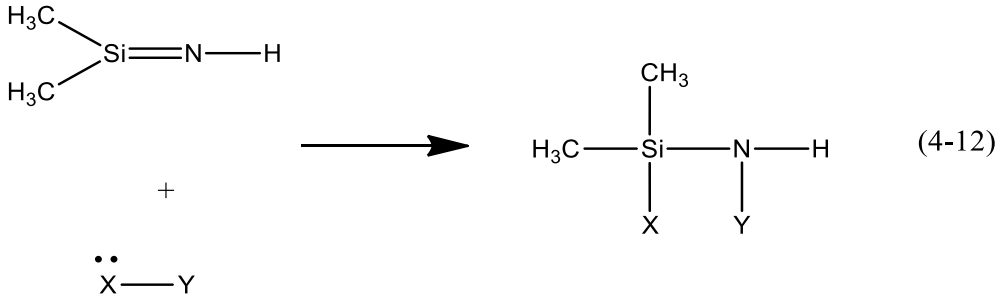

(4-12)

Nucleophiles containing O atoms such as water,[134] alcohol,[134, 139-141] silanols,[134] and silyl ethers, including $(CH_3)_3SiOCH_3$,[134, 142] $((CH_3)_2SiO)_3$,[134] $HSi(OC_2H_6)_3$,[143, 144] and $(CH_3)_3Si(OCH_3)_3$,[143, 144] all add to the S=N bond. Similarly, nitrogen-containing nucleophiles, such as $(CH_3)_2SiNSi(CH_3)_3$ and $(CH_3)_3SiN(CH_3)_2$[134] can also be added to silanimines. In our experiment, the peak at m/z 234 (octamethyltrisilazane) could be attributed to the nucleophilic attack by the abundant HMDSZ molecules to 1,1-dimethylsilanimine produced in the reactor, leading to the addition reaction as shown in Equation (4-13). The peak at m/z 234 can lose one methyl group leading to the observation of peak at m/z 219 upon ionization by the VUV radiation.

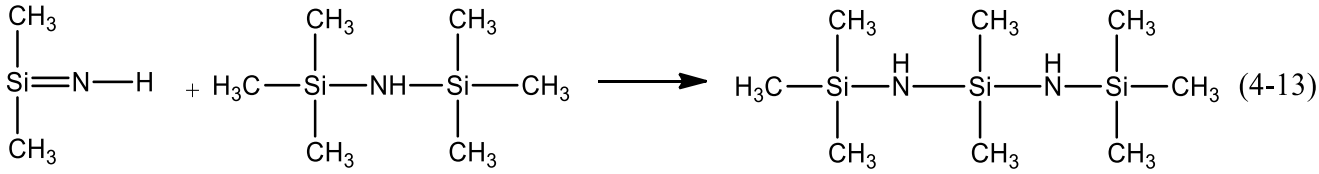

(Octamethyltrisilazane)

(234 amu)

(4-13)

4.3 Experiments with Deuterated Isotopomers on W filament

In order to help assign the mass peaks observed in the HWCVD reactor when using HMDSZ, experiments with deuterated isotopomers, including bis(trimethylsilyl)-N-deuterioamine (HMDSZ-d_1) and 1,1,1,3,3,3-hexa(deuteratedmethyl)disilazane (HMDSZ-d_{18}), were carried out under the same experimental conditions. For this, 12 Torr of 0.9% HMDSZ-d_1/He and 0.9 % HMDSZ-d_{18}/He were prepared, and mass spectra were recorded after filament was turned on in the filament temperature range of 1200 - 2000 ^oC.

4.3.1 Experiments with bis(trimethylsilyl)-N-deuterioamine

Figure 4-5 shows the mass spectra of 12 Torr 0.9% HMDSZ-d_1 in HWCVD reactor with W filament at 1700 ^oC. As mentioned earlier, with 0.9 % HMDSZ/He, the room-temperature 10.5 eV SPI mass spectrum was dominated by the parent HMDSZ ion at m/z 161 and the photofragment ion peak at m/z 146. When HMDSZ was replaced with bis(trimethylsilyl)-N-deuterioamine (HMDSZ-d1), the dominant peaks at m/z 146 and 161 were clearly shifted to m/z 147 and 162, respectively, and the dominance of these peaks are preserved, as shown in Figure 4-5(a). From the enlarged mass spectra shown in Figure 4-5(b) in the mass region between 2 and 140 amu, mass peaks at m/z 75 and 90 were observed. The peaks at m/z 75 and 90 are the corresponding peaks at m/z 74 and 89,

respectively, in the room-temperature mass spectrum of HMDSZ. In the enlarged mass spectra illustrated in Figure 4-5 (c), only the background peak at m/z 219 was observed.

It can be seen from Figure 4-5 (b) that a new peak at m/z 74 was observed when the filament was turned on. This indicates the formation of the isotopomer of 1,1-dimethylsilanimine-d_1, ($DN=Si(CH_3)_2$), with a mass of 74 amu. As described in Section 4.2.1.2, the formation of 1,1-dimethylsilanimine ($HN=Si(CH_3)_2$, 73 amu) occurred via the decomposition of (trimethylsilylamino)dimethylsilyl radical as represented by Equation (4-4). When HMDSZ-d1 was used, the corresponding radical product by the cleavage of Si-C bond is (trimethylsilylamino-d1)dimethylsilyl radical. Its decomposition according to Equation (4-14) produced 1,1-dimethylsilanimine-d_1. Therefore, the observation of the new peak at m/z 74 provided strong support for the existence of 1,1-dimethylsilanimine and its formation via the decomposition of the (trimethylsilylamino)dimethylsilyl radical.

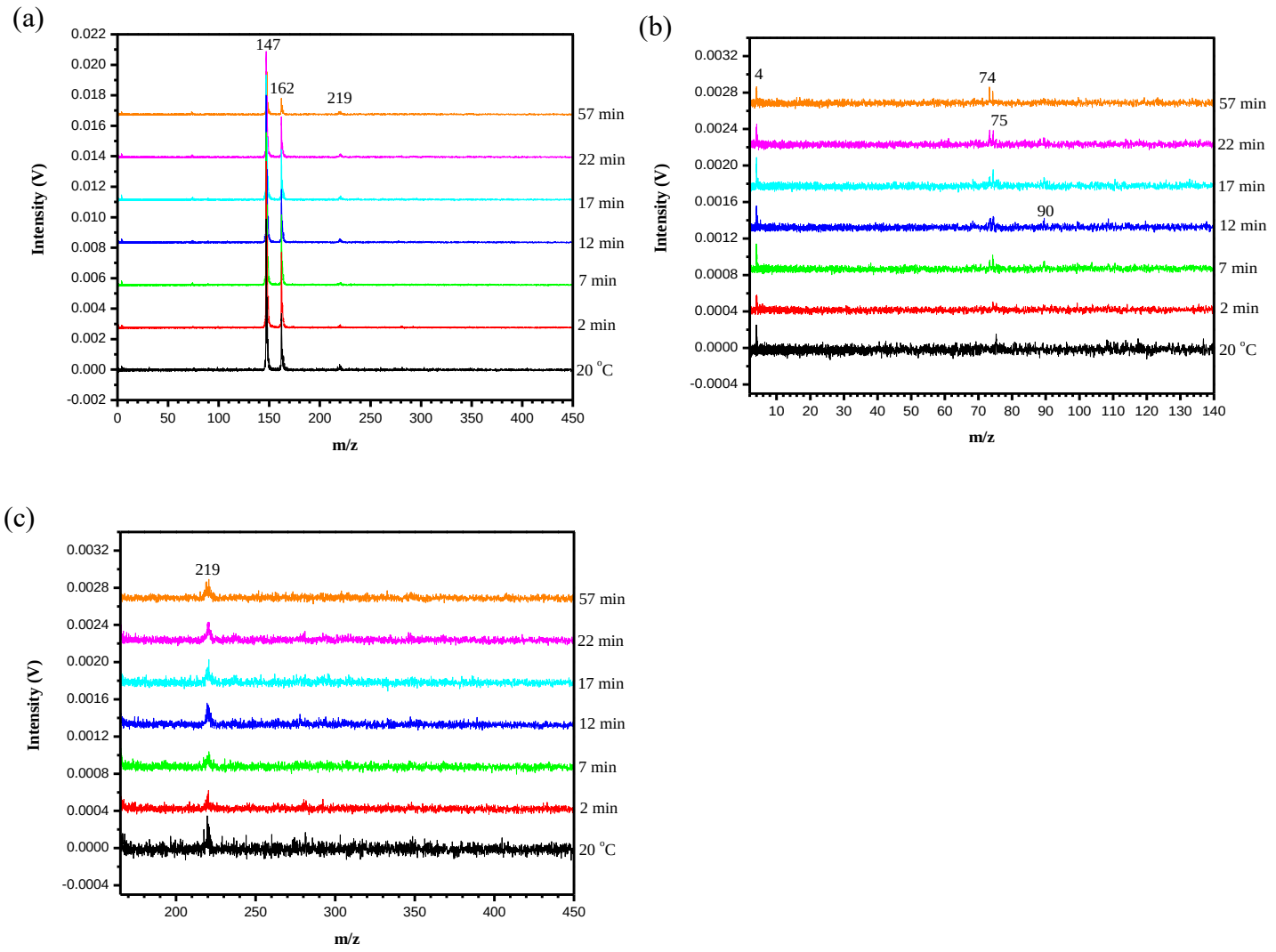

Figure 4-5: (a) 10.5 eV VUV SPI TOF mass spectra of 12 Torr 0.9 % HMDSZ-d1/He in HWCVD reactor with W filament at 1700 ºC. The spectrum at 20 ºC is recorded when the filament is off. (b) An enlarged picture of (a) in the mass region between 2 amu and 140 amu. (c) An enlarged picture of (a) in the mass region between 170 amu and 450 amu

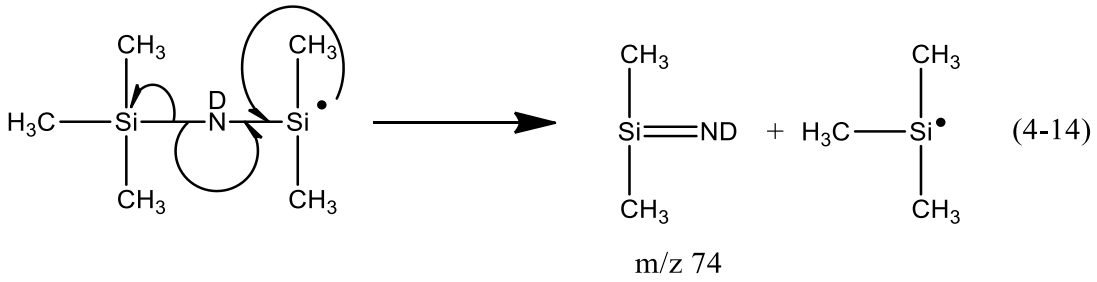

(4-14)

m/z 74

As shown in Figure 4-5(c), the usage of the HMDSZ-d1 isotopomer was not helpful in assigning peaks in the high mass regions. There was no new mass peaks observed in the high mass regions with HMDSZ-d1. This could be a result of their weak intensities and the fact that temperatures higher than 1700 ºC were not explored experimentally in this work. The peak at m/z 219 is a background peak, it is observed even when there is no source gas introduced into the system.

4.3.2 Experiments with 1,1,1,3,3,3-Hexa(deuteratedmethyl)disilazane

Figure 4-6 shows the mass spectra of 12 Torr 0.9 % HMDSZ-d18 in HWCVD reactor with W filament at 1700 ºC. As can be seen from Figure 4-6, when the filament was turned on, no new peaks were observed in both the low mass regions and high-mass regions. This is due to their weak intensities and the fact that temperatures higher than 1700 ºC were not explored experimentally in this work.

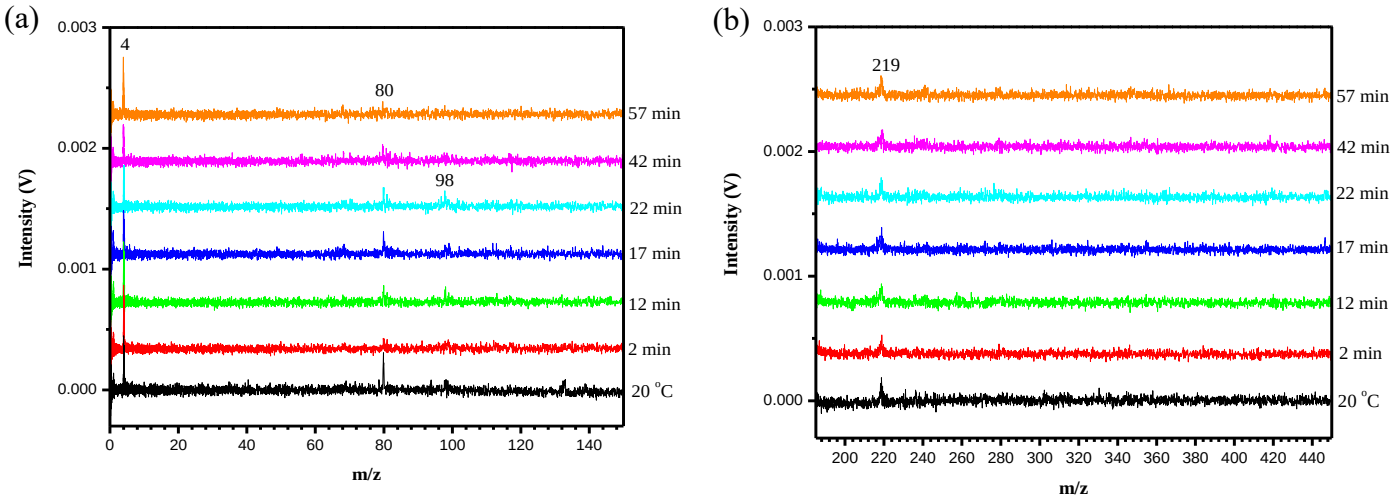

Figure 4-6: 10.5 eV VUV SPI TOF mass spectra of 12 Torr 0.9 % HMDSZ-d18/He in HWCVD reactor with W filament at 1700 ºC in the mass region of (a) 2 amu and 150 amu. (b) 170 amu and 450 amu. The spectrum at 20 ºC is recorded when the filament is off.

4.4. Secondary Gas-phase Reactions of HMDSZ in a HWCVD Reactor with Ta Filaments

Similarly, the secondary gas-phase reaction chemistry of HMDSZ on Ta was studied by introducing 12 Torr of 0.9 % HMDSZ/He in the HWCVD reactor in the temperature range of 1200 - 2000 ^{o}C. When the filament was turned on, the parent ion peak at m/z 161 and the predominant photofragment ion peak at m/z 146 also decreased with increasing filament temperature as shown in Figure 4-7(a). From the enlarged mass spectrum, at temperatures of 1900 - 2000 ^{o}C, the intensities of peak at 146 and 161 are just discernable from the baseline. This shows that the parent HMDSZ molecules decompose and consume more quickly at higher temperatures. In Figure 4-7(b), the enlarged mass spectrum shows similar new mass peaks at m/z 17, 73, 88, 130, and 131 when Ta was used as filament. Figure 4-8 illustrates the intensity distributions of peaks at m/z 146 and 161, respectively for both W and Ta filaments. On W, at 1900 ^{o}C, the intensity of peaks at m/z 146 and 161 show continual decrease with increasing filament-on time, whereas, at 2000 ^{o}C, the intensity plateaued after 25 minutes of reaction time. With regard to Ta, the intensity of peaks at m/z 146 and 161 plateaued after 5 minutes of reaction time at both 1900 ^{o}C and 2000 ^{o}C.

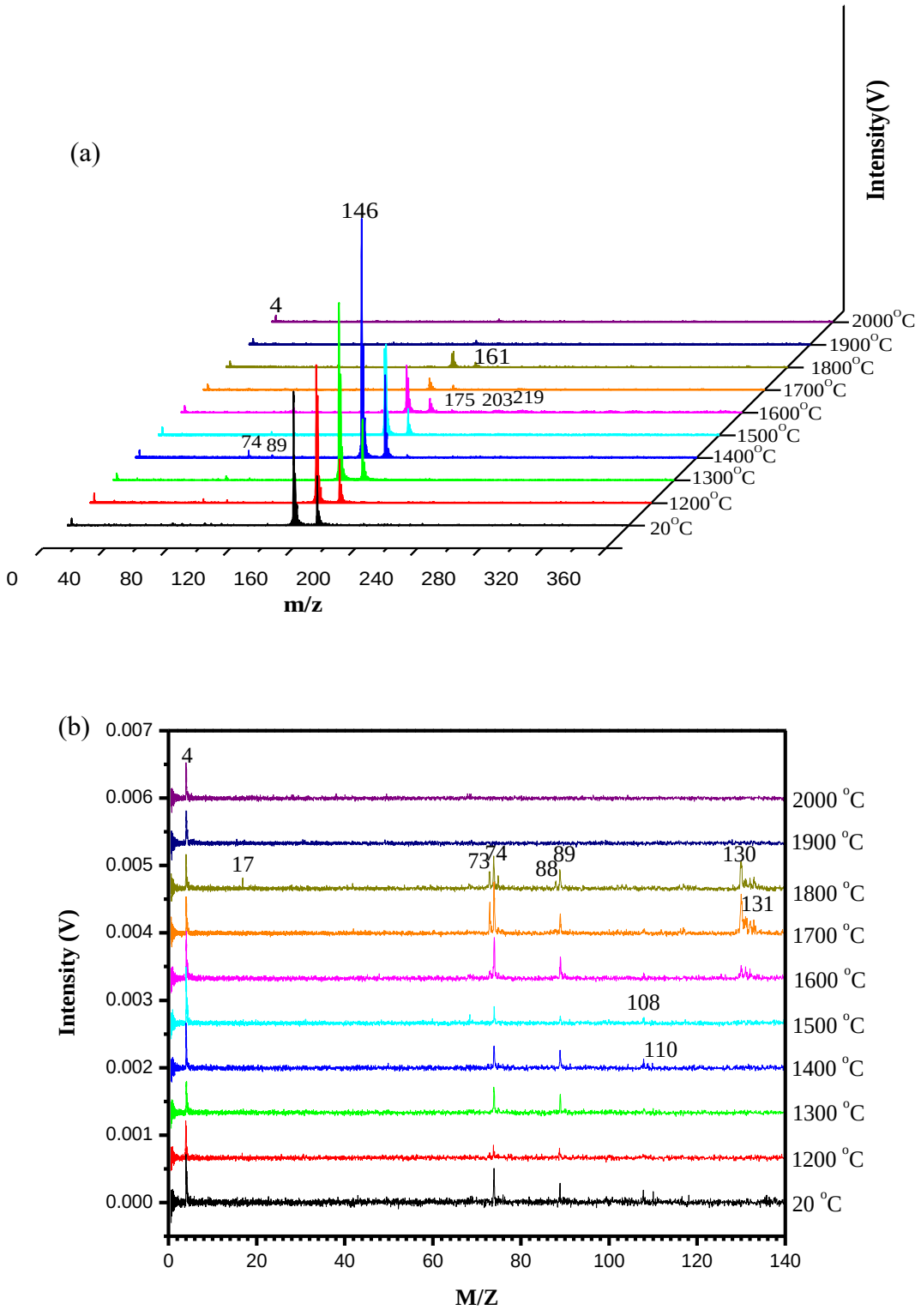

Figure 4-7: (a) 10.5 eV VUV SPI TOF mass spectra of 12 Torr 0.9% HMDSZ/He at Ta filament temperatures between 1200 ºC and 2000 ºC. The spectrum at 20 ºC is recorded when the filament is off (b) Enlarge spectra in mass regions between 2 amu and 140 amu

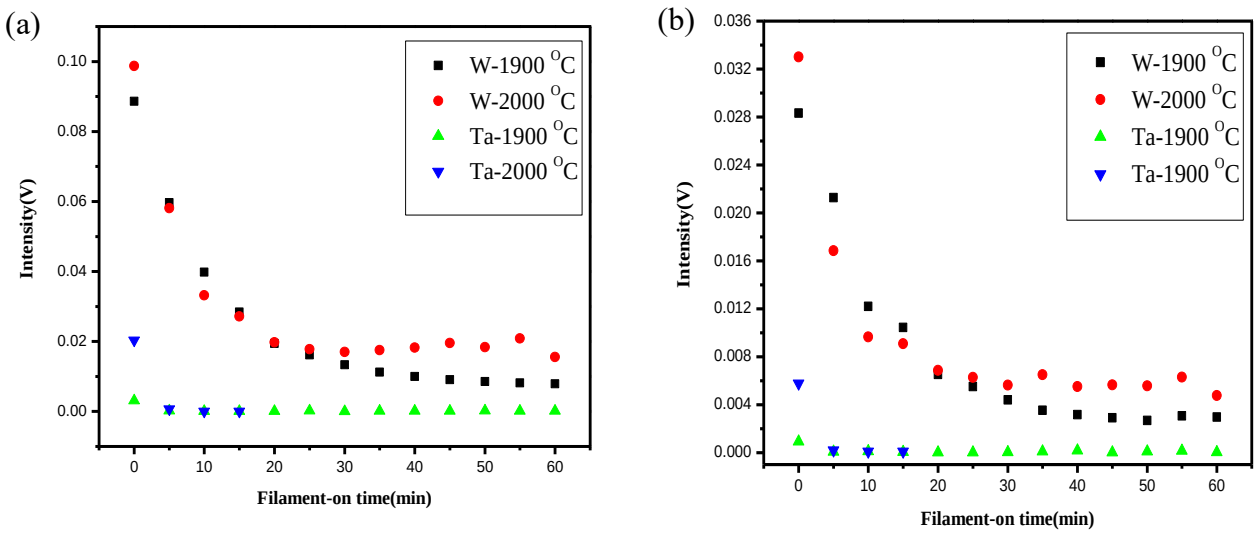

Figure 4-8: The peak intensity of (a) m/z 146 (b) m/z 161 as a function of filament-on time at 1900 ºC and 2000 ºC with W and Ta

From the enlarged picture shown in Figure 4-9, weak high mass peaks at m/z 175, 189, 203, 219, 234, 264, 277, 292, 308, and 320 were observed when the filament was turned on**.** The optimum temperatures for active chemistry in the high mass regions on W was observed in the range of 1500-2000 ºC, whereas, that of Ta was in the range of 1600-1800 ºC. It can, therefore, be concluded that the gas-phase chemistry of HMDZ was not affected by W or Ta materials.

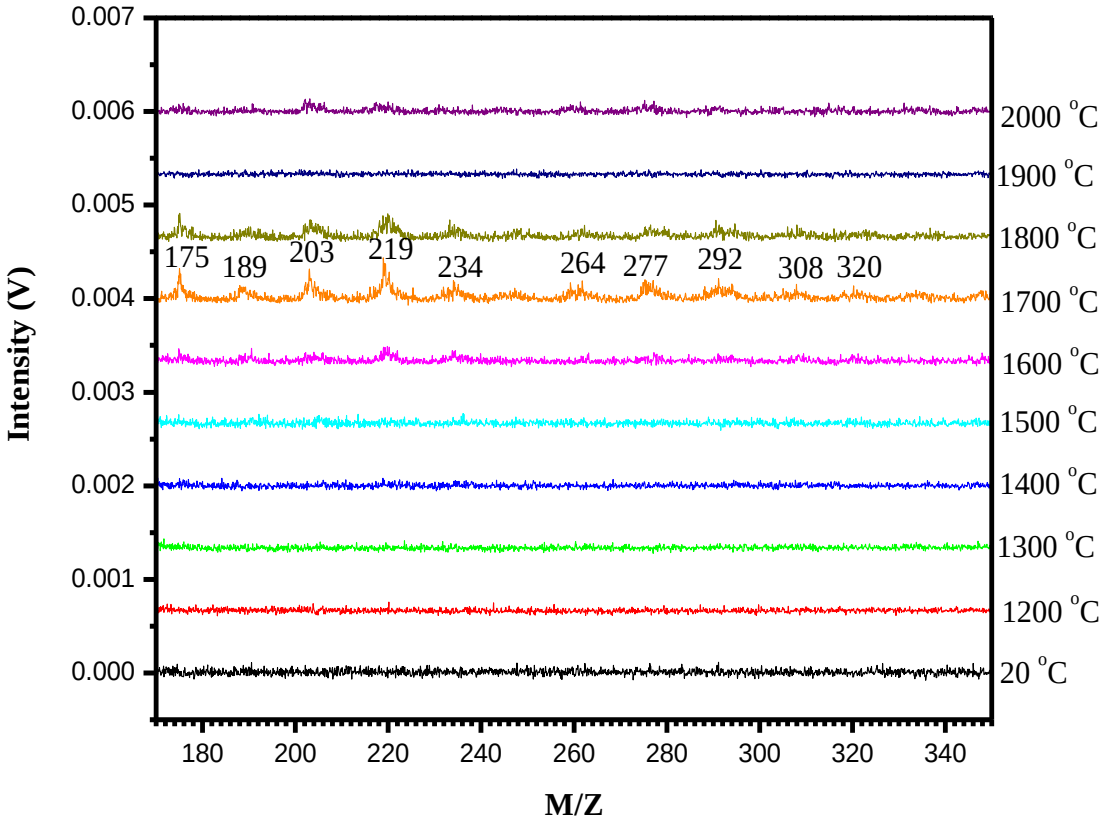

Figure 4-9: 10.5 eV SPI TOF mass spectra of 1% HMDSZ/He in HWCVD reactor of Ta filament temperature ranging from 1200 – 2000 º C at 32 minutes of reaction time in the mass regions of 165-360 amu

4.5 Summary

The secondary gas-phase reactions of HMDSZ in the HWCVD reactor when using W and Ta filaments were examined using SPI with a 118nm VUV wavelength coupled with TOF MS. In the secondary gas-phase reactions, species generated from the primary decomposition of HMDSZ react with each other and with the abundant HMDSZ molecules. The room-temperature 10.5 eV SPI mass spectrum was dominated by the parent HMDSZ ion at m/z 161 and the photofragment ion peak at m/z 146. When the filament was turned on, the intensity of the parent ion peak at m/z 161 and the predominant photofragment ion peak at m/z 146 decreased with an increase in filament temperature. This indicates that the parent HMDSZ decomposes on the filament and gets consumed in the secondary gas-phase reactions in the HWCVD reactor. When the filament was turned on, a new peak at m/z 73 (1,1-dimethylsilanimine) was observed in both W and Ta filaments, which increase with increase in temperature. This is as a result of fragmentation of (trimethylsilylamino)dimethylsilyl radical in the reactor. Experiments with the isotopomer, bis(trimethylsilyl)-N-deuterioamine (HMDSZ-d_1), confirmed the existence of 1,1-dimethylsilanimine and its formation via the decomposition of the (trimethylsilylamino)dimethylsilyl radical. Silanimines are known to dimerize easily to form cyclodisilazane. The 1,1-dimethylsilanimine formed in the reactor dimerizes to form 1,1,3,3-tetramethylcyclodisilazane (146 amu), shown in our experiments with the presence of its photofragment peak at m/z 131 upon ionization by the 10.5 eV SPI. Silanimines also undergo nucleophilic addition reactions. The peak at m/z 234 (octamethyltrisilazane) is attributed to the nucleophilic attack by the abundant parent molecules to 1,1-dimethylsilanimine produced in the reactor.

Another mechanism that operated in the secondary gas-phase reactions in the HWCVD reactor with HMDSZ is the free radical short-chain reaction. The primary decomposition of HMDSZ on the metal filaments to produce methyl radicals initiates the chain reaction. The hydrogen abstraction by methyl radical is the main propagation step in the reactor. The biradical recombination reactions terminate the chain reaction, leading to the formation of various stable products in the high mass regions. These high-molecular-mass products include those observed at m/z 175, 189, 203, 292 and 320.

Chapter Five: Conclusions and Future Work

5.1 Conclusions

Hot-wire chemical vapor deposition (HWCVD), also known as catalytic CVD (Cat-CVD), is a promising method for preparing silicon-based thin films. HWCVD has many advantages compared to the conventionally used CVD techniques such as low-pressure CVD (LPCVD) and plasma-enhanced CVD (PECVD). The technique of HWCVD offers the advantages of low substrate temperature, high deposition rate, minimal damage to the deposited film, and low equipment cost. HWCVD consists of three processes: (a) catalytic decomposition of source gas by resistively heated metal filament to produce reactive radical species; (b) gas-phase reactions of these reactive radical species with each other and with the abundant source gas; and (c) surface reactions with the final mixture of growth precursors on the substrate placed near the heated filament, but kept at relatively low temperature (~300 ^{o}C), leading to film growth. Film growth in HWCVD is induced by reactive species in the gas phase and these film growth precursors come from direct decomposition on the filament or from the secondary reactions in the gas phase. The properties and quality of the deposited films are governed by the gas-phase film growth precursor species. Therefore, it is important to identify the gas-phase chemical species for a better understanding of the HWCVD processes.

Silicon nitride (SiN_x) and silicon carbonitride (SiC_yN_z) thin films deposited by HWCVD have attracted great attention due to the combination of Si-C and Si-N binary compounds properties, which makes them suitable for many applications such as solar cell, flat panel display, optical memory and anti-reflective coatings. Most CVD growths of SiN_x and SiC_yN_z proceed through the use of separate Si-containing molecules (e.g., SiH_4), C-bearing molecules (*e.g.,* CH_4) and NH_3 as source gases. Handling of pyrophoric

silane is difficult, and the process of optimization with multiple source gases is extremely complex. This has urged interest in exploring alternative single-source precursors for SiN_x and SiC_yN_z deposition. 1,1,1,3,3,3-Hexamethyldisilazane (HMDSZ), a methyl-substituted disilazane molecule, contains both Si-C and Si-N bonds which can readily be incorporated into the SiC_yN_z films. In addition, HMDSZ is non-explosive, non-toxic, inexpensive, and commercially available.

In this work, the primary decomposition of HMDSZ on W and Ta filaments were investigated using single-photon ionization (SPI) with a vacuum ultraviolet (VUV) laser radiation of a 118-nm wavelength coupled with time-of-flight mass spectrometry (TOF MS). The formation of methyl radicals was found to be the common decomposition pathway on heated W and Ta metal surfaces. The intensity of the methyl radical increases with increase in filament temperature for both W and Ta when the temperature is higher than 1700 – 1800 ºC. The apparent activation energy for the formation of methyl radical on W filament was determined to be 71.2 ± 9.1 $kJmol^{-1}$, whereas that for Ta filament was 76.7 ± 8.1 $kJmol^{-1}$. This indicates that W and Ta exhibit similar apparent activation energies for methyl radical production.

In order to better understand the role that metal filaments play in the dissociation processes of HMDSZ, the decomposition pathways of HMDSZ in the gas phase were examined using *ab initio* methods. From the theoretical calculations, the reaction enthalpy for the homolytic cleavage of Si-C bond was determined to be 86.8 kcal/mol (*i.e.*, 363.2 kJ/mol) The experimentally determined activation energies for the production of CH_3, 71.2 ± 9.1 kJ/mol and 76.7 ± 8.1 kJ/mol for W and Ta respectively are much lower than the theoretically determined value of 86.8 kcal/mol (*i.e.*, 363.2 kJ/mol) for the

Si-C bond cleavage in HMDSZ. This clearly suggests that the dissociation of HMDSZ on both W and Ta filaments is a catalytic process. W or Ta metal wire serves as a catalyst in the cracking of HMDSZ molecules.

Aside from the homolytic cleavage of Si-C, Si-N, and N-H bonds, concerted and stepwise decomposition pathways of HMDSZ have been systematically explored using *ab initio* methods at the CCSD(T)/6-311++G(d,p)//B3LYP/6-311++G(d,p) level of theory. Four concerted decomposition routes were identified, leading to the formation of 1,1-dimethyl silanimine (P1) and tetramethylsilane (P2) in the concerted CR-1 route, 1,1-dimethylsilene (P3) and trimethylsilylamine (P4) in CR-2, (trimethylsilyl)dimethylsilanimine (P5) and methane (P6) in CR-3, and 1-trimethylsilylamino-1-methylsilene (P8) and P6 in CR-4. The transition state for all four concerted routes were successfully located. A comparison of all the four concerted pathways showed that the formation of P3 and P4 in route CR-2 is most energetically favourable with the lowest activation enthalpy of 66.4 kcal/mol, whereas methane elimination in CR-4 has the highest value of 88.9 kcal/mol. In the stepwise routes, the transition states for SR-1b-1 (the elimination of trimethylsilyl (I3) from I1), SR-1b-3 (1,2-H shift in I1), SR-2b-3 (1,2-H shift in I3) were successfully located. The elimination of H from the C atom attached to a Si atom in a silyl radical proceeds with no activation barrier. This is illustrated in the two routes of SR-1b-2 (elimination of H from I1) and SR-2b-2 (elimination of H from I3). Also, the elimination of CH_3 radical from a methylated silylamino radical proceeds with no transition state, as is shown in SR-2b-1 (elimination of CH_3 from I4) and SR-3b (elimination of CH_3 from I6). A comparison of all the stepwise pathways revealed that the elimination of trimethylsilyl (I3) from I1 in

SR-1b-1 route is most energetically favourable with the lowest activation enthalpy of 60.6 kcal/mol, whereas the SR-2b-3 route (1,2-H shift in I3) has the highest value of 64.0 kcal/mol.

In order to understand the effect of temperature on the reaction kinetics and thermochemistry, the kinetic ($\Delta H^{\ddagger}_{298}$, $\Delta G^{\ddagger}_{298}$, $\Delta S^{\ddagger}_{298}$) and thermochemical ($\Delta H_{298}$, ΔG_{298}, ΔS_{298}) parameters were computed for the room temperature of 298 K to examine the effect of temperature change on the activation and reaction enthalpy ($\Delta H^{\ddagger}$, ΔH), entropy ($\Delta S^{\ddagger}$, ΔS), and Gibbs free energy ($\Delta G^{\ddagger}$, ΔG). From the *ab initio* calculations, increasing the temperature to 298 K did not affect much the reaction kinetics and thermochemistry.

The secondary gas-phase reaction chemistry of HMDSZ in the HWCVD reactor under practical deposition pressures with W or Ta filaments was explored by introducing 12 Torr of 0.9 % HMDSZ diluted in He in the HWCVD reactor. When the filament was turned on, the intensity of the parent ion at m/z 161 and the predominant photofragment ion at m/z 146 decreases with the increase in temperature. This shows that the parent HMDSZ decomposes on the filament and gets consumed in the secondary gas-phase reactions in the HWCVD reactor. At the same time, new peaks at m/z 17 and 73 were observed. The peaks at m/z 17 and 73 were assigned to ammonia and 1,1-dimethylsilanimine, respectively. The NH_3 peak at m/z 17 increases with increase in temperature. It is believed that NH_3 is produced in-situ in a HWCVD reactor with HMDSZ in the presence of the filament. The 1,1-dimethylsilanimine peak at m/z 73 is as a result of fragmentation of (trimethylsilylamino)dimethylsilyl radical in the reactor and this was confirmed by an isotopomer experiment with bis(trimethylsilyl)-N-deuterioamine (HMDSZ-d1).

Silanimines are known to dimerize to form cycloaddition. The 1,1-dimethylsilanimine undergo dimerization to form 1,1,3,3-tetramethylcyclodisilazane (146 amu). The peak observed at m/z 234 (octamethyltrisilazane) is a result of nucleophilic attack by the abundant parent molecules to 1,1-dimethylsilanimine produced in the reactor. Free radical short-chain reaction is another mechanism utilized in the secondary gas-phase reactions. This is initiated by the primary decomposition of HMDSZ on the metal filaments to produce methyl radicals. The hydrogen abstraction by methyl radical is the main propagation step in the reactor and the chain is terminated by biradical recombination reactions to form various stable products in the high mass regions.

5.2 Future Work

In this work, primary decomposition of HMDSZ on W and Ta filaments and its secondary reaction chemistry in a HWCVD reactor were investigated. As discussed in Chapter 4, the hydrogen abstraction reaction by the methyl radical constitutes the main chain propagation step. This reaction also forms a stable methane molecule, which was not observed due to its high IE of 12.6 eV. In order to observe the methane and other species such as hydrogen with IE > 10.5 eV, a dual ionisation source developed in the Shi laboratory can be proposed. A dual ionization source consists of SPI and laser induced electron impact ionization (LIEI). In this source the LiF lens after the gas cell is removed and the path of the laser adjusted to aim at the repeller plate. This technique is versatile and capable of ionising all species of interest. In addition, it is achieved in one source, without the need to switch between the SPI and LIEI modes.

In order to assign the new peaks unambiguously, experiments with the isotopomers of HMDSZ-d1 and HMDSZ-d18 at temperatures higher than 1700 ^{o}C will be performed.

Also, to further confirm the existence and production of 1,1-dimethylsilanimine in the reactor, trapping experiment with *t*-butanol is proposed. 1,1-dimethylsilanimine is known to react with t-butanol to form 1-*t*-Butoxy-1,1-dimethylsilanamine.

As decomposition reactions studied in this work occurred at high temperatures, the kinetic and thermochemical parameters of relevant reactions, such as the formation of methyl radical via homolytic Si-CH_3 bond cleavage along with the stepwise and concerted formation of 1,1-dimethylsilanimine at high temperatures (900 – 2000 ºC) need to be calculated.

In the future, it will be interesting to examine another methyl-substituted disilazane containing Si-C, Si-N and Si-H, for example 1,1,3,3-tetramethyldisilazane (TMDSZ) both experimentally and theoretically to test if the Si-H bond will have an effect on the decomposition chemistry, for example the production of methyl radical and 1,1-dimethylsilanimine, in the process of HWCVD.

References

1. Seshan, K., Handbook of thin film deposition processes and techniques. **2001**.
2. Vossen, J. L.; Kern, W., Thin film processes II. **1991**.
3. Maissel, L. I.; Glang, R., Handbook of thin film technology. **1970**.
4. Mattox, D. M., Handbook of physical vapor deposition (PVD) processing. **2010**.
5. Hugh, O. P., Handbook of chemical vapor deposition: Principles, Technology and Applications. **1999**.
6. Park, J. H.; Sudarshan, T. S., Chemical vapor deposition. **2001**.
7. Pierson, H. O., Handbook of chemical vapor deposition (CVD): Principles, technology, and applications. **1992**.
8. Bunshah, F. R., Handbook of deposition technologies for films and coatings: Science, technology and applications. **1994**.
9. Mahan, A. H.; Nelson, B. P.; Salamon, S.; Crandall, R. S., Deposition of device quality, low H content a-Si-H by the hot-wire technique. *Journal of Non-Crystalline Solids* **1991,** *137*, 657-660.
10. Matsumura, H., High-quality amorphous silicon germanium produced by catalytic chemical vapor deposition. *Applied Physics Letters* **1987,** *51* (11), 804-805.
11. Matsumura, H., Formation of silicon-based thin films prepared by catalytic chemical vapor deposition (Cat-CVD) method. *Japanese Journal of Applied Physics Part 1-Regular Papers Short Notes & Review Papers* **1998,** *37* (6A), 3175-3187.
12. Tabata, A.; Nakajima, T.; Mizutani, T.; Suzuoki, Y., Preparation of wide-gap hydrogenated amorphous silicon carbide thin films by hot-wire chemical vapor deposition at a low tungsten temperature. *Japanese Journal of Applied Physics Part 2-Letters* **2003,** *42* (1A-B), L10-L12.
13. Mahan, A. H.; Carapella, J.; Nelson, B. P.; Crandall, R. S.; Balberg, I., Deposition of device quality, low H content amorphous-silicon. *Journal of Applied Physics* **1991,** *69* (9), 6728-6730.
14. Matsumura, H., Summary of research in NEDO Cat-CVD project in Japan. *Thin Solid Films* **2001,** *395* (1-2), 1-11.
15. Matsumura, H.; Umemoto, H.; Masuda, A., Cat-CVD (hot-wire CVD): how different from PECVD in preparing amorphous silicon. *Journal of Non-Crystalline Solids* **2004,** *338*, 19-26.
16. Grunsky, D.; Kupich, M.; Hofferberth, B.; Schroeder, B., Investigation of the tantalum catalyst during the hot wire chemical vapor deposition of thin silicon films. *Thin Solid Films* **2006,** *501* (1-2), 322-325.
17. Sakai, M.; Tsutsumi, T.; Yoshioka, T.; Masuda, A.; Matsumura, H., High performance amorphous-silicon thin film transistors prepared by catalytic chemical vapor deposition with high deposition rate. *Thin Solid Films* **2001,** *395* (1-2), 330-334.
18. Shumpei, K. W.; Ichiro, T., Silicon nitride prepared by the SiH_4-NH_3 reaction with catalysts*. *Japanese Journal of Applied Physics* **1970,** *9* (12), 1467-1477.
19. Wiesmann, H.; Ghosh, A. K.; McMahon, T.; Strongin, M., A-Si-H produced by high-temperature thermal-decomposition of silane. *Journal of Applied Physics* **1979,** *50* (5), 3752-3754.
20. Matsumura, H.; Tachibana, H., Amorphous-silicon produced by a new thermal chemical vapor-deposition method using intermediate species SiF_2. *Applied Physics Letters* **1985,** *47* (8), 833-835.
21. Matsumura, H.; Ihara, H., Catalytic chemical vapor-deposition method to prepare high-quality hydrofluorinated amorphous-silicon. *Journal of Applied Physics* **1988,** *64* (11), 6505-6509.

22. Matsumura, H., Silicon-nitride produced by catalytic chemical vapor-deposition method. *Journal of Applied Physics* **1989,** *66* (8), 3612-3617.
23. Matsumura, H., Formation of polysilicon films by catalytic chemical vapor-deposition (cat-CVD) method. *Japanese Journal of Applied Physics Part 2-Letters & Express Letters* **1991,** *30* (8B), L1522-L1524.
24. Li, X. M.; Eustergerling, B. D.; Shi, Y. J., Mass spectrometric study of gas-phase chemistry in a hot-wire chemical vapor deposition reactor with tetramethylsilane. *International Journal of Mass Spectrometry* **2007,** *263* (2-3), 233-242.
25. Toukabri, R.; Shi, Y. J., Effect of pressure on the gas-phase chemistry when using monomethylsilane and dimethylsilane in hot-wire chemical vapor deposition. *Canadian Journal of Chemistry* **2015,** *93* (1), 82-90.
26. Badran, I., Hot-wire chemical vapor deposition chemistry and kinetics of new precursors in gas phase and on the wire surface. *PhD., University of Calgary (Canada)* **2014**.
27. Doyle, J.; Robertson, R.; Lin, G. H.; He, M. Z.; Gallagher, A., Production of high-quality amorphous-silicon films by evaporative silane surface decomposition. *Journal of Applied Physics* **1988,** *64* (6), 3215-3223.
28. Matsumura, H., Study on catalytic chemical vapor-deposition method to prepare hydrogenated amorphous-silicon. *Journal of Applied Physics* **1989,** *65* (11), 4396-4402.
29. Brogueira, P.; Conde, J. P.; Arekat, S.; Chu, V., Low filament temperature deposition of a-Si-H by hot-wire chemical-vapor-deposition. *Journal of Applied Physics* **1995,** *78* (6), 3776-3783.
30. Schropp, R. E. I., Advances in solar cells made with hot wire chemical vapor deposition (HWCVD): superior films and devices at low equipment cost. *Thin Solid Films* **2002,** *403*, 17-25.
31. Field, J. E., The properties of natural and synthetic diamond. **1992**.
32. Spitsyn, B. V.; Bouilov, L. L.; Derjaguin, B. V., Vapor growth of diamond on diamond and other surfaces. *Journal of Crystal Growth* **1981,** *52* (APR), 219-226.
33. Matsumoto, S.; Sato, Y.; Kamo, M.; Setaka, N., Vapor-deposition of diamond particles from methane. *Japanese Journal of Applied Physics Part 2-Letters* **1982,** *21* (4), L183-L185.
34. Motahari, H.; Moemen Bellah, S.; Malekfar, R., *A new tubular hot-wire CVD for diamond coating*. 2017; Vol. 123.
35. Anderson, D. A.; Spear, W. E., Electrical and optical-properties of amorphous silicon-carbide, silicon-nitride and germanium carbide prepared by glow-discharge technique. *Philosophical Magazine* **1977,** *35* (1), 1-16.
36. Tehrani, F. S.; Badaruddin, M. R.; Rahbari, R. G.; Muhamad, M. R.; Rahman, S. A., Low-pressure synthesis and characterization of multiphase SiC by HWCVD using CH_4/SiH_4. *Vacuum* **2012,** *86* (8), 1150-1154.
37. Kamble, M.; S. Waman, V.; Mayabadi, A.; Ghosh, S.; B. Gabhale, B.; Rondiya, S.; Rokade, A.; Khadtare, D. S.; Sathe, V.; Shripathi, T.; Pathan, H.; W. Gosavi, S.; Jadkar, S., Hydrogenated silicon carbide thin films prepared with high deposition rate by hot wire chemical vapor deposition method. *Journal of Coatings* 2014; Vol. *2014*, p 1-11.
38. Lee, M. S.; Bent, S. F., Spectroscopic and thermal studies of a-SiC : H film growth: Comparison of mono-, tri-, and tetramethylsilane. *Journal of Vacuum Science & Technology a-Vacuum Surfaces and Films* **1998,** *16* (3), 1658-1663.
39. Mahan, A. H., An update on silicon deposition performed by hot wire CVD. *Thin Solid Films* **2006,** *501* (1-2), 3-7.
40. Umeda, T.; Mochizuki, Y.; Miyoshi, Y.; Nashimoto, Y., Charge-trapping defects in Cat-CVD silicon nitride films. *Thin Solid Films* **2001,** *395* (1-2), 266-269.

41. Takano, M.; Niki, T.; Heya, A.; Osono, T.; Yonezawa, Y.; Minamikawa, T.; Muroi, S.; Minami, S.; Masuda, A.; Umemoto, H.; Matsumura, H., Preparation of low-stress SiN_x films by catalytic chemical vapor deposition at low temperatures. *Japanese Journal of Applied Physics Part 1-Regular Papers Brief Communications & Review Papers* **2005,** *44* (6A), 4098-4102.
42. Stannowski, B.; Rath, J. K.; Schropp, R. E. I., Growth process and properties of silicon nitride deposited by hot-wire chemical vapor deposition. *Journal of Applied Physics* **2003,** *93* (5), 2618-2625.
43. Verlaan, V.; Houweling, Z. S.; van der Werf, C. H. M.; Romijn, I. G.; Weeber, A. W.; Goldbach, H. D.; Schropp, R. E. I., Deposition of device quality silicon nitride with ultra high deposition rate (> 7 nm/s) using hot-wire CVD. *Thin Solid Films* **2008,** *516* (5), 533-536.
44. Mahan, A. H.; Dillon, A. C.; Gedvilas, L. M.; Williamson, D. L.; Perkins, J. D., Properties of thin film silicon nitride deposited by hot wire chemical vapor deposition using silane, ammonia, and hydrogen gas mixtures. *Journal of Applied Physics* **2003,** *94* (4), 2360-2367.
45. Liu, F. Z.; Ward, S.; Gedvilas, L.; Keyes, B.; To, B.; Wang, Q.; Sanchez, E.; Wang, S. L., Amorphous silicon nitride deposited by hot-wire chemical vapor deposition. *Journal of Applied Physics* **2004,** *96* (5), 2973-2979.
46. Ansari, S. G.; Umemoto, H.; Morimoto, T.; Yoneyama, K.; Izumi, A.; Masuda, A.; Matsumura, H., H-2 dilution effect in the Cat-CVD processes of the SiH_4/NH_3 system. *Thin Solid Films* **2006,** *501* (1-2), 31-34.
47. Eustergerling, B.; Heden, M.; Shi, Y. J., Application of laser induced electron impact ionization to the deposition chemistry in the hot-wire chemical vapor deposition process with SiH_4-NH_3 gas mixtures. *Journal of the American Society for Mass Spectrometry* **2007,** *18* (11), 1950-1958.
48. Holt, J. K. M., M. S.; Goodwin, D. F.; Atwater, H. A., In Amorphous and heterogeneous silicon-base films. *Material Research Society Symposium Proceedings* **2002,** *Vol 715. Abelson, J. R.; Boyce, J. B.; Cohen, J. D.; Matsumura, H.; Robertson, J., Eds.; Warrendale, p A10.2.*
49. Chu, T. L.; Lee, C. H.; Gruber, G. A., Preparation and properties of amorphous silicon nitride films. *Journal of the Electrochemical Society* **1967,** *114* (7), 717-&.
50. Grieco, M. J.; Worthing, F. L.; Schwartz, B., Silicon nitride thin films from $SiCl_4$ plus NH_3 - preparation and properties. *Journal of the Electrochemical Society* **1968,** *115* (5), 525-+.
51. Roger, C.; Corbitt, T. S.; Hampdensmith, M. J.; Kodas, T. T., Aerosol-assisted chemical-vapor-deposition of copper - a liquid delivery approach to metal thin-films. *Applied Physics Letters* **1994,** *65* (8), 1021-1023.
52. Hampden-smith, M. J., Kodas, T.T., Chemical vapor deposition of metals: Part 1. An overview of CVD processes. *Chemical Vapor Deposition* **1995,** *1*, 8-23.
53. Wrobel, A. M.; Blaszczyk-Lezak, I.; Uznanski, P.; Glebocki, B., Remote hydrogen microwave plasma chemical vapor deposition of amorphous silicon carbonitride (a-SiCN) coatings derived from tris(dimethylamino)silane. *Plasma Processes and Polymers* **2011,** *8* (6), 542-556.
54. Blaszczyk-Lezak, I.; Wrobel, A. M.; Kivitorma, M. P. M.; Vayrynen, I. J.; Aoki, T., Remote hydrogen microwave plasma chemical vapor deposition of silicon carbonitride films from a (dimethylamino)dimethylsilane precursor: Characterization of the process, chemical structure, and surface morphology of the films. *Diamond and Related Materials* **2006,** *15* (9), 1484-1491.
55. Blaszczyk-Lezak, I.; Wrobel, A. M., Silicon carbonitride by remote microwave plasma CVD from organosilicon precursor: Physical and mechanical properties of deposited Si : C : N films. *Applied Surface Science* **2007,** *253* (18), 7404-7411.

56. Fainer, N. I.; Rumyantsev, Y. M.; Kosinova, M. L.; Yurjev, G. S.; Maximovskii, E. A.; Kuznetsov, F. A., The investigation of properties of silicon nitride films obtained by RPECVD from hexamethyldisilazane. *Applied Surface Science* **1997,** *113-114*, 614-617.
57. Wrobel, A. M.; Walkiewicz-Pietrzykowska, A.; Blaszczyk-Lezak, I., Reactivity of organosilicon precursors in remote hydrogen microwave plasma chemical vapor deposition of silicon carbide and silicon carbonitride thin-film coatings. *Applied Organometallic Chemistry* **2010,** *24* (3), 201-207.
58. Taguchi, K.; Yoshimoto, M.; Saraie, J., Reduction of carbon impurity in silicon nitride films deposited from metalorganic source. *Japanese Journal of Applied Physics Part 2-Letters* **2004,** *43* (2A), L148-L150.
59. Izumi, A.; Oda, K., Deposition of SiCN films using organic liquid materials by HWCVD method. *Thin Solid Films* **2006,** *501* (1-2), 195-197.
60. Collins, R. H. D., F. T., Process for improving photoresist adhesion. *United State Patent* **1970,** *3,549,368*.
61. Morimoto, T.; Ansari, S. G.; Yoneyama, K.; Nakajima, T.; Masuda, A.; Matsumura, H.; Nakamura, M.; Umemoto, H., Mass-spectrometric studies of catalytic chemical vapor deposition processes of organic silicon compounds containing nitrogen. *Japanese Journal of Applied Physics Part 1-Regular Papers Brief Communications & Review Papers* **2006,** *45* (2A), 961-966.
62. Rahman, M. M.; Hasan, S. K., Ellipsometric, XPS and FTIR study on SiCN films deposited by hot-wire chemical vapor deposition method. *Materials Science in Semiconductor Processing* **2016,** *42*, 373-377.
63. Belmahi, M.; Bulou, S.; Thouvenin, A.; de Poucques, L.; Hugon, R.; Le Brizoual, L.; Miska, P.; Geneve, D.; Vasseur, J. L.; Bougdira, J., Microwave plasma process for SiCN:H thin films synthesis with composition varying from SiC:H to SiN:H in H-2/N-2/Ar/hexamethyldisilazane gas mixture. *Plasma Processes and Polymers* **2014,** *11* (6), 551-558.
64. Bulou, S.; Le Brizoual, L.; Miska, P.; de Poucques, L.; Bougdira, J.; Belmahi, M., Wide variations of SiC_xN_y:H thin films optical constants deposited by H-2/N-2/Ar/hexamethyldisilazane microwave plasma. *Surface & Coatings Technology* **2012,** *208*, 46-50.
65. Duan, H. L.; Zaharias, G. A.; Bent, S. F., Detecting reactive species in hot wire chemical vapor deposition. *Current Opinion in Solid State & Materials Science* **2002,** *6* (5), 471-477.
66. Nozaki, Y.; Kongo, K.; Miyazaki, T.; Kitazoe, M.; Horii, K.; Umemoto, H.; Masuda, A.; Matsumura, H., Identification of Si and SiH in catalytic chemical vapor deposition of SiH_4 by laser induced fluorescence spectroscopy. *Journal of Applied Physics* **2000,** *88* (9), 5437-5443.
67. Nozaki, Y.; Kitazoe, M.; Horii, K.; Umemoto, H.; Masuda, A.; Matsumura, H., Identification and gas phase kinetics of radical species in Cat-CVD processes of SiH_4. *Thin Solid Films* **2001,** *395* (1-2), 47-50.
68. Crosley, D. R., Laser-induced fluorescence in spectroscopy, dynamics, and diagnostics. *Journal of Chemical Education* **1982,** *59* (6), 446-455.
69. Berden, G.; Peeters, R.; Meijer, G., Cavity ring-down spectroscopy: Experimental schemes and applications. *International Reviews in Physical Chemistry* **2000,** *19* (4), 565-607.
70. Ledingham, K. W. D.; Singhal, R. P., High intensity laser mass spectrometry - A review. *International Journal of Mass Spectrometry and Ion Processes* **1997,** *163* (3), 149-168.
71. McEnally, C. S.; Pfefferle, L. D.; Mohammed, R. K.; Smooke, M. D.; Colket, M. B., Mapping of trace hydrocarbon concentrations in two-dimensional flames using single-photon photoionization mass spectrometry. *Analytical Chemistry* **1999,** *71* (2), 364-372.

72. Duan, H. L.; Zaharias, G. A.; Bent, S. F., Probing radicals in hot wire decomposition of silane using single photon ionization. *Applied Physics Letters* **2001,** *78* (12), 1784-1786.
73. Tange, S.; Inoue, K.; Tonokura, K.; Koshi, M., Catalytic decomposition of SiH_4 on a hot filament. *Thin Solid Films* **2001,** *395* (1-2), 42-46.
74. Ashfold, M. N. R.; May, P. W.; Petherbridge, J. R.; Rosser, K. N.; Smith, J. A.; Mankelevich, Y. A.; Suetin, N. V., Unravelling aspects of the gas phase chemistry involved in diamond chemical vapour deposition. *Physical Chemistry Chemical Physics* **2001,** *3* (17), 3471-3485.
75. Rego, C. A.; May, P. W.; Henderson, C. R.; Ashfold, M. N. R.; Rosser, K. N.; Everitt, N. M., In-situ mass-spectrometric study of the gas-phase species involved in CVD of diamond as a function of filament temperature. *Diamond and Related Materials* **1995,** *4* (5-6), 770-774.
76. Wu, C. H.; Tamor, M. A.; Potter, T. J.; Kaiser, E. W., A study of gas chemistry during hot-filament vapor-deposition of diamond films using methane hydrogen and acetylene hydrogen gas-mixtures. *Journal of Applied Physics* **1990,** *68* (9), 4825-4829.
77. Shi, Y. J.; Li, X. M.; Toukabri, R.; Tong, L., Effect of Si-H bond on the gas-phase chemistry of trimethylsilane in the hot wire chemical vapor deposition process. *Journal of Physical Chemistry A* **2011,** *115* (37), 10290-10298.
78. Toukabri, R.; Shi, Y. J., Effect of trimethylsilane pressure on hot-wire chemical vapor deposition chemistry using vacuum ultraviolet laser ionization mass spectrometry. *Journal of Vacuum Science & Technology A* **2013,** *31* (6).
79. Toukabri, R.; Shi, Y. J., Unraveling the complex chemistry using dimethylsilane as a precursor gas in hot wire chemical vapor deposition. *Physical Chemistry Chemical Physics* **2014,** *16* (17), 7896-7906.
80. Toukabri, R.; Shi, Y. J., Dominance of silylene chemistry in the decomposition of monomethylsilane in the presence of a heated metal filament. *Journal of Physical Chemistry A* **2014,** *118* (22), 3866-3874.
81. Shi, Y. J.; Lo, B.; Tong, L.; Li, X.; Eustergerling, B. D.; Sorensen, T. S., In situ diagnostics of the decomposition of silacyclobutane on a hot filament by vacuum ultraviolet laser ionization mass spectrometry. *Journal of Mass Spectrometry* **2007,** *42* (5), 575-583.
82. Badran, I.; Forster, T. D.; Roesler, R.; Shi, Y. J., Competition of silene/silylene chemistry with free radical chain reactions using 1-methylsilacyclobutane in the hot-wire chemical vapor deposition process. *The Journal of Physical Chemistry A* **2012,** *116* (41), 10054-10062.
83. Tong, L.; Shi, Y. J., Decomposition of 1,1-dimethyl-1-silacyclobutane on a tungsten filament - evidence of both ring C-C and ring Si-C bond cleavages. *Journal of Mass Spectrometry* **2010,** *45* (2), 215-222.
84. Badran, I.; Rauk, A.; Shi, Y. J., Theoretical study on the ring-opening of 1,3-disilacyclobutane and H_2 elimination. *The Journal of Physical Chemistry A* **2012,** *116* (48), 11806-11816.
85. Tong, L.; Shi, Y. J., A mechanistic study of gas-phase reactions with 1,1,3,3-tetramethyl-1,3-disilacyclobutane in the hot-wire chemical vapor deposition process. *Thin Solid Films* **2009,** *517* (12), 3461-3465.
86. Eustergerling, B. D.; Shi, Y. J., Formation of aminosilanes in the hot-wire chemical vapor deposition process using SiH_4 - NH_3 gas mixtures. *Arkivoc* **2009**, 75-89.
87. Shi, Y. J.; Eustergerling, B. D.; Li, X. M., Mass spectrometric study of gas-phase chemistry in the hot-wire CVD processes of SiH_4/NH_3 mixtures. *Thin Solid Films* **2008,** *516* (5), 506-510.

88. Umemoto, H.; Morimoto, T.; Yamawaki, M.; Masuda, Y.; Masuda, A.; Matsumura, H., Deposition chemistry in the Cat-CVD processes of the SiH_4/NH_3 system. *Thin Solid Films* **2003,** *430* (1-2), 24-27.
89. Yoshimura, S.; Sugimoto, S.; Takeuchi, T.; Murai, K.; Kiuchi, M., Identification of fragment ions produced from hexamethyldisilazane and production of low-energy mass-selected fragment ion beam. *Nuclear Instruments & Methods in Physics Research Section B-Beam Interactions with Materials and Atoms* **2018,** *430*, 1-5.
90. Schuhle, U.; Pallix, J. B.; Becker, C. H., Surface-analysis of bulk polymers using single-photon and multiple-photon ionization. *Journal of Vacuum Science & Technology a-Vacuum Surfaces and Films* **1988,** *6* (3), 936-940.
91. Kung, A. H., Generation of tunable picosecond VUV radiation. *Applied Physics Letters* **1974,** *25* (11), 653-654.
92. Wiley, W. C.; McLaren, I. H., Time-of-flight mass spectrometer with improved resolution. *Review of Scientific Instruments* **1955,** *26* (12), 1150-1157.
93. Sauer, R. O., Derivatives of the methylchlorosilanes I trimethylsilanol and its simple ethers. *Journal of the American Chemical Society* **1944,** *66*, 1707-1710.
94. Becke, A. D., Density-functional thermochemistry .1. the effect of the exchange-only gradient correction. *Journal of Chemical Physics* **1992,** *96* (3), 2155-2160.
95. Lee, C. T.; Yang, W. T.; Parr, R. G., Development of the colle-salvetti correlation-energy formula into a functional of the electron-density. *Physical Review B* **1988,** *37* (2), 785-789.
96. Bartlett, R. J., Coupled-cluster approach to molecular-structure and spectra - a step toward predictive quantum-chemistry. *Journal of Physical Chemistry* **1989,** *93* (5), 1697-1708.
97. Tirado-Rives, J.; Jorgensen, W. L., Performance of B3LYP density functional methods for a large set of organic molecules. *Journal of Chemical Theory and Computation* **2008,** *4* (2), 297-306.
98. Olson, E. W.; Standard, J. M., Structure and bonding in hexamethyldisilazane and a series of analogues, $(XH_3)(2)YH$ (X = CSi, Ge and Y=N, P, As), by ab initio and density functional methods. *Journal of Molecular Structure-Theochem* **2005,** *719* (1-3), 17-30.
99. Fleischer, H.; McKean, D. C.; Torto, I., A quantum-chemical study of the structure, vibrations and SiH bond properties of disilylamine, $NH(SiH_3)(2)$. *Spectrochimica Acta Part a-Molecular and Biomolecular Spectroscopy* **2002,** *58* (5), 911-925.
100. Scott, A. P.; Radom, L., Harmonic vibrational frequencies: An evaluation of Hartree-Fock, Moller-Plesset, quadratic configuration interaction, density functional theory, and semiempirical scale factors. *Journal of Physical Chemistry* **1996,** *100* (41), 16502-16513.
101. Frisch, M. J. T., G.W.; Schlegel, H.B.; Scuseria, G.E.; Robb, M.A; Cheeseman, J.R.; Scalmani, G.; Barone, V.; Petersson, G.A; Nakatsuji, H.; Li, X.; Caricato, M.; Marenich, A.V.; Bloino, J.; Janesko, B.G.; Gomperts, R.; Mennucci, B.; Hratchian, H.P.; Ortiz, J.V.; Izmaylov, A.F.; Sonnenberg, J.L.; Williams-Young, D.; Ding, F.; Lipparini, F.; Egidi, F.; Goings, J.; Peng, B.; Petrone, A.; Henderson, T.; Ranasinghe, D.; Zakrzewski, V.G.; Gao, J., Rega, N.; Zheng, G.; Liang, W.; Hada, M.; Ehara, M.; Toyota, K.; Fukuda, R.; Hasegawa, J.; Ishida, M.; Nakajima, T.; Honda, Y.; Kitao, O.; Nakai, H.; Vreven, T.; Throssell, K.; Montgomery, J.A., Jr.; Peralta, J.E.; Ogliaro, F.; Bearpark, M.J.; Heyd, J.J.; Brothers, E.N.; Kuden, K.N.; Staroverov, V.N.; Keith, T.A.; Kobayashi, R.; Normand, J.; Raghavachari, K.; Rendell, A.P.; Burant, J.C.; Iyenger, S.S.; Tomasi, J.; Cossi, M.; Millam, J.M.; Adamo, C.; Cammi, R.; Ochterski, J.W.; Martin, R.L.; Morokuma, K.; Farkas, O.; Foresman, J.B.; Fox, D.J., Gaussian 16, Revision A.03, Gaussian, Inc., Wallingford CT, 2016.

102. Kuo, D. H.; Yang, D. G., Plasma-enhanced chemical vapor deposition of silicon carbonitride using hexamethyldisilazane and nitrogen. *Thin Solid Films* **2000,** *374* (1), 92-97.
103. Kleps, I.; Caccavale, F.; Brusatin, G.; Angelescu, A.; Armelao, L., LPCVD silicon-carbide and silicon carbonitride films using liquid single precursors. *Vacuum* **1995,** *46* (8-10), 979-981.
104. Limmanee, A.; Otsubo, M.; Sugiura, T.; Sato, T.; Miyajima, S.; Yamada, A.; Konagai, M., Effect of thermal annealing on the properties of a-SiCN : H films by hot wire chemical vapor deposition using hexamethyldisilazane. *Thin Solid Films* **2008,** *516* (5), 652-655.
105. Olesko, K.; Szymanowski, H.; Gazicki-Lipman, M.; Balcerzak, J.; Szymanski, W.; Pawlak, W.; Sobczyk-Guzenda, A., Thin $Si_xN_yC_z$ films deposited from hexamethyldisilazane by RF PECVD technique for optical filter applications. *Materials Science-Poland* **2018,** *36* (1), 56-68.
106. Fainer, N. I.; Rumyantsev, Y. M.; Golubenko, A. N.; Kosinova, M. L.; Kuznetsov, F. A., Synthesis of nanocrystalline silicon carbonitride films by remote plasma enhanced chemical vapor deposition using the mixture of hexamethyldisilazane with helium and ammonia. *Journal of Crystal Growth* **2003,** *248*, 175-179.
107. Yates, D. J. C.; Chern, C. S.; Witzke, H.; Kear, B. H., Thin-film formation by the thermal-decomposition of hexamethyldisilazane in a hot wall reactor. *Scripta Metallurgica Et Materialia* **1991,** *25* (9), 2071-2074.
108. Nakayamada, T.; Matsuo, K.; Hayashi, Y.; Izumi, A.; Kadotani, Y., Evaluation of corrosion resistance of SiCN films deposited by HWCVD using organic liquid materials. *Thin Solid Films* **2008,** *516* (5), 656-658.
109. Stelzner, T.; Arold, M.; Falk, F.; Stafast, H.; Probst, D.; Hoche, H., Single source precursors for plasma-enhanced CVD of SiCN films, investigated by mass spectrometry. *Surface & Coatings Technology* **2005,** *200* (1-4), 372-376.
110. Shi, Y. J., Hot wire chemical vapor deposition chemistry in the gas phase and on the catalyst surface with organosilicon compounds. *Accounts of Chemical Research* **2015,** *48* (2), 163-173.
111. Toukabri, R.; Alkadhi, N.; Shi, Y. J., Formation of methyl radicals from decomposition of methyl-substituted silanes over tungsten and tantalum filament surfaces. *The Journal of Physical Chemistry A* **2013,** *117* (33), 7697-7704.
112. Eustergerling, B. D.; Heden, M.; Shi, Y. J., Development of a new laser induced electron impact ionization source for studying the hot-wire chemical vapor deposition chemistry of silane-ammonia mixtures. *Journal of Analytical Atomic Spectrometry* **2008,** *23* (12), 1590-1598.
113. Owusu-Ansah, E.; Rajendran, A.; Shi, Y., Catalytic dissociation of tris(dimethylamino)silane on hot tungsten and tantalum filament surfaces. *Physical Chemistry Chemical Physics* **2019**.
114. Tamas, J.; Miklos, P., Mass-spectrometric study of hexamethyldisilazane and some of its n-substituted derivatives. *Organic Mass Spectrometry* **1975,** *10* (10), 859-866.
115. Schuhle, U.; Pallix, J. B.; Becker, C. H., Sensitive mass spectrometry of molecular adsorbates by stimulated desorption and single-photon ionization. *Journal of the American Chemical Society* **1988,** *110* (7), 2323-2324.
116. Shi, Y. J.; Consta, S.; Das, A. K.; Mallik, B.; Lacey, D.; Lipson, R. H., A 118 nm vacuum ultraviolet laser/time-of-flight mass spectroscopic study of methanol and ethanol clusters in the vapor phase. *Journal of Chemical Physics* **2002,** *116* (16), 6990-6999.

117. Shi, Y.; Li, X.; Tong, L.; Toukabri, R.; Eustergerling, B., Decomposition of hexamethyldisilane on a hot tungsten filament and gas-phase reactions in a hot-wire chemical vapor deposition reactor. *Physical Chemistry Chemical Physics* **2008,** *10* (18), 2543-2551.
118. Duan, H. L.; Bent, S. F., The influence of filament material on radical production in hot wire chemical vapor deposition of a-Si:H. *Thin Solid Films* **2005,** *485* (1), 126-134.
119. Zeigarnik, A. V.; Valdes-Perez, R. E.; Myatkovskaya, O. N., C-C bond scission in ethane hydrogenolysis. *Journal of Physical Chemistry B* **2000,** *104* (45), 10578-10587.
120. Wang, G. C.; Li, J.; Xu, X. F.; Li, R. F.; Nakamura, J., The relationship between adsorption energies of methyl on metals and the metallic electronic properties: A first-principles DFT study. *Journal of Computational Chemistry* **2005,** *26* (9), 871-878.
121. Kua, J.; Faglioni, F.; Goddard, W. A., Thermochemistry for hydrocarbon intermediates chemisorbed on metal surfaces: CHn-m(CH_3)(m) with n=1, 2, 3 and m <= n on Pt, Ir, Os, Pd, Ph, and Ru. *Journal of the American Chemical Society* **2000,** *122* (10), 2309-2321.
122. Lin, J. L.; Bent, B. E., 2 Mechanisms for formation of methyl radicals during the thermal-decomposition of CH_3I on a Cu(111) surface. *Journal of Physical Chemistry* **1993,** *97* (38), 9713-9718.
123. Truhlar, D. G.; Garrett, B. C., Variational transition-state theory. *Accounts of Chemical Research* **1980,** *13* (12), 440-448.
124. Ge, Y.; Gordon, M. S.; Battaglia, F.; Fox, R. O., Theoretical study of the pyrolysis of methyltrichlorosilane in the gas phase. 3. Reaction rate constant calculations. *The Journal of Physical Chemistry A* **2010,** *114* (6), 2384-2392.
125. Badran, I.; Shi, Y., A kinetic study of the gas-phase reactions of 1-methylsilacyclobutane in hot wire chemical vapor deposition. *Physical Chemistry Chemical Physics* **2018,** *20* (1), 75-85.
126. Fleischer, H.; McKean, D. C., Ab initio studies of disilazanes: Structures and vibrational properties of hexachloro-, hexamethyl-, and tetrachlorodisilazane. *Journal of Physical Chemistry A* **1999,** *103* (6), 727-738.
127. Fjeldberg, T., The molecular structure and conformation of hexamethyldisilazane, NH(Si(CH3)3)2, as determined by gas phase electron diffraction. *Journal of Molecular Structure* **1984,** *112* (1), 159-167.
128. Guruvenket, S.; Andrie, S.; Simon, M.; Johnson, K. W.; Sailer, R. A., Atmospheric-pressure plasma-enhanced chemical vapor deposition of a-SiCN:H Films: Role of precursors on the film growth and properties. *Acs Applied Materials & Interfaces* **2012,** *4* (10), 5293-5299.
129. Saloum, S.; Alkhaled, B., Structural, optical and electrical properties of plasma deposited thin films from hexamethyldisilazane compound. *Acta Physica Polonica A* **2011,** *119* (3), 369-373.
130. Neethirajan, S.; Ono, T.; Masayoshi, E., Characterization of catalytic chemical vapor-deposited SiCN thin film coatings. *International Nano Letters* **2012,** *2* (1), 4.
131. Metail, V.; Joanteguy, S.; Chrostowska-Senio, A.; Pfister-Guillouzo, G.; Systermans, A.; Ripoll, J. L., Gas-phase characterization of unhindered silanimines by photoelectron spectroscopy: Experimental and theoretical study of the SiN double bond1. *Inorganic Chemistry* **1997,** *36* (7), 1482-1487.
132. Raabe, G.; Michl, J., Multiple bonding to silicon. *Chemical Reviews* **1985,** *85* (5), 419-509.
133. Kuhn, A.; Sander, W., Photochemistry of dimethylsilyl Azide: Formation and reactivity of 1,1-dimethylsilanimine. *Organometallics* **1998,** *17* (2), 248-254.

134. Wiberg, N., Unsaturated compounds of silicon and group homologues: VIII. Unsaturated silicon and germanium compounds of the types R2E□C(SiR3)2 and R2E□N(SiR)3) (E = Si, Ge). *Journal of Organometallic Chemistry* **1984,** *273* (2), 141-177.
135. Zhinkin, D. Y.; Varezhkin, Y. M.; Morgunova, M. M., Advances in the chemistry of compounds with the cyclodisilazane structure. *Russian Chemical Reviews* **1980,** *49* (12), 1149-1162.
136. Letulle, M.; Systermans, A.; Ripoll, J.-L.; Guenot, P., The generation of 1,1-dimethylsilanimine by flash vacuum thermolysis. *Journal of Organometallic Chemistry* **1994,** *484* (1), 89-91.
137. Kerr, J. A.; Stephens, A.; Young, J. C., Hydrogen-abstraction reactions from organosilicon compounds. The reactions of methyl, trideuteromethyl, trifluoromethyl, and ethyl radicals with tetramethylsilane. *International Journal of Chemical Kinetics* **1969,** *1* (3), 339-351.
138. Chaudhry, A. U.; Gowenlock, B. G., Arrhenius parameters for the reactions of methyl radicals with group IV tetramethyls. *Journal of Organometallic Chemistry* **1969,** *16* (2), 221-226.
139. Zigler, S. S.; Johnson, L. M.; West, R., Generation of silanimines by photolysis of hindered azidosilanes. *Journal of Organometallic Chemistry* **1988,** *341* (1), 187-198.
140. Ando, W.; Tsumaki, H.; Ikeno, M., Photolysis of diazidosilanes. Generation and reactions of digonal silicon intermediates such as silacarbodi-imides. *Journal of the Chemical Society, Chemical Communications* **1981,** (12), 597-598.
141. Sekiguchi, A.; Ando, W.; Honda, K., Matrix isolation of silaacrylate and its photochemical reaction. *Tetrahedron Letters* **1985,** *26* (19), 2337-2340.
142. Kazoura, S. A.; Weber, W. P., Flash vacuum pyrolysis of dimethoxymethylsilyl-bis(trimethylsilyl)amine: 1,3-Sigmatropic rearrangements of silaimine intermediates. *Journal of Organometallic Chemistry* **1984,** *268* (1), 19-30.
143. Elsheikh, M.; Pearson, N. R.; Sommer, L. H., Evidence for silicon-carbon and silicon-nitrogen multiple-bonded (p.pi.-p.pi.) intermediates from photolysis. Dipolar character of the unsaturated linkages. *Journal of the American Chemical Society* **1979,** *101* (9), 2491-2492.
144. Elseikh, M.; Sommer, L. H., Unsaturated bridgehead silicon intermediates. Dipolar character of unsaturated silicon nitrogen bonds in such intermediates. *Journal of Organometallic Chemistry* **1980,** *186* (3), 301-308.

APPENDIX A: HYDROLYSIS OF HMDSZ

A. Gas Chromatography/Mass Spectrometry (GC-MS) of hydrolysed HMDSZ

As discussed in section 3.2.1, HMDSZ has been shown to hydrolyse in humid airstream to HMDSO and TriMSO plus ammonia. Using our TOF MS, it has been proven that, HMDSZ can easily undergo hydrolysis in humid conditions. GC-MS experiment was performed using electron ionization source. As shown in the chromatogram below, there are three integrated peaks in the chromatogram. A NIST (National Institute of Standards and Technology) search confirms that peak (a) and (b) with retention time 1.36 min and 1.66 are impurities from H_2O and HMDSO/TriMSO respectively.

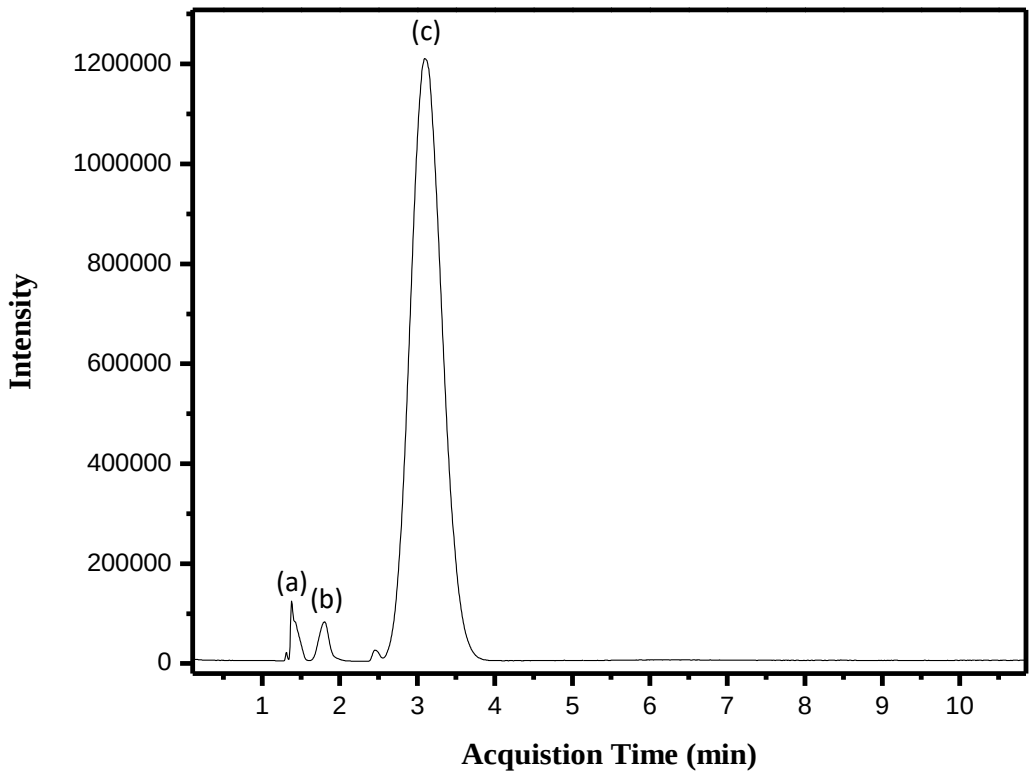

Appendix A. Chromatogram of HMDSZ obtained by GC showing integrated area of various constituents in HMDSZ.

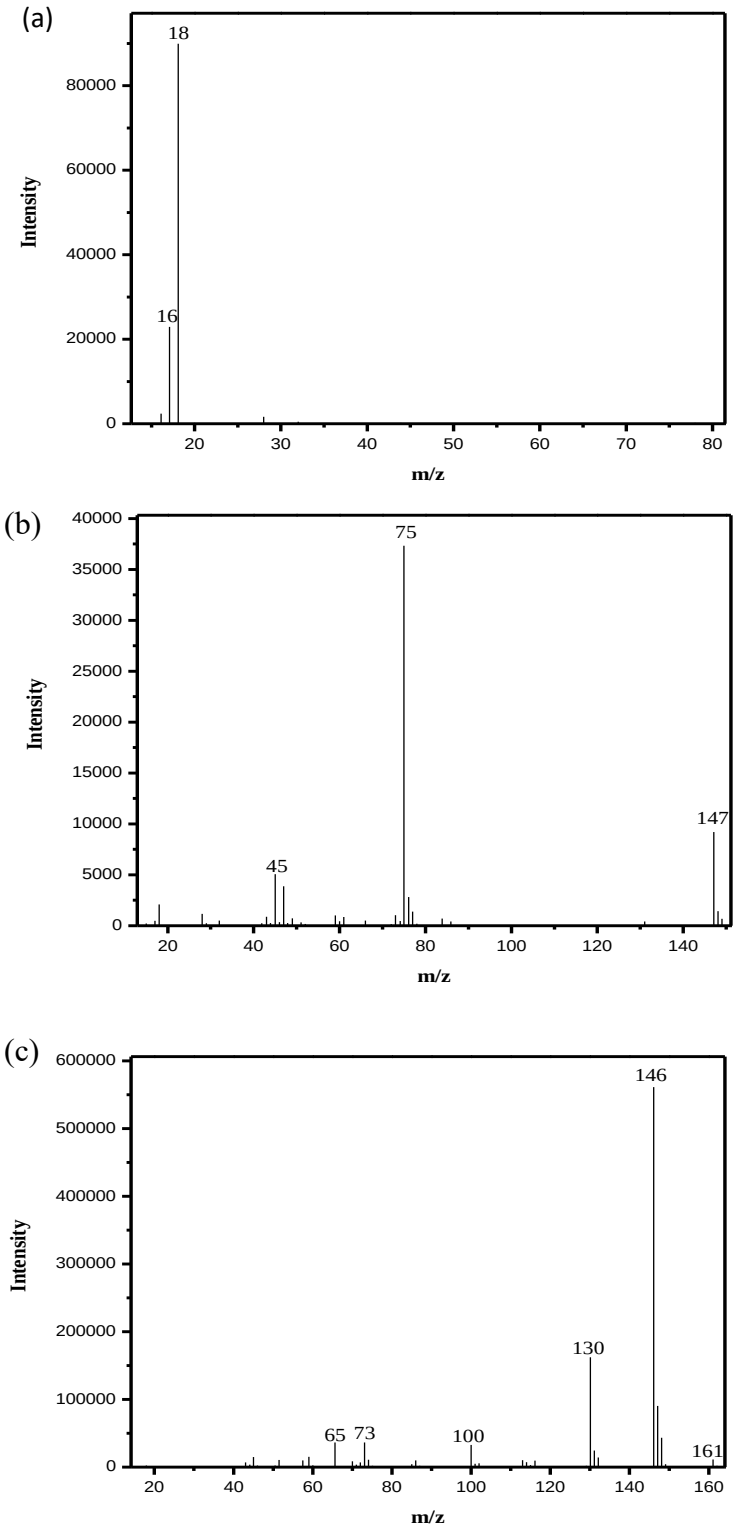

Appendix A. Mass spectra of various peaks in the GC (a) water (b) TriMSO and HMDSO (c) HMDSZ

B. AMERICAN CHEMICAL SOCIETY LICENSE

Title: Hot Wire Chemical Vapor Deposition Chemistry in the Gas Phase and on the Catalyst Surface with Organosilicon Compounds

Author: Yujun Shi

Publication: Account of Chemical Research

Publisher: American Chemical Society

Date: Jan. 14, 2015 Copyright © 2015 American Chemical Society

PERMISSION/LICENSE IS GRANTED FOR YOUR ORDER AT NO CHARGE

This type of permission/license, instead of the standard Terms & Conditions, is sent

to you because no fee is being for your order. Please note the following:

- This type of permission /license, instead of the standard Terms & Conditions, is sent to you because no fee is being charged for your order. Please note the following:
- Permission is granted for your request in both print and electronic formats, and translations.
- If figures and/ or tables were requested, they may be adapted or used in part.
- Appropriate credit for the requested material should be given as follows: "Reprinted (adapted) with permission from (Acc. Chem. Res. 2015, 48, 2, 163-173). Direct link (https://pubs.acs.org/doi/full/10.1021/ar500241x). Copyright (2015) American Chemical Society.
- One-time permission is granted only for the use specified in your request. No additional uses are granted (such as derivative works or other editions). For any other uses, please submit a new request.